



Thèse

2023

Open Access

This version of the publication is provided by the author(s) and made available in accordance with the copyright holder(s).

Accurate and Precise Nuclear Magnetic Moments of Radioactive Nuclei for β -NMR

Croese, Jared

How to cite

CROESE, Jared. Accurate and Precise Nuclear Magnetic Moments of Radioactive Nuclei for β -NMR. Doctoral Thesis, 2023. doi: 10.13097/archive-ouverte/unige:172023

This publication URL: <https://archive-ouverte.unige.ch/unige:172023>

Publication DOI: [10.13097/archive-ouverte/unige:172023](https://doi.org/10.13097/archive-ouverte/unige:172023)

© The author(s). This work is licensed under a Creative Commons Attribution (CC BY)

<https://creativecommons.org/licenses/by/4.0>

UNIVERSITÉ DE GENÈVE

Département de physique nucléaire et corpusculaire

FACULTÉ DES SCIENCES

Professeure M. Kowalska

Directrice de thèse

UNIVERSITÉ DE MAASTRICHT

Centre de biologie des systèmes de Maastricht

FACULTÉ DES SCIENCES

ET D'INGÉNIERIE

Professeur R. B. Jolivet

Co-directeur de thèse

**Accurate and Precise Nuclear Magnetic Moments of Radioactive
Nuclei for β -NMR.**

THÈSE

Présentée à la Faculté des sciences de l'Université de Genève
pour obtenir le grade de Docteur ès sciences, mention Physique

par

ir. Jared CROESE

de

Rotterdam (Les Pays-Bas)

Thèse N°5756



**UNIVERSITÉ
DE GENÈVE**

GENÈVE

2023

The work done within the context of this thesis has given rise to the following publications reproduced therein:

High-accuracy liquid-sample β -NMR setup at ISOLDE, Nucl. Ints. & Meth. A (1020), 2021, 165862

Magnetic moments of short-lived nuclei with part-per-million accuracy, Phys. Rev. X (10), 2020, 041061



**UNIVERSITÉ
DE GENÈVE**

FACULTÉ DES SCIENCES

DOCTORAT ÈS SCIENCES, MENTION PHYSIQUE

Thèse de Monsieur Jared CROESE

intitulée :

**«Accurate and Precise Nuclear Magnetic Moments of
Radioactive Nuclei for β -NMR»**

La Faculté des sciences, sur le préavis de Madame M. KOWALSKA, professeure titulaire et directrice de thèse (Département de physique nucléaire et corpusculaire), Monsieur R. JOLIVET, professeur et codirecteur de thèse (MaCSBio, Maastricht University, Maastricht, Pays-Bas), Monsieur Z. SALMAN, docteur (LMU, NUM, Paul Scherrer Institut, Villigen) et Monsieur M. AFZELIUS, docteur (Département de physique appliquée), autorise l'impression de la présente thèse, sans exprimer d'opinion sur les propositions qui y sont énoncées.

Genève, le 22 août 2023

Thèse - 5756 -



La Doyenne

N.B. - La thèse doit porter la déclaration précédente et remplir les conditions énumérées dans les "Informations relatives aux thèses de doctorat à l'Université de Genève".

Résumé

La résonance magnétique nucléaire détectée par asymétrie de désintégration bêta (β -RMN) est une technique de résonance magnétique de spin qui utilise des isotopes émetteurs bêta radioactifs comme sondes. Deux des principaux avantages de la technique sont la large gamme d'isotopes ayant des propriétés nucléaires différentes pour le même élément chimique et sa grande sensibilité. Traditionnellement, cette technique a été utilisée pour la recherche en science des matériaux, pour étudier les champs électromagnétiques internes d'hôtes à l'état solide, et pour la recherche en physique nucléaire, pour étudier comment les moments électromagnétiques changent dans différents noyaux en fonction de leur distribution propre de protons et de neutrons. La présente thèse explique les techniques et méthodes utilisées pour appliquer β -RMN à des hôtes à l'état liquide. Ces techniques et méthodes sont démontrées par la détermination du moment dipolaire magnétique de ^{26}Na avec une précision en ppm. Les mêmes étapes pourront être utilisées à l'avenir pour des études chimiques, biochimiques et de moment électromagnétique nucléaires de haute précision.

Au cœur de ces mesures se trouve la boucle de stabilisation et de mesure du champ magnétique basée sur la mesure RMN des protons dans des molécules d'eau, dont la mise en œuvre a été décrite dans *High-accuracy liquid-sample β -NMR setup at ISOLDE, Nucl. Int. & Meth. A (1020), 2021, 165862*, ainsi que d'autres adaptations de la ligne de faisceau β -RMN d'ISOLDE.

La méthode de mesure des moments dipolaires magnétiques nucléaires de haute précision, telle qu'énoncée dans *Magnetic moments of short-lived nuclei with part-per-million accuracy, Phys. Rev. X (10), 2020, 041061*, contient les éléments suivants: Tout d'abord, une mesure de la fréquence de Larmor nucléaire avec une largeur de raie inférieure au kHz, ceci ayant été réalisé en utilisant un liquide ionique à température ambiante (LITA) comme hôte d'implantation, en

réduisant les écarts spatiaux du champ magnétique (homogénéité) au niveau ppm au moyen de bobines de calage PCB, et en stabilisant les fluctuations temporelles au niveau ppm en utilisant une boucle de rétroaction; Deuxièmement, une référence externe et une carte de champ précise pour déterminer le rapport des fréquences de Larmor entre l'isotope d'intérêt et la référence; Troisièmement, le même rapport pour un isotope stable du même élément chimique dans le même matériau hôte (un LITA) par rapport à la même référence; Quatrièmement, une mesure précise de la fréquence de Larmor de l'isotope stable; Cinquièmement, une constante de blindage RMN précise pour l'environnement dans lequel la mesure précise de l'isotope stable a été effectuée, par exemple déterminée par des calculs de blindage RMN *ab initio*; Enfin, le déplacement chimique entre les environnements de mesure chimiques utilisés dans les troisième et quatrième étapes.

En combinant ces éléments, on peut calculer un moment magnétique très précis de l'isotope stable et l'utiliser pour calculer le moment magnétique de l'isotope d'intérêt au moyen du rapport corrigé du déplacement chimique des fréquences de Larmor. Le résultat obtenu pour ^{26}Na est de 2,849390(20) magnétons nucléaires. Ceci est en accord avec, mais deux ordres de grandeur plus précis que, la détermination précédente du moment dipolaire magnétique de ^{26}Na . Étant donné que les moments dipolaires magnétiques de $^{27-31}\text{Na}$ étaient déterminés par leur rapport à ^{26}Na , leurs moments dipolaires magnétiques pourraient également être améliorés.

Summary

Beta decay asymmetry detected Nuclear magnetic resonance (β -NMR) is a spin magnetic resonance technique that uses radioactive beta-emitting isotopes as probes. Two of the main benefits of the technique are the wide selection of isotopes with different nuclear properties for the same chemical element and its high sensitivity. Traditionally this technique has been used for material science research to study internal electromagnetic fields of solid-state hosts, and for nuclear physics research to study how the electromagnetic moments change for different nuclei based on their proton and neutron distribution. This thesis expounds on the techniques and methods used to apply β -NMR to liquid state hosts. They are demonstrated by the determination of the magnetic dipole moment of ^{26}Na with ppm precision. The same steps can be used in the future for chemical, biochemical, and high-precision nuclear electromagnetic moment studies.

Central to this measurement has been the magnetic field stabilization and measurement loop based on the NMR measurement of protons in water molecules. The implementation of which has been described in *High-accuracy liquid-sample β -NMR setup at ISOLDE, Nucl. Ints. & Meth. A (1020), 2021, 165862* together with other adaptations of ISOLDE's β -NMR-beamline.

The method for measuring high-precision nuclear magnetic dipole moments as set forth in *Magnetic moments of short-lived nuclei with part-per-million accuracy, Phys. Rev. X (10), 2020, 041061* contains the following elements. First, a measurement of the nuclear Larmor frequency with sub-kHz line-width. This has been achieved by using a room temperature ionic liquid (RTIL) as implantation host, reducing the spatial deviations of the magnetic field (homogeneity) to the ppm level by means of PCB shimming coils, and stabilizing the temporal fluctuations to the ppm level using a feedback loop. Second, an external ref-

erence and an accurate field map to determine the ratio of Larmor frequencies between the isotope of interest and the reference. Third, the same ratio for a stable isotope of the same chemical element in the same host material (a RTIL) with respect to the same reference. Fourth, a precise measurement of the Larmor frequency of the stable isotope. Fifth, an accurate NMR shielding constant for the environment in which the precise measurement of the stable isotope was performed, e.g. determined by *ab initio* NMR shielding calculations. Last, the chemical shift between chemical measurement environments used in the third and fourth steps.

Combining these elements one can compute a very accurate magnetic moment of the stable isotope and use it to compute the magnetic moment of the isotope of interest by means of the chemical shift corrected ratio of Larmor frequencies. The result obtained for ^{26}Na is 2.849390(20) nuclear magnetons. This is in agreement with, but two orders of magnitude more precise than, the previous determination of the magnetic dipole moment of ^{26}Na . Because the magnetic dipole moments of $^{27-31}\text{Na}$ were determined by their ratio to ^{26}Na their magnetic dipole moments could be improved as well.

Acknowledgments

Nothing in life is to be feared, it is only to be understood. Now is the time to understand more, so that we may fear less. – **Marie Curie** (As quoted in *Our Precarious Habitat* (1973) by Melvin A. Benarde)

"I think physicists are the Peter Pans of the human race. They never grow up, and they keep their curiosity." – **I.I Rabi** (As quoted in "The Atomic Scientists, the Sense of Wonder and the Bomb" by Mark Fiege in *Environmental History*, Vol. 12, Issue 3, July 2007).

Working at an online facility like ISOLDE has been a really special experience. One can not work in isolation and is constantly standing on the shoulders of those that have come before. As such the work presented in this thesis has been directly and indirectly affected and made possible by the work and lives of so many people. Even though I can not mention each one of them there are some that I need to mention at this stage because of their effect on me and or the project. So not in any particular order let's start with Stephan Etenaur-Malbrunot. Thank you for contacting me after I filled out the CERN doctoral student application form. If you wouldn't have done so, I would have continued to think that the chance of working at CERN was infinitesimally small. Next to that, I would have never known about ISOLDE or about β -NMR.

I'm very grateful to Magda, for giving me the opportunity to spend my PhD research at CERN and supporting me along the way. I've always had the feeling you valued my opinion on technical matters. I thoroughly enjoyed having physics discussions whenever we had the time for it. I appreciate the level of equality I experienced when I joined the group, which gave me the opportunity to make mistakes, learn and grow. I'm grateful for the opportunity you gave me to join an experimental campaign at TRIUMF, and for all of the many other

things you allowed me to try. Though my time within the group has felt like a roller-coaster ride, with highs, lows, and being tossed in every direction. It was all over in the blink of an eye. I think the β -NMR experiments that we have done are super interesting and still think about it often. The beamline that we have (re)-build is very dear to me.

Renaud thank you very much for going above and beyond my expectations. For bringing me with you to Saudi Arabia to the conference at KAUST even though I have/had zero understanding of neuroscience. For regularly checking in with me, to see how I'm doing, and caring about my well-being and future career. For helping me out with the administration at the university. For all your advice and for being a great sounding board. Also thank you for your patience with my lack of writing skills and your patience with me as I was trying to figure out what future career steps would make the most sense for me and my family.

Jean-Noel you must be the most sincere person I know in academia. Thanks for opening your lab for me and being an active part of our collaborative experiments and for being such a nice guy.

Rob, this section would not be complete without mentioning you. From the start, you treated me as an equal. While we were rebuilding the beamline together you taught me a lot about what it takes to make this experimental setup work. I can honestly say that without you there would not have been a working beamline for the experiments in 2018. I really enjoyed working together and thinking about what next upgrades or changes would improve this exceptional piece of equipment.

Lina as the senior PhD-student/post-doc on the project when I arrived, you made a significant impact on my work. I admire your work ethic and your determination to reach your goals. Thank you so much for our chats, the kindness, and understanding you have shown me, and all of the advice you have given me. Also thank you very much for your love for my family.

Beatrice thank you for being the best post-doc I could have asked for, for being super patient with me, encouraging me when I got stuck, acting as a "rubber duck" and keeping some of the stress away when that was needed. You really made a huge difference in my PhD. I had so much fun at the office with you and Emma, and the Germanic language similarities. I learned a lot from you about NMR, academic work, and how to take a step back when things are getting

tense. I wish you and Hendrik the best and hope that your archery/leather-working/sword-fighting plans will come to fruition.

Kasia thank you for being yourself. Even though we had a bit of a rocky start when you just joined the group I'm really grateful for your friendship. I admire your ability to push through even though your path ahead might seem to be blocked up. How you tenaciously use any opening you see to achieve your goals. Your skill at devouring and organizing literature. And for the way that you have taken ownership of your own research path. I really miss our many chats, whether it was the latest "gossip" or our constant discussions about NMR (although often it felt like we were speaking two different languages). Thank you for the many ways in which you helped me. I fully expect you will "Excel" at anything you will do in the future. I wish you and David lots of luck and hope your dream to work, live, and travel overseas will arrive sooner rather than later.

Frank, technically we haven't worked together, and to be honest, my first impression of you wasn't the best. But I still want to thank you for turning out to be a very kind and approachable person, with a low tolerance for bull shit, for helping out with advice and devices, and for your constant critical review/feedback. When you were not part of the project anymore and eventually even left ISOLDE you left some big shoes to fill and a high technical standard to live up to. I wish you and your family all the best.

Mark your expertise with lasers and your experience at ISOLDE have been essential to this project. Thank you very much for your critical feedback and relaxed attitude.

Mik & Nikolay or should I say Pat and Mat, you two are great. Working alongside you two has been hilarious, insightful, and instructive at the same time. Time and again I'm amazed at the inventiveness and skill with which you make things work. You really combine in-depth knowledge with practical expertise.

Dalibor no beamtime has been complete without you. You have been super kind, down-to-earth, and knowledgeable. I enjoyed listening to your many personal and ISOLDE experiences.

Wouter thanks for always showing up at beamtimes when that was needed, even though you were not part of the local-group anymore, your contribution to

the experiments, and especially the night shifts which you somehow were always assigned to, was essential.

Phillip and Ahbi thank you so much for welcoming me into the group when I just arrived. I knew you two would be leaving soon after but I wished you could have stayed longer. Working with you and getting to know you has been an absolute pleasure.

Marcus it's been so nice to have come to know you, and to work and to live alongside you. Your initial enthusiasm rekindled my drive. Thank you for enduring my endless explanations and stories and for stepping up to the challenge of understanding the experiment and managing the beamline. You have done, and are still doing some tremendous work in a very challenging environment. I admire your drive and wish you all the best with the remainder of your PhD.

Maxime thanks for always being there whenever I need someone to complain to, and for being a better friend than I have been.

Tassos you were definitely the best-dressed physicist at ISOLDE. Thank you for your social and cheerful attitude and for being my support when I was the only man on the team.

Emma you've been the most memorable student that has passed through the group during my time at ISOLDE. Both the physics discussions and the countless chats on language and cultural differences were a blast. You really brought a positive spirit into the group. And thank you very much for your love for my family.

Stu even though we had our struggles I want to thank you for everything you did to the beamline and the amazing shape that it was when I left. Without your hard work, input and experience, the integration of the new magnet would not have gone so smoothly. Thanks for your explanations about mechanical design, beam optics, and of course for your always interesting stories and hobbies.

I wanted to thank the local group at ISOLDE with a special mention to Dinko, Peter, Simon, Simon, Hanne, Karl, Jonas, Liss, Victoria, Jenny, Gerda, and Erwin. I have often felt very lost in all of the nuclear physics talks but notwithstanding all of that, you have really made it into an amazing and educational experience.

Most thanks go to my family, and most of all to my wife, Celeste, without

whom, I would not have even dared to start this adventure. You have been so supportive, patient, and encouraging. I also want to thank my parents for all the help that they offered us.

Last I want to thank some of my friends from church (Thomas, Phillip, Andrea & Olivia, Gregoire & Isabel, Camille & Simon, Floriane & Lucas, Iris & Mathew, and Jenny & Thomas), who have welcomed us so kindly and have really made us feel at home. Because of your loving friendship, you've made our journey back to the Netherlands so much more difficult, we miss you dearly.

Contents

1	Introduction	16
1.1	Motivation	16
1.2	Nuclear Magnetic Resonance	17
1.2.1	Spin	18
1.2.2	Larmor Precession	19
1.2.3	Spin orientation	21
1.2.4	Rotating reference frame	23
1.2.5	Resonant field	25
1.3	β -NMR	26
1.3.1	Simple radioactive decay	26
1.3.2	Beta particle emission in all space	27
1.3.3	Emission asymmetry	27
1.3.4	Relaxed Asymmetry	28
1.3.5	Experimental Asymmetry	30
1.3.6	Resonance detection	31
1.4	Optical Pumping	31
1.5	Applications	33
1.5.1	Guanine Quadruplexes	34
1.5.2	Hyperfine anomaly	35
1.6	CERN	36
1.7	ISOLDE	38
1.7.1	Production and separation	38
1.8	Versatile Ion-polarized Techniques On-line	43
1.8.1	Ion/laser beam overlap	44
1.8.2	Doppler tuning and neutralization	45

1.8.3	Optical Pumping and Spin Rotation	45
2	Paper 01: High-accuracy liquid-sample β-NMR setup at ISOLDE	49
2.1	Introduction	51
2.2	Methods	54
2.2.1	Field locking	54
2.2.2	Absolute-field measurement	55
2.2.3	Magnetic field shimming	55
2.2.4	β -detectors	56
2.2.5	Sample exchange system	56
2.2.6	Experimental vacuum chamber	59
2.3	Results	61
2.4	Discussion	66
2.4.1	Locking system	66
2.4.2	Shimming coils	67
2.4.3	Sample handling system	68
2.4.4	Beta detectors	70
2.4.5	Experimental chamber	70
2.5	Conclusion	71
2.6	Acknowledgements	71
3	Paper 02: Magnetic Moments of Short-Lived Nuclei with Part-	
	per-Million Accuracy	73
3.1	Introduction	75
3.2	Techniques	77
3.2.1	β -NMR on short-lived ^{26}Na	77
3.2.2	Conventional NMR on stable ^{23}Na	81
3.3	Results	82
3.4	Discussion and future perspectives	90
3.5	Conclusions	93
3.6	Acknowledgements	94
3.7	Appendix A - <i>Ab initio</i> NMR shielding calculations	95
3.8	Appendix B - Effect of bulk magnetic susceptibility	96
4	Discussion & Outlook	98

Acronyms	106
List of Figures	107
List of Tables	109
Bibliography	110

Chapter 1

Introduction

”Our imagination is stretched to the utmost, not, as in fiction, to imagine things which are not really there, but just to comprehend those things which ‘are’ there.” – **Richard Feynman** (chapter 6, “Probability and Uncertainty — the Quantum Mechanical View of Nature,” p. 127-128)

”And now as I said concerning faith - faith is not to have a perfect knowledge of things; therefore if ye have faith ye hope for things which are not seen, which are true.” – **Alma the younger** (Alma 32:21, The Book of Mormon)

1.1 Motivation

Recently there has been an increased interest in the potential application of beta decay asymmetry detected nuclear magnetic resonance (β -NMR) to (bio-)chemical studies [1], [2]. The reason for this interest can be attributed to three main advantages of this technique over conventional nuclear magnetic resonance (NMR) spectroscopy. First, an increased sensitivity (of up to 10 orders of magnitude) due to the high polarisation of the nuclear ensemble used as probes and due to the sensitive detection by means of beta decay asymmetry [3]. Second, radioactive ion beam (RIB)-facilities allow for a wide selection of isotopes with beneficial nuclear properties compared to their stable counterparts [4], [5]. Last, one of the prerequisites for (bio-)chemical investigations, viz. liquid (bio-compatible) samples can potentially lead to an improved accuracy for β -NMR

investigations for nuclear (structure) physics. In solid-state samples NMR resonance peaks are widened due to anisotropic spin interactions [6], [7]. In liquids, on the other hand, due to molecular tumbling, these anisotropic interactions are averaged out and thus the observed resonance peaks are very narrow [7]. This effect could be used to increase the precision of the measured resonance frequencies by two to three orders of magnitude leading to a similar increase in the precision of the derived nuclear magnetic dipole moment which is one of the parts needed to learn more about the still little understood distribution of magnetization within the nucleus [8], [9].

In the following sections, some background to NMR, β -NMR, and a proof of principle biochemical experiment will be given. Following this, the facility and the beamline where this research took place will be shortly described. After that two publications are introduced and added as chapters. The first "High-accuracy liquid-sample β -NMR setup at ISOLDE" [10] describes in detail the additions to the beamline that enabled the experiments done within the scope of this thesis. It will thus function more or less like a traditional "Methods" chapter. The second "Magnetic Moments of Short-Lived Nuclei with Part-per-Million Accuracy: Toward Novel Applications of β -Detected NMR in Physics, Chemistry, and Biology" [11] describes the main results gained by this experimental setup and discusses the potential application of this new methodology.

This thesis will be finalized with a discussion and outlook chapter in which the main points already discussed in the publications will be summarized and slightly expanded upon and an outlook will be given to plans for future modifications and expansions of the setup including potential new investigations.

1.2 Nuclear Magnetic Resonance

From its first measurement in molecular beams by I.I Rabi [12] and its consecutive post world war II development by Bloch and Purcell [13], [14] the NMR phenomenon has become widely applied in spectroscopic and imaging techniques in physics, material science, (bio)chemistry, medicine, and many more fields. At its core, it is a spin magnetic resonance technique, like Electron Paramagnetic Resonance (EPR) and Muon Spin Resonance (μ SR). Many excellent textbooks exist that give either an introductory or in-depth explanation of the matter, for

example references [7], [15]–[17]. In this thesis, the explanation of NMR will be kept as general as possible, accompanied by some useful mental models, while mostly touching on the essentials needed to understand the importance of the presented results.

1.2.1 Spin

A particle can have a quantum mechanical property called spin angular momentum, or spin for short, whose mathematical description is analogous to the classical angular momentum. Because of this analogy, nuclei and other particles with spin are often depicted as a sphere rotating or spinning around its axis. It must however be stated that even though this spinning globe serves as a useful mental image, for elementary (point) particles, like the electron, spin is an intrinsic property and they are not actually spinning. All quantum mechanical particles can be divided into two categories: those whose spin has an integer value (0, 1, ..) are called bosons, and those for which it is half-integer (1/2, 3/2, ..) are called fermions. Bosons follow Bose-Einstein statistics, while fermions follow Fermi-Dirac statistics and the Pauli exclusion principle, meaning that no two identical fermions can be in the same quantum state.

In the case of composite particles, like nuclei, the charge and current distribution can be described by a multipole expansion of the electric and magnetic moments. The electric moment $\mathbb{Q}(\mathbf{r})$ and the magnetic moment $\mathbb{M}(\mathbf{r})$ can thus be expanded as follows:

$$\mathbb{Q}(\mathbf{r}) = \mathbb{Q}^{(0)}(\mathbf{r}) + \mathbb{Q}^{(1)}(\mathbf{r}) + \mathbb{Q}^{(2)}(\mathbf{r}) + \dots \quad (1.1)$$

$$\mathbb{M}(\mathbf{r}) = \mathbb{M}^{(0)}(\mathbf{r}) + \mathbb{M}^{(1)}(\mathbf{r}) + \mathbb{M}^{(2)}(\mathbf{r}) + \dots \quad (1.2)$$

with (0) being the monopole term, (1) the dipole term, (2) the quadrupole term and so forth. One can find the proof that the magnetic monopole term $\mathbb{M}^{(0)} = 0$ in many introductory textbooks on electrodynamics [18]. Furthermore for nuclei, when assuming conservation of parity, all odd electric and even magnetic multipole terms vanish [19]. Using the Wigner-Eckart theorem the following relation between the shape of the nucleus (and thus its charge and current distributions) and the nuclear spin I can be found [15], [16].

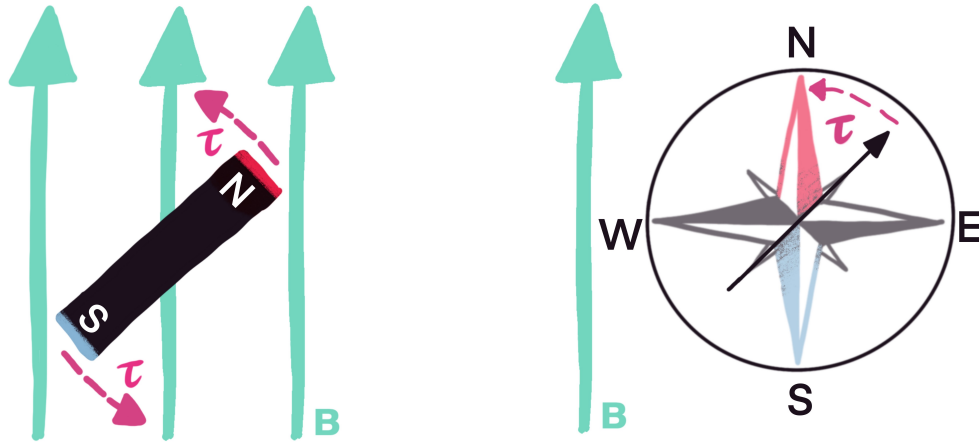


Figure 1.1 A magnetic dipole placed in a magnetic field acts like a compass needle does in the earth's magnetic field.

$$\mathbb{Q}^{(n)} = 0 \ \& \ \mathbb{M}^{(n)} = 0 \ \text{for all } n > 2I \quad (1.3)$$

This means that the order of the multipole expansion is limited to 2 times the I . For example, a nucleus with $I = 0$ will have an electric monopole term $\mathbb{Q}^{(0)}$ (the total charge of the nucleus), but not a magnetic dipole term $\mathbb{M}^{(1)}$. A nucleus with $I = 1/2$ will also have an $\mathbb{M}^{(1)}$ but won't have an electric quadrupole term $\mathbb{Q}^{(2)}$ and so forth.

The spin is related to the magnetic dipole moment $\mu = \mathbb{M}^{(1)}$ in the following way:

$$\mu = \gamma \mathbf{S}, \quad (1.4)$$

where \mathbf{S} is the spin angular momentum vector and $\gamma \equiv g \times q/(2m)$ is the gyromagnetic ratio, with g the g -factor of the particle, q its charge, m its mass.

1.2.2 Larmor Precession

When placed in a magnetic field a dipole moment will experience a torque which will bring it into alignment with the external field. One can think of this as the spindle of a compass that aligns with the earth's magnetic field as illustrated in figure 1.1 (In fact, the spindle of a compass is a dipole magnet).

However, a particle with non-zero spin also has an (intrinsic) angular momentum. Therefore, when placed in a magnetic field the torque exerted on the

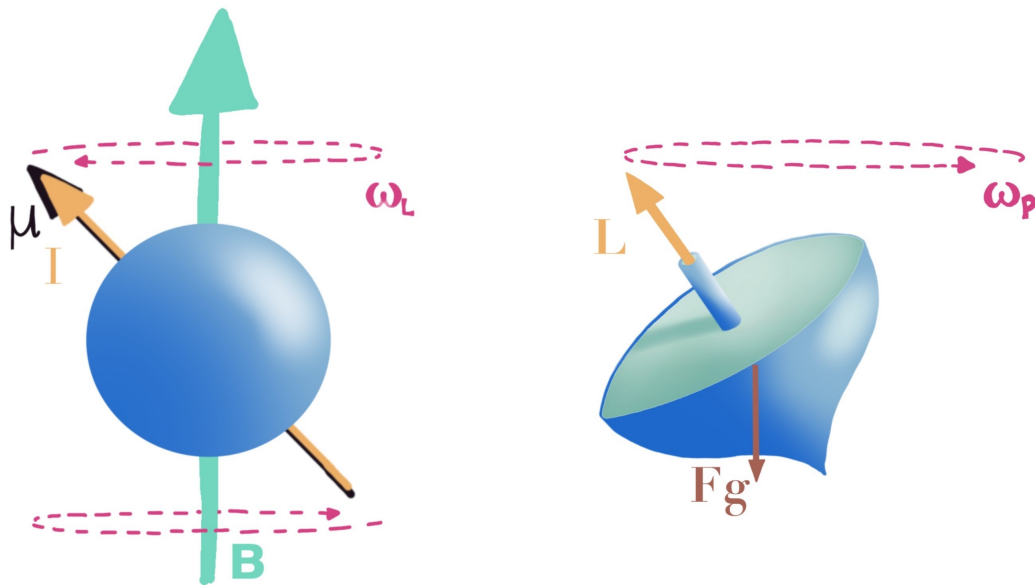


Figure 1.2 A particle with non-zero spin undergoes precessional motion when placed in a magnetic field similar to a gyroscope or spinning top under the influence of gravity.

particle functions similarly to gravity on a spinning top or a gyroscope, making the particle precess around the axis of the magnetic field as shown in figure 1.2

This precession of a magnetic moment around the magnetic field is called Larmor precession and the associated angular frequency of this motion is called the Larmor frequency ω_L , which is given by:

$$\omega_L = \gamma B, \quad (1.5)$$

where B is the magnitude of the magnetic field vector \mathbf{B} .

Speaking about the nuclear Larmor precession, and experiments to measure its frequency, Edward Mills Purcell made the following poetic remark during his Nobel Lecture.

Commonplace as such experiments have become in our laboratories, I have not yet lost that sense of wonder, and delight, that this delicate motion should reside in all ordinary things around us, revealing itself only to him who looks for it. – E. M. Purcell (Nobel Lecture, 1952)

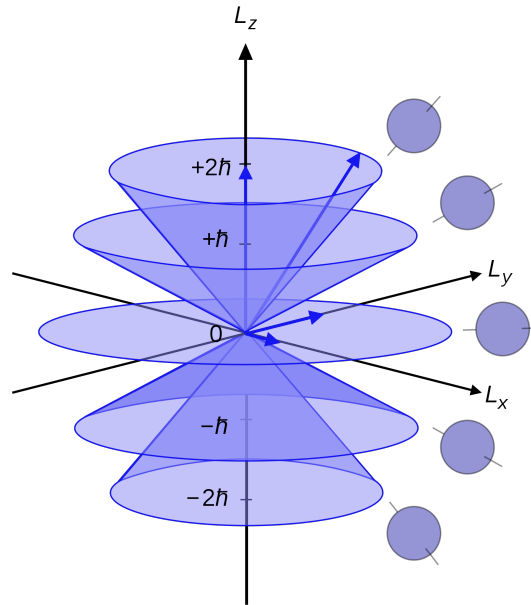


Figure 1.3 The eigenvalues of the angular momentum operator along the z-axis can be seen as the projections of the angular momentum along the z-axis. *Maschen, Public domain, via Wikimedia Commons*

1.2.3 Spin orientation

Since spin is an angular momentum, the corresponding quantum mechanical operators apply to it. It is customary to choose the coordinate system in such a way that the z-axis lies along the magnetic field. The angular momentum operator along the z-axis \hat{l}_z has $2l + 1$ eigenstates with eigenvalues $-l, -l + 1, \dots, l - 1, l$. As this eigenvalue describes the quantum state, it is also called the projection quantum number. This name becomes very intuitive as the eigenvalues of \hat{l}_z can be seen as the different projections of the angular momentum vector on the z-axis, as shown in figure 1.3.

The magnetic energy of a particle with spin \mathbf{S} is given by:

$$\mathbb{H}^{mag} = -\boldsymbol{\mu} \cdot \mathbf{B} \quad (1.6)$$

Notice the minus sign in front of this dot product, which implies that the magnetic energy is lowest when the magnetic moment is aligned with the field. Combining equations 1.6 and 1.4 and the eigenstates of \hat{l}_z directly leads to the Zeeman effect: the degeneracy of the projection substates is lifted when the

particle is exposed to a magnetic field. They are therefore also referred to as magnetic or Zeeman substates.

When looking at an ensemble of spins, a metric is useful that describes the distribution of the ensemble over these magnetic substates. Since the substates identify the orientation of the spin angular momentum vector by its projection on the z-axis, the parameters describing the distribution over the sub states are called orientation parameters. The first and second-order orientation parameters are named Polarisation P^0 and Alignment P^1 [20], [21]:

$$P^0 = \frac{\langle I_z \rangle}{I} = \sum_m (m/I) a_m \quad (1.7)$$

$$P^1 = \sum_m (m^2/I^2) a_m - \frac{I+1}{3I}, \quad (1.8)$$

with $\langle \rangle$ denoting the expectation value, m the projection quantum number and a_m the normalized population or the population probability of the sub-state m . Though each individual spin in the ensemble might be in an arbitrary superposition state, P^0 gives a measure on how much the ensemble on average is oriented with or opposite to the quantization axis. P^1 indicates how well the ensemble on average lies along the quantization axis.

The equilibrium distribution over the Zeeman states is temperature dependent and is given by the Boltzmann distribution:

$$a_m = \frac{e^{-E_m/k_B T}}{\sum_s e^{-E_s/k_B T}}, \quad (1.9)$$

with k_B the Boltzmann constant and \sum_s indicating the sum over all Zeeman states.

When the distribution deviates from the thermal equilibrium the ensemble will return or relax back to an equilibrium distribution due to interactions with the environment. Two time constants are important in the description of relaxation. The first, T_1 , is the longitudinal relaxation time constant, which describes the return to the thermal equilibrium state distribution. The second, T_2 , is the transverse relaxation time constant which describes the loss of coherent behavior of the spin ensemble in the transversal plane.

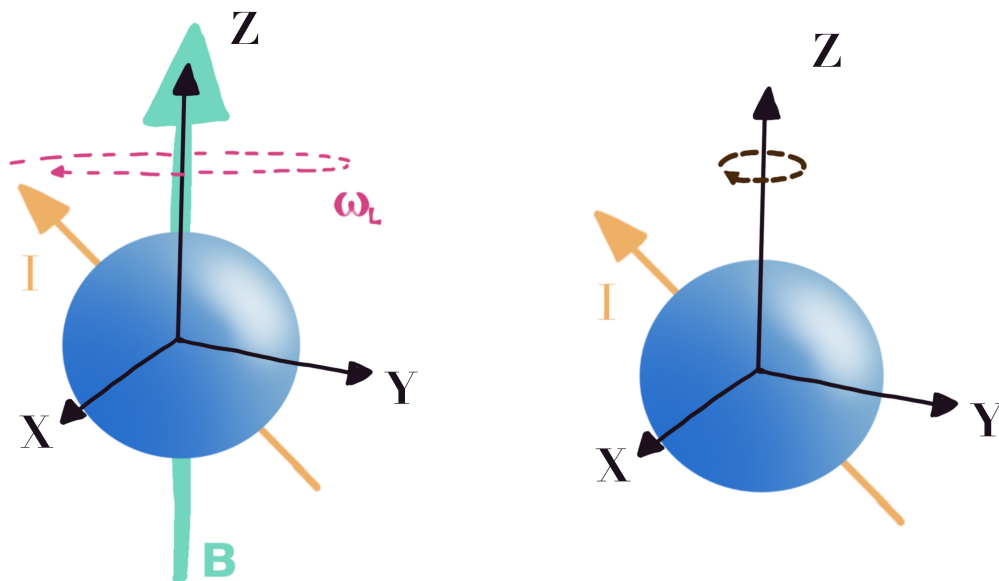


Figure 1.4 Moving to a rotating reference frame makes it easier to visualize the dynamic behavior of spins.

1.2.4 Rotating reference frame

To visualize the effect of longitudinal and transversal relaxation on the spin ensemble one needs to expand further on our mental model of a precessing and spinning sphere. First of all, the sphere now should not represent a single spin, but the ensemble average. Second, it would be useful to perform a reference frame transformation. Moving to a reference frame that is rotating at exactly the Larmor frequency allows one to evaluate the dynamic behavior of the spins in a static picture. Figure 1.4 depicts the reference frame transformation.

Figure 1.5 shows how the two relaxation effects can be depicted in the rotating reference frame. The top three images show that as the individual spins move back to their equilibrium the polarisation vector shrinks and/or moves back to its equilibrium position and magnitude. The bottom three images show that as individual spins in the ensemble might experience slightly different magnetic fields they precess at slightly different frequencies causing them to fan out in the rotating frame and thus the coherent behavior of the ensemble is lost and the transversal polarisation vector shrinks.

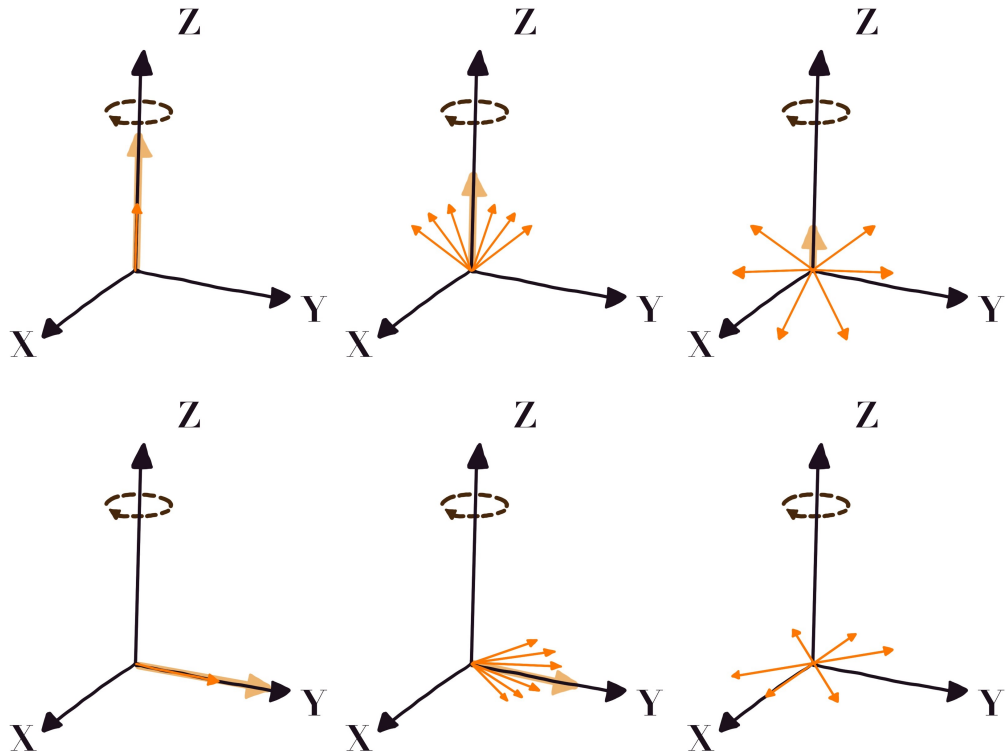


Figure 1.5 T_1 and T_2 can be depicted in the rotating frame as shrinking polarisation vectors. The thick arrow represents the ensemble polarization vector and the small arrows represent the orientation of some individual spins from the ensemble. From left to right the images depict the effect of relaxation on the individual spins as well as on of the ensemble over time. The top three figure show that starting from a non-equilibrium polarization, the amount of polarization (magnitude of the thick arrow) decreases as time progresses, and the individual spins re-orient due to longitudinal relaxation. The bottom three figures show that because not each individual spin in the ensemble constantly experiences the same magnetic field, in the rotating frame they will start to fan out (transversal relaxation). This eventually leads to 0 transversal polarization.

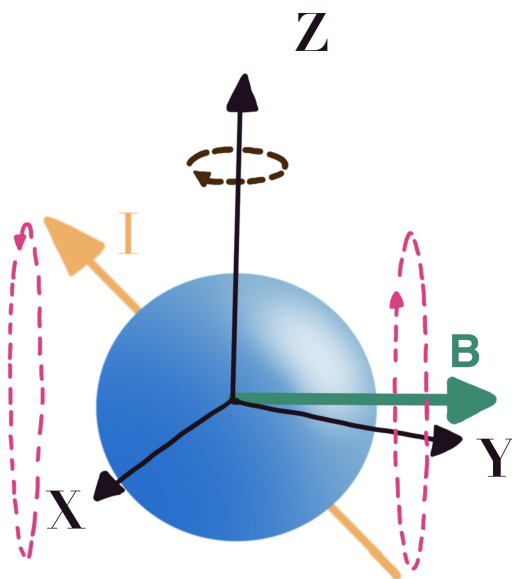


Figure 1.6 A resonantly applied rotating magnetic field B perpendicular to the quantization axis will be seen as a static field in the rotating frame, (green arrow). In the rotating frame, the spin precesses around this field (purple arrows). Due to this precession, the angular momentum vector of the spin (orange arrow) will move from one angular momentum eigenstate (i.e. the projection or magnetic substrates) to the next. In between two eigenstates, the spin will be in a superposition. This rotation between (two) different sub-states is a Rabi oscillation.

1.2.5 Resonant field

One last thing is to show how a magnetic field rotating at the same frequency as the rotating frame, applied at an angle to the quantization axis would look like in this reference frame. Please note that as the spin is not precessing in the rotating frame, the magnitude of the static magnetic field along the quantization axis reduces to 0 within this reference frame. The aforementioned rotating magnetic field, however, would appear static in the rotating reference frame. The direction of its projection on the x-y plane is determined by the phase difference between the rotating reference frame and the applied rotating magnetic field. The spin will now start to precess within the rotating frame around this field, making the spin shift between orientation states and effectively perform Rabi oscillations, as shown in figure 1.6.

Detecting this resonance condition, or the frequency at which one starts to drive the Rabi oscillation will enable the measurement of the Larmor frequency. In Continuous Wave (CW)-NMR and CW-EPR this is identified by an increased absorption of the applied rotating field. In pulse-NMR and EPR and with the Qubit gate operations in Quantum Computing and Communication, the applied field is turned on (pulsed) for only a very short time, allowing for a controlled rotation of the polarisation vector. With pulse-NMR and -EPR one measures the field induced by the precessing magnetization after such a pulse. In β -NMR and μ SR the resonance condition is observed by a decrease in β -decay asymmetry.

1.3 β -NMR

Anisotropically emitted radiation from ensembles of oriented nuclei have become a staple technique in the toolbox of nuclear physicists. The profile of the anisotropic distribution can be used to determine the spin and parity of either the decaying nucleus or its product. When coupled with other techniques it can be used as a very sensitive means of measuring the HyperFine Structure (HFS) in radioactive atoms and ions, or detecting NMR resonances.

In the following subsections the decay profile measured during a β -NMR measurement will be described.

1.3.1 Simple radioactive decay

Given a pure isotopic ensemble of radioactive nuclei the number of remaining nuclei after a time period t can be found by solving the following first order differential equation that describes the expected change in the number of nuclei dependent on the amount of nuclei present.

$$-\frac{dN}{dt} = \lambda N, \quad (1.10)$$

where N is the number of radioactive nuclei, t the time and λ the decay constant, which is correlated with the half-life ($t_{1/2}$) as $\lambda = \frac{\ln(2)}{t_{1/2}}$.

The solution describes the amount of expected nuclei left after the passage of an amount of time t dependent on N_0 the number of nuclei present at time $t = 0$.

$$N(t) = N_0 e^{-t \frac{\ln(2)}{t_{1/2}}} \quad (1.11)$$

1.3.2 Beta particle emission in all space

Assuming a uniform spherical distribution the radiation resulting from this decay will be evenly emitted in all directions. The amount of radiation emitted in a time window dt is equal to the change in the number radioactive nuclei in the sample within dt . Thus $N_{\beta}^{dt}(T) = N(T) - N(T + dt)$. Differentiating equation 1.11 for $N(t)$ gives:

$$\frac{dN}{dt} = -\frac{\ln(2)}{t_{1/2}} N_0 e^{-t \frac{\ln(2)}{t_{1/2}}} \quad (1.12)$$

Because of the geometry of the experimental setup the detectors typically will not cover all directions from the source. Therefore, the number of beta particles detected will be modified by the solid angle Ω that the detectors cover, as well as the efficiency ϵ_{det} of these detectors. This will modify equation 1.12 as follows:

$$\frac{dN}{dt} = -\Omega \epsilon_{det} \frac{\ln(2)}{t_{1/2}} N_0 e^{-t \frac{\ln(2)}{t_{1/2}}} \quad (1.13)$$

1.3.3 Emission asymmetry

For a spin-polarized ensemble, due to the parity non-conservation of the weak interaction governing beta-decay, the emission of beta particles is not equal in all directions as first observed by Wu et. al. [22]. The anisotropy that can be observed can be described by the angular distribution formula which in its well-known form is given by:

$$W(\theta) = 1 + a \frac{v}{c} P_I^0 \cos(\theta), \quad (1.14)$$

where θ is the angle between the orientation axis of the polarized ensemble and the direction of emission, v is the velocity of the emitted beta particle, c is the speed of light in vacuum, P_I^0 is the nuclear spin polarization as given by equation 1.7, and a the asymmetry factor which is dependent on the difference of the nuclear spin ΔI between initial and final state. The values of the a parameter for $\Delta I = -1, 0$ or 1 are given in table ??.

Table 1.1 The Spin change dependent value of the Asymmetry factor a .

Asymmetry factor	Spin change
-1	$\Delta I = -1$
$I_i/(I_i + 1)$	$\Delta I = +1$
$-1/(I_i + 1)$	$\Delta I = 0$ (Gamow-Teller transition)
0	$\Delta I = 0$ (Fermi transition)

Since the asymmetry factor depends on the beta decay branch, a total asymmetry factor for a given isotope can be defined as $a_{iso} = \sum_d a_d br_c^v$ in which a_d is the asymmetry factor for the given decay branch and br its probability (branching ratio).

Replacing the fixed solid angle Ω from the radioactive decay with the above angular distribution, one obtains the following formula for the number of beta particles emitted over time dt at an angle θ :

$$\frac{\partial N(t, \theta)}{\partial t} = -\epsilon_{det} \frac{\ln(2)}{t_{1/2}} N_0 e^{-t \frac{\ln(2)}{t_{1/2}}} [1 + a_{iso} P_I \cos(\theta)] \quad (1.15)$$

1.3.4 Relaxed Asymmetry

The spin polarization of a nuclear ensemble in an environment will eventually relax back to thermal equilibrium in the following way:

$$P_I(t) = P_0 \sum_n b_n e^{-\frac{t}{T_{1n}}} \quad (1.16)$$

Here, P_0 is the initial polarization, b_n the fraction of nuclei experiencing a specific chemical environment with $b_n > 0$ and $\sum_n b_n = 1$ and T_{1n} the longitudinal relaxation constant belonging to environment n . This gives the following equation that has to be integrated from T to $T + dt$ to determine the amount of beta radiation emitted during a time window dt after time T .

$$\frac{\partial N(t, \theta)}{\partial t} = -\epsilon_{det} \frac{\ln(2)}{t_{1/2}} N_0 e^{-t \frac{\ln(2)}{t_{1/2}}} \left[1 + a_{iso} \cos(\theta) P_0 \sum_n b_n e^{-\frac{t}{T_{1n}}} \right] \quad (1.17)$$

Integrating this formula from time T to $T + dt$ and over the solid angle of the detectors gives the following formula for the expected amount of beta's seen by

a detector in a time window dt after time T :

$$\begin{aligned}
 N_{\beta}^{dt}(T) &= \int_T^{T+dt} \int_0^{2\pi} \int_{\alpha}^{\beta} -dN(t, \theta) d\theta d\phi dt \\
 &= \int_T^{T+dt} \int_0^{2\pi} \int_{\alpha}^{\beta} \epsilon_{det} \frac{\ln(2)}{t_{1/2}} N_0 e^{-t \frac{\ln(2)}{t_{1/2}}} \left[1 + a_{iso} \cos(\theta) P_0 \sum_n b_n e^{-\frac{t}{T_1 n}} \right] d\theta d\phi dt,
 \end{aligned} \tag{1.18}$$

with α and β the opening and closing angles of the detector respective to the axis of orientation (with $0 \leq \alpha, \beta \leq \pi$). When ϵ_{det} and $n = 1$, $v \approx c$, $\alpha = 0$, and $\beta = \pi/12$, the equation reduces to:

$$N_{\beta}^{dt}(T) = \int_T^{T+dt} \int_0^{2\pi} \int_0^{\pi/12} \frac{\ln(2)}{t_{1/2}} N_0 e^{-t \frac{\ln(2)}{t_{1/2}}} \left[1 + a_{iso} \cos(\theta) P_0 e^{-\frac{t}{T_1}} \right] d\theta d\phi dt \tag{1.19}$$

or

$$N_{\beta}^{dt}(T) = \frac{\ln(2)}{t_{1/2}} N_0 \int_0^{2\pi} d\phi \int_T^{T+dt} \int_0^{\pi/12} e^{-t \frac{\ln(2)}{t_{1/2}}} + a_{iso} P_0 e^{-t \left(\frac{1}{T_1} + \frac{\ln(2)}{t_{1/2}} \right)} \cos(\theta) d\theta dt \tag{1.20}$$

Solving the integrals gives:

$$\begin{aligned}
 N_{\beta}^{dt}(T) &= \frac{\ln(2)}{t_{1/2}} N_0 [\phi]_0^{2\pi} \left\{ \int_T^{T+dt} \int_0^{\pi/12} e^{-t \frac{\ln(2)}{t_{1/2}}} d\theta dt \right. \\
 &\quad \left. + \int_T^{T+dt} \int_0^{\pi/12} a_{iso} P_0 e^{-t \left(\frac{1}{T_1} + \frac{\ln(2)}{t_{1/2}} \right)} \cos(\theta) d\theta dt \right\} \\
 &= \frac{\ln(2)}{t_{1/2}} N_0 2\pi \left\{ \int_0^{\pi/12} d\theta \int_T^{T+dt} e^{-t \frac{\ln(2)}{t_{1/2}}} dt \right. \\
 &\quad \left. + a_{iso} P_0 \int_0^{\pi/12} \cos(\theta) d\theta \int_T^{T+dt} e^{-t \left(\frac{1}{T_1} + \frac{\ln(2)}{t_{1/2}} \right)} dt \right\} \tag{1.21} \\
 &= \frac{\ln(2)}{t_{1/2}} N_0 2\pi \left\{ [\theta]_0^{\pi/12} \left[-\frac{t_{1/2}}{\ln(2)} e^{-t \frac{\ln(2)}{t_{1/2}}} \right]_T^{T+dt} \right. \\
 &\quad \left. + a_{iso} P_0 [\sin(\theta)]_0^{\pi/12} \left[-\frac{1}{\frac{1}{T_1} + \frac{\ln(2)}{t_{1/2}}} e^{-t \left(\frac{1}{T_1} + \frac{\ln(2)}{t_{1/2}} \right)} \right]_T^{T+dt} \right\}
 \end{aligned}$$

$$\begin{aligned}
 &= \frac{\ln(2)}{t_{1/2}} N_0 2\pi \left\{ -\frac{\pi}{12} \frac{t_{1/2}}{\ln(2)} \left[e^{-t \frac{\ln(2)}{t_{1/2}}} \right]_T^{T+dt} \right. \\
 &\quad \left. - a_{iso} P_0 \frac{-1 + \sqrt{3}}{2\sqrt{2}} \frac{1}{\frac{1}{T_1} + \frac{\ln(2)}{t_{1/2}}} \left[e^{-t \left(\frac{1}{T_1} + \frac{\ln(2)}{t_{1/2}} \right)} \right]_T^{T+dt} \right\} \\
 &= -2\pi N_0 \left\{ \frac{\pi}{12} e^{-T \frac{\ln(2)}{t_{1/2}}} \left(e^{-dt \frac{\ln(2)}{t_{1/2}}} - 1 \right) \right. \\
 &\quad \left. + a_{iso} P_0 \frac{-1 + \sqrt{3}}{2\sqrt{2}} \frac{T_1 \ln(2)}{t_{1/2} + T_1 \ln(2)} e^{-T \left(\frac{1}{T_1} + \frac{\ln(2)}{t_{1/2}} \right)} \left(e^{-dt \left(\frac{1}{T_1} + \frac{\ln(2)}{t_{1/2}} \right)} - 1 \right) \right\}
 \end{aligned}$$

Notice that when $dt = 0$, then $N_\beta^{dt}(T) = 0$ because in a time window of size 0, no β particles can be physically detected. Following these same steps the general equation will be:

$$\begin{aligned}
 N_\beta^{dt}(T) = & -2\pi \epsilon_{det} N_0 \left\{ (\beta - \alpha) e^{-T \frac{\ln(2)}{t_{1/2}}} \left(e^{-dt \frac{\ln(2)}{t_{1/2}}} - 1 \right) + a_{iso} P_0 (\sin(\beta) - \sin(\alpha)) \right. \\
 & \left. \sum_n b_n \frac{\ln(2) T_{1n}}{t_{1/2} + \ln(2) T_{1n}} e^{-T \left(\frac{1}{T_{1n}} + \frac{\ln(2)}{t_{1/2}} \right)} \left(e^{-dT \left(\frac{1}{T_{1n}} + \frac{\ln(2)}{t_{1/2}} \right)} - 1 \right) \right\} \quad (1.22)
 \end{aligned}$$

1.3.5 Experimental Asymmetry

Equation 1.22 can be used to compute the expected amount of radiation counted by one of the detectors used in a β -NMR experiment. However, because the asymmetry is usually in the per-cent range, during an experiment, it is difficult to see the effect of the asymmetry by looking at absolute counts registered in each detector. When one takes the normalized difference of the radiation counts of two detectors positioned on opposing sides of the quantization axis, the effect of radioactive decay on the number of counts cancels out and only the β -decay asymmetry is left. This normalized difference, known as the Experimental Asymmetry A_{Exp} , is given by equation 1.23.

$$A_{exp} = N_{DetA} - N_{DetB} / N_{DetA} + N_{DetB}, \quad (1.23)$$

with N_{DetA} and N_{DetB} being the counts measured in detector "A" and "B", respectively. If an ensemble of beta-emitting nuclei is polarized, an asymmetry

will be observed due to the angular distribution. The moment an ensemble has a non-equilibrium polarization the spins start to relax back to thermal equilibrium due to interactions with the environment and the polarization starts to decrease. This can be observed by a change in the Experimental Asymmetry. The relaxation curve can be fitted to determine the longitudinal relaxation time constant T_1 .

1.3.6 Resonance detection

If a magnetic field B_1 perpendicular to the static magnetic field B_0 and rotating at the resonance frequency is applied for a relatively long time to the sample during the implantation and observation time, the ensemble of spins will start to perform Rabi oscillations. Because the angular distribution is defined in reference to the polarization vector of the spins, this distribution will follow the Rabi oscillations, effectively averaging out the experimental asymmetry. Thus, to measure the resonance frequency the polarization, implantation, and relaxation observation steps are repeated while applying B_1 with different frequencies. When the observation window is chosen to be in the order of T_1 and the integrated asymmetry is plotted against the frequency of B_1 a change in asymmetry can be observed around the resonance frequency.

1.4 Optical Pumping

The amount of equilibrium polarization produced by the Boltzmann distribution at room temperature in a 1 T field is generally on the order of parts-per-million (ppm). To increase the amount of polarization of the ensemble upon implantation the laser optical pumping method is used. Here, the atoms are allowed to interact repeatedly with resonant circularly polarized light. This will excite the atom while transferring angular momentum to it. Fig. 1.7 shows this process on the example of a ^{26}Na atom. Following the selection rules, this excitation also shifts the atom into a magnetic substate with a higher (or lower) m_F quantum number. Upon de-excitation, following the selection rules the m_F quantum number can only change by $-1, 0$ or 1 . Repeated excitation and de-excitation cycles will eventually transfer all (or most) of the atoms to the magnetic substate

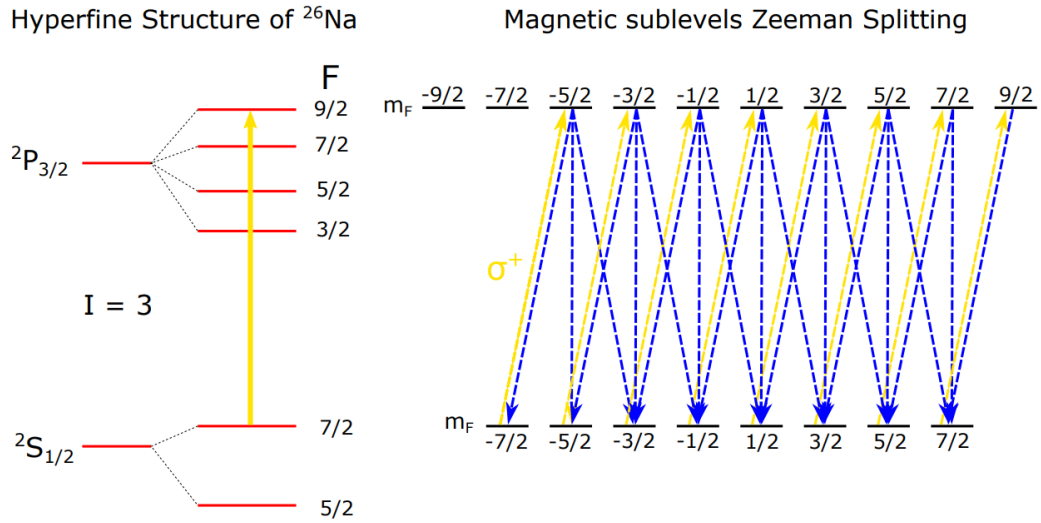


Figure 1.7 The hyperfine structure of the D2 line of ^{26}Na is shown on the left. On the right, the magnetic m_F substates of the $F = 7/2$ $^2\text{S}_{1/2}$ ground state and the $F = 9/2$ $^2\text{P}_{3/2}$ excited state are shown. The yellow arrows indicate excitation with circularly σ^+ polarized light. The blue lines indicate the decay back to the ground stage. Repeated cycles of excitation and de-excitation will move (most off) the atomic population into the $m_F = 7/2$ $^2\text{S}_{1/2}$ ground state leading to atomic polarization. Figure from [23]

with the highest or lowest m_F quantum number, leading to atomic polarization.

As the magnetic field is increased the splitting of the magnetic substates due to the Zeeman effect increases. At a certain point this stops being linear and even later the coupling between the nuclear spin I and the electron spin J breaks. From that magnetic field strength onward the atomic magnetic substate can no longer be described by the m_F quantum number but only by the combination of the nuclear m_I and electron m_J spin magnetic substates. The breaking of the coupling between the nuclear and electron spin at high magnetic fields is called the Paschen-Back effect. The splitting and re-arranging of selected magnetic substrates of ^{26}Na is shown in figure 1.8.

After a controlled transition from a low magnetic field area where optical pumping was achieved, to a high magnetic field area, the ensemble will be left with nuclear polarization.

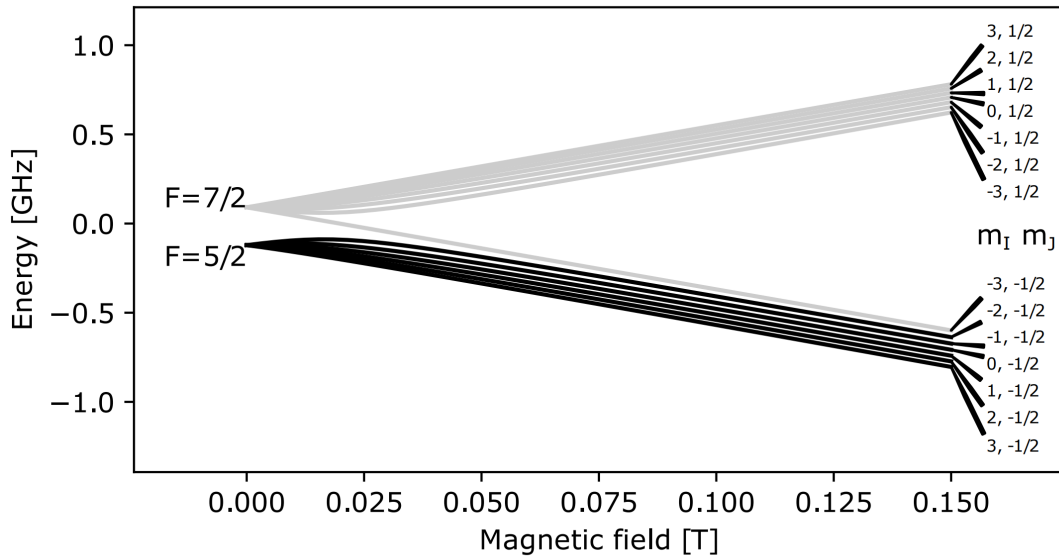


Figure 1.8 The splitting and reordering of some of the magnetic sub-states of ^{26}Na showing the Paschen-Back effect. Figure from [23]

1.5 Applications

Equations 1.4 and 1.5 give a direct relation between the Larmor frequency, the magnetic dipole moment, and the magnetic field. When one of these is known a measurement of the second allows a determination of the third. For example, in a known magnetic field, a measurement of the Larmor frequency gives the magnetic dipole moment of a particle with spin greater than zero. This is of keen interest in the realm of nuclear (structure) physics, where the measurement of the ground-state electromagnetic moments is a vital tool to learn more about the shape and structure of the nucleus. This includes the distribution of electric charge as well as magnetization within the nucleus. The reverse measurement also holds where a particle with a known magnetic dipole moment can be used as a local magnetometer by measuring its Larmor frequency. The use of spins as local magnetometers leads to many interesting applications. Within the field of NMR spectroscopy, for example, the minute shielding effect the neighboring electrons have on the magnetic field experienced by the nuclei causes small shifts in the measured Larmor frequency. The available electrons and their orbits depend to some extent on the chemical bonds between the atoms, thus this shift

in the Larmor frequency is known as the chemical shift σ . The chemical shift can be used to identify molecules and, when the effect of different interactions is taken into account, can be used to elucidate the chemical structure. As another example, β -NMR measurements have been used routinely to determine the internal magnetic fields of solid-state samples as a function of temperature and applied external magnetic field [24]. An interesting test case for applying this technique to non-solid state samples would be the interaction between a bio-molecule and an (implanted) atom/ion. An example of such a molecule is a Guanine Quadruplex (GQ).

1.5.1 Guanine Quadruplexes

The DNA molecules play a central role in molecular biology, and thus life in general. They fulfill the role of the long-term storage of genetic information. Within DNA, the blueprints (genes) for the proteins that life depends on, are encoded via four nucleobases: adenine (A), cytosine (C), guanine (G), and thymine (T). The genes encoded in DNA are preserved, accessed, copied, and used through the protein machinery involved in duplication, transcription, and translation. Due to hydrogen bonding, the nucleobases pair up. The most common type of base-pairing called the "Watson–Crick–Franklin" base-pairing leads to the familiar double helical structure of DNA. Another type of base-pairing, "Hoogsteen" base-pairing, allows for other DNA structures. One of the DNA structures in which "Hoogsteen" base pairing is observed is the GQ. GQs are observed in nucleic acid regions that are rich in guanine. This is the case in the transcriptional regulatory regions of several genes and in the repeat sequence section at the ends of chromosomes (the telomeric regions). At these places GQs are involved in several processes that have been identified to contribute to aging [25], gene regulation [26], and oxidative damage compensation [27]. For these reasons alone the study of GQs is of high interest. Outside of living systems GQs have been used as catalysts for chemical reactions [28] and in therapeutics [29].

A GQ is formed by the stacking of Guanine tetrads, squares of planar G bases formed through Hoogsteen bonding. These stacks are stabilized by the presence of an alkali metal cation (e.g. sodium or potassium) in the central channel in between the tetrads as seen in figure 1.9.

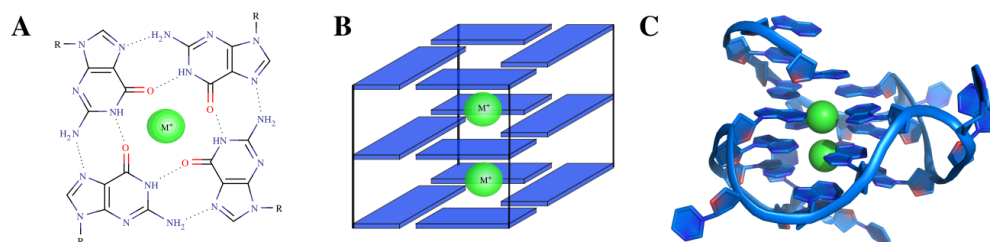


Figure 1.9 The G-Quadruplex structure: **A** Guanine bases coordinated in a tetrad around a central monovalent cation. **B** Schematic structure of G4 with metal ions located in-between tetrads coordinating the partial charges of 8 oxygen-groups. **C** 3-dimensional structure of a G4 (pdb: 1XAV) [30]. Figure and caption from [2]

The alkali metal ions in the GQ have an influence on its stability, structure, and dynamics. A better understanding of the interactions of the alkali metal ion with the GQ could help to better comprehend its influence and could help with better understanding the folding landscape. However, NMR on stable Na and K is very difficult due to the large electric quadrupole moments of stable ^{23}Na and $^{39,41}\text{K}$, which lead to broad resonance peaks.

As β -NMR uses unstable isotopes, an isotope with a smaller electric quadrupole could be selected for these studies. And because β -NMR is an implantation-based technique it lends itself exceptionally well for fast titration (like) experiments.

1.5.2 Hyperfine anomaly

The magnetic hyperfine interaction is the interaction between the nucleus and (its atomic) electrons that happens because the electrons and the nucleus have a spin. It gives rise to a splitting in the atomic energy levels known as the hyperfine splitting (HFS), which is proportional to the nuclear magnetic moment. The hyperfine anomaly is a small correction needed in the derivation of the value of the nuclear magnetic moment from HFS. It appears because the HFS formula includes an approximation that the nucleus is a point-like particle. However, nuclei have an extended distribution of charge and magnetisation inside them. The extended magnetisation gives rise to the magnetic hyperfine anomaly, or the so called Bohr-Weisskopf effect [31]. This correction is at the level of a per-

cent or less. To derive it one needs to compare the independently determined nuclear magnetic moment (e.g through (β -)NMR) with a magnetic moment for a (hypothetical) point-like nucleus derived from HFS data. To determine it with high-enough precision both the Magnetic moment and the HFS need to be measured with high enough accuracy.

The size of the hyperfine anomaly, or size difference between two isotopes of the same element is very interesting for nuclear structure studies. Namely, the magnetisation distribution is mostly determined by the unpaired nucleon. Thus, it might give unique access to determine the distribution of valence neutrons which are otherwise much more difficult to address than protons. This can be especially interesting for halo nuclei, such as ^{11}Li or ^{11}Be , in which 1 to 2 neutrons are very far away from the core. A proposal to study ^{11}Be has been recently accepted by ISOLDE [32].

1.6 CERN

The work presented in the thesis was performed at ISOLDE, CERN's RIB facility. CERN, the European Organization for Nuclear Research, is located on the French-Swiss border near Geneva, Switzerland. It was founded in 1954, right after the Second World War, to help unite European physics research, and to set up a laboratory that provides the larger infrastructure needed for nuclear and particle physics research. CERN currently maintains and operates a series of accelerators as shown in Figure 1.10. The protons commence along this accelerator chain when H_2 gas is injected into a linear accelerator (LINAC). LINAC 4 (LINAC 2 before 2020, at the time when most of this work was done) accelerates H^- ions to an energy of 160 MeV and feeds them through a stripper foil to remove the electrons, before injecting them into the proton synchrotron booster (PSB). The PSB, with its four superimposed synchrotron rings, in turn, accelerates the created proton bunch to 1.4 GeV and sends it with an average intensity of 2.1 μA to ISOLDE. The proton bunches arrive at ISOLDE at intervals which are an integer multiple of 1.2 s [34]. Because the PSB has to provide proton bunches to all subsequent accelerators in the chain, the operators arrange the proton bunches in a sequence dependent on their final destination. This sequence is called the super-cycle. There is no fixed length of the super-cycle [35],

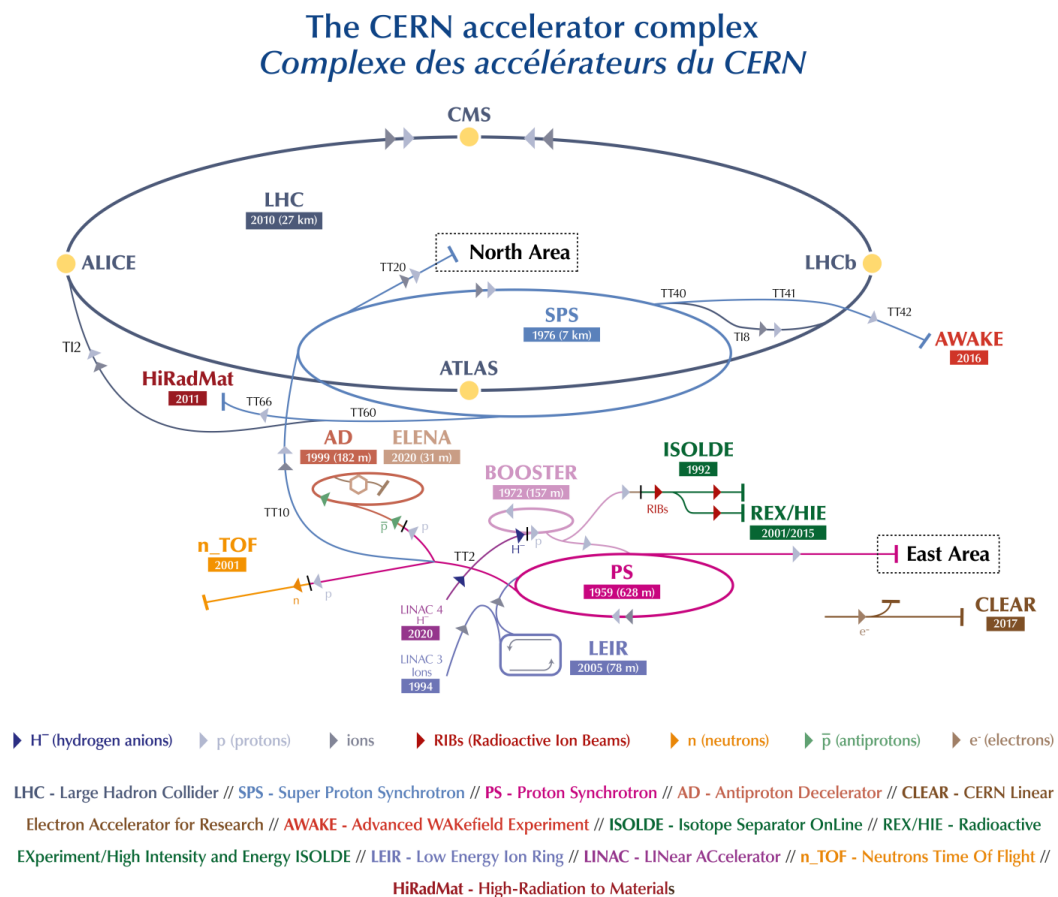


Figure 1.10 A schematic representation of CERN's accelerator complex showing the different accelerators, facilities, and experiments. The dark purple line in the bottom center represents linear accelerator (LINAC) 4, which feeds the proton synchrotron booster (PSB), shown in pink. This is the start of all the accelerated protons at CERN. From the PSB the protons are delivered to ISOLDE, shown in green, with an energy of 1.4 GeV[33]

but it usually consists of around 20-40 cycles. ISOLDE generally receives more than 50 % of all the protons accelerated by the PSB [36], [37].

1.7 ISOLDE

ISOLDE (Isotope Separator OnLine DEvice) is CERN's oldest still running facility. The first experiments were performed in 1967 when ISOLDE was still connected to CERN's first accelerator, the 600 MeV Synchro-Cyclotron (SC) [34]. In the more than fifty years since then, ISOLDE has seen multiple major upgrades, numbered II to IV. These upgrades allowed the facility to make use of more intense beams from the SC (II), have an increased mass resolving power by use of an additional separator with higher resolution(III) [38], and move to its current location at the PSB in 1992 (IV)[39]. Even though ISOLDE is still thought of as being at version IV, it has seen several extensions and improvements to the building and the equipment since then. Additional laboratories, more space in the experimental hall, a normal conducting LINAC, a superconducting LINAC[40] and a Radio Frequency Quadrupole (RFQ) cooler-buncher have been added over the years. Several plans have been and are being made for even further additions to the facility to be able to cater to the ever-increasing demands of beam time at ISOLDE[41], [42]. Currently, as part of the EPIC (Exploiting the Potential of ISOLDE at CERN) project, it is also planned to take advantage of the recent increase in energy and intensity of the PSB beams[42]. So far, ISOLDE has delivered beams of 1300 different isotopes from 73 chemical elements to the experimental setups[43]. The current layout of the Low-Energy side of the ISOLDE Experimental hall is shown in figure 1.11.

1.7.1 Production and separation

At ISOLDE, the proton bunch coming from the PSB impinges on a thick target of material usually containing elements with a high mass number (A). Figure 1.12 shows a 3D CAD model of a typical ISOLDE target unit. One of the most commonly used target materials at ISOLDE (>60 %) is Uranium Carbide (UC_x). The target material is contained in a Tantalum tube of 20 cm in length with a radius of 1 cm. The high-energy proton beam induces spallation, frag-

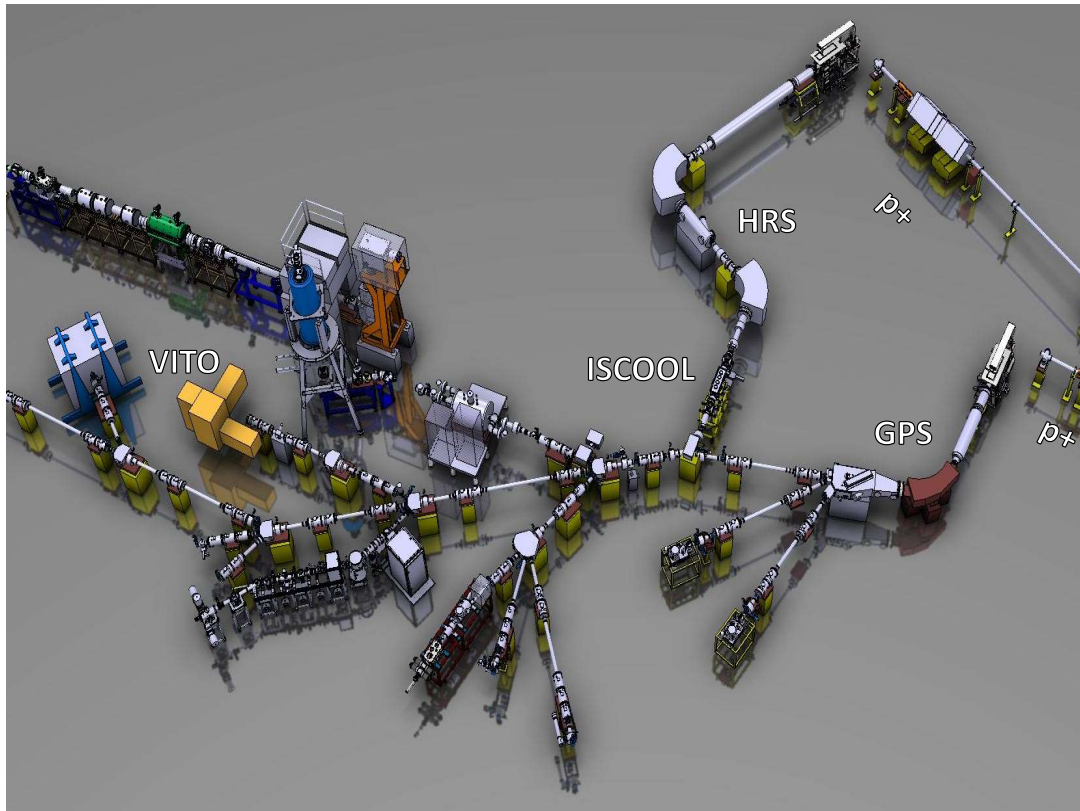


Figure 1.11 An overview of the ISOLDE Low-Energy Experimental Hall. The proton lines coming from the proton synchrotron booster are indicated with p^+ . The General Purpose and High-Resolution Separators, indicated with GPS and HRS respectively, each have their own Front Ends and target stations. The HRS is followed by ISCOOL, the ISOLDE Radio Frequency Quadrupole Cooler-Buncher. From there, both separators feed into the merging switch-yard which allows for the radioactive ion beams to be guided into the central beamline and onwards to the different experiments. The Versatile Ion-polarized Techniques On-line (VITO) beamline, which includes the polarization beamline and β -NMR setup, is located at the center of the experimental hall[44].

mentation, and fission reactions in this irradiated material, creating a plethora of different isotopes. Alternatively, the proton bunch impinges on a tungsten rod, located next to the target material, to create spallation neutrons. The target material is then irradiated by these neutron-inducing fission reactions[45]–[48]. The produced isotopes are stopped in the target material and need to diffuse to the surface and evaporate in order to be extracted. To increase the diffusion and evaporation rate, the target container is usually heated to around 2200 K by applying a current of about 800 A. To further increase the diffusion rate, there have been ongoing efforts to reduce the grain size of the target material. An example of this is the nano-UC_x target[48]. The trade-off for using ever smaller grain sizes is that the maximum heating temperature of the target is limited by the sintering temperature, which decreases with smaller grain sizes. Notwithstanding the lower maximum temperature, the decreased grain size has led to an increased yield. Once the isotopes are out of the target material, they effuse out of the target container into the transfer line. This line can be heated or cooled, which allows for coarse means of chemical selection. Next, the isotopes are ionized by one of the three available techniques: plasma ionization, resonant laser ionization, and surface ionization. Due to their small ionization potential, caused by the single electron in their outer shell, alkali metals are readily surface ionized. For example, sodium has an ionization potential of only 5.139 076(2) eV[49]. The surface ion source consists of a 3 cm long hot tungsten cavity which is heated to 2000-2600 K. Within 2 ms after the proton bunch arrives at the target, an electric potential of 30-60 kV is applied to the target unit [50]. The extraction electrode (shown in figure 1.12) is kept at ground potential and this potential difference supplies the electric field which accelerates the isotopes once they are ionized. The typical ISOLDE yield for ²⁶Na is around 5×10^7 ions/ μ C[4].

A target unit is used for one to two weeks and is highly radioactive after use. Thus, a pair of industrial robots handle the target changes. The ISOLDE front-end (see figure 1.13) is therefore designed in such a way that the target units can be easily taken off. The front ends furthermore supply all connections needed by the target e.g. vacuum, current, cooling, gas-inlet, acceleration potential, etc. It also houses the extraction electrode. Next, the now accelerated ion beam arrives at one of two mass separators. Depending on which target station is used, this

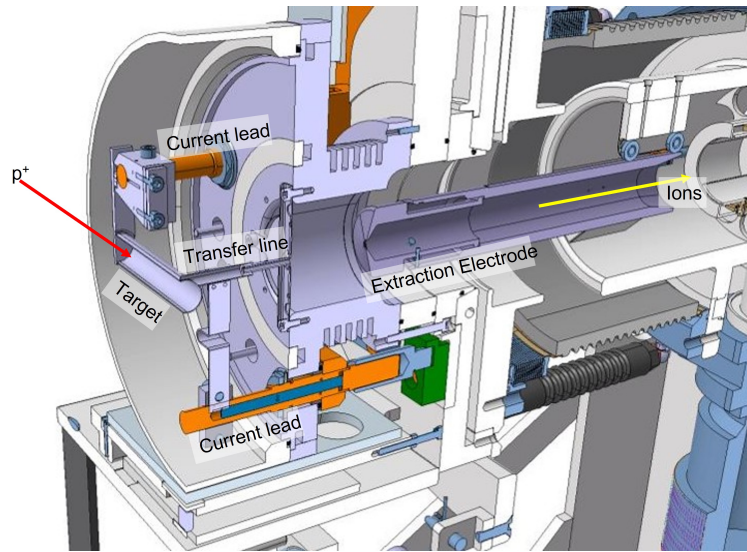


Figure 1.12 A cut-through of a 3D CAD Model of an ISOLDE target unit. Indicated are the tantalum target tube (20 cm), transfer line, extraction electrode, current leads used to heat the target by applying up to 1000 A, the direction of the incoming proton beam, and the direction of the outgoing ion beam consisting of a mixture of the produced isotopes. CAD Image courtesy of M. Delonca

is either the General Purpose Separator (GPS) or the High Resolution Separator (HRS). Both are essentially magneto-static mass-spectrometers spatially separating the incoming beam based on the mass-over-charge (m/q), by use of the Lorentz force. The GPS has an H-magnet type with a bending radius of 1.5 m and a bending angle of 70° . Its resolution $m/\Delta m$ is approximately 800 [50]. Two pairs of movable electrostatic plates are located inside the vacuum chamber between the magnet poles. These plates allow for the deflection of parts of the separating ion beam into two different beamlines. The m/q of the beam that is guided in these beamlines is up to 15% higher or lower compared to that of the beam transported into the central beamline. The lower mass fraction is sent to the General Low Mass (GLM) beamline and the higher mass fraction to the General High Mass (GHM) beamline [23]. The HRS has a 90° and a 60° C-magnet type magnet, with a bending radius of 1 m. The combined resolution of the HRS magnets has been measured to go up to 6000 [50], which is for a very large part determined by the emittance and vertical size of the beam entering the HRS. Due to the limited space in the ISOLDE hall and due to the con-

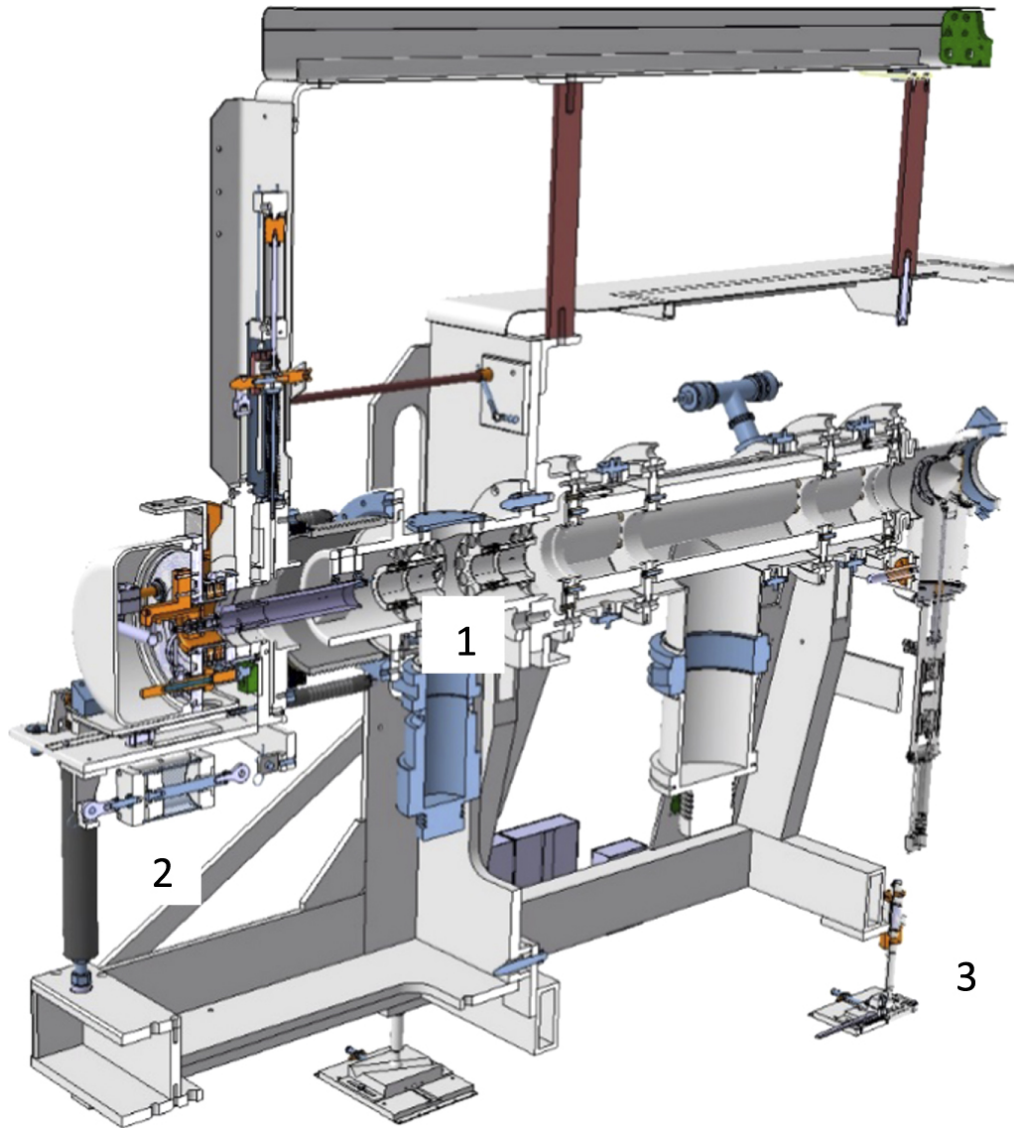


Figure 1.13 A cross-section view of the ISOLDE Frontend showing 1. The X–Y deflector plates 2. The modified piston for target coupling and 3. The tripod support system. Image and caption from [50].

figuration of the beamlines, the RFQ-Cooler-Buncher could only be positioned behind the HRS [50]. It is known as ISCOOL. It allows for the cooling and bunching of the ion beam. Cooling the beam is achieved by thermal collisions with a low density (0.1 mbar) He gas. The rest of the beamlines operate at high vacuum. To maintain a constant pressure of 0.1 mbar within ISCOOL, without destroying the vacuum in other parts of ISOLDE, a cooled gas is continuously leaked into its vacuum chamber. At the same time, a series of apertures on its entrance and exit makes it possible to apply differential pumping. To prevent the scattering of the ions, the RFQ is used as a linear Paul trap, constricting the beam to its central axis [51]. The bunching is done by creating a potential well by applying a gradually decreasing and then a sharply increasing potential on the RFQ's electrodes. The ions get trapped in this potential well, effectively bunching the beam. By pulsing the potential on the final electrodes, the ion bunch can be released towards the rest of ISOLDE. Up to 1×10^7 ions can be contained in ISCOOL, this is limited due to space charge effects[51]. The transmission efficiency lies between 50-80 %, depending heavily on the emittance of the incoming beam, as well as on the mass of the selected isotope [50]. After ISCOOL or after the GPS the beam arrives at the merging switchyard which allows either the beam from the GPS or the HRS to be sent down the central beamline. For the measurement of the longitudinal relaxation, it is beneficial for all nuclei to be implanted at the "same" time (within a very narrow time window). For this reason, the HRS separator was used for all the experiments described in this thesis, as it allowed to bunch the beam for the measurements of the longitudinal relaxation using β -NMR.

1.8 Versatile Ion-polarized Techniques On-line

The central beamline is divided up into four sections (CA0, CB0, CC0 and CD0). In between these sections there are kicker-bender type switchyards which allow the beam to travel to the different branches of the ISOLDE beamline. Versatile Ion-polarized Techniques On-line (VITO)[52] is located at the RB0 beamline, this means that it is the right branch of the beamline after the second section of the central beamline (CB0). An extensive description of the different parts of the VITO beamline is given in references [23], [53]–[55]. For completeness, an

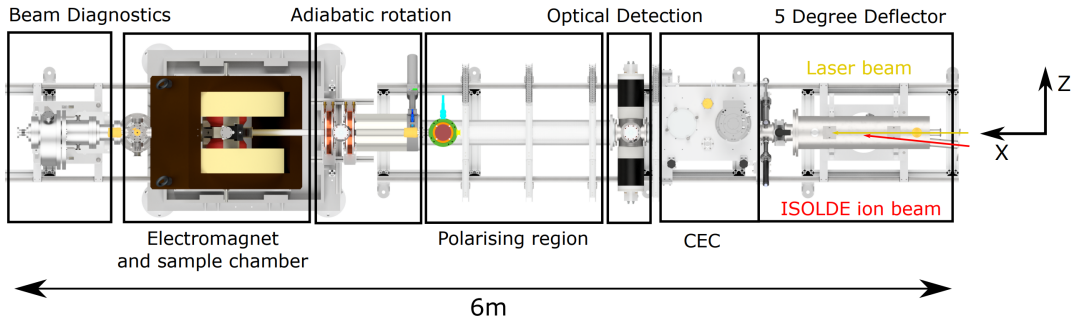


Figure 1.14 Top view of the VITO beamline. The axes indicate the magnetic field directions referenced in this section. The ion and laser beams enter from the right and are overlapped in the 5° Deflector. The ions are Doppler tuned and neutralized in the Charge Exchange Chamber (CEC). The optical detection section allows for the detection of fluorescent photons coming from the atom beam. The polarising region lets the laser light and atom beam interact repeatedly resulting in an atomic spin polarised ensemble. The Adiabatic rotation section causes the spin polarisation to rotate from the X-direction toward the Z-direction. Next, the electronic and nuclear spins are decoupled in the fringe field of the magnet resulting in a nuclear spin polarized ensemble which is implanted on the sample in the sample chamber housed between the poles of the electromagnet. At the end of the beamline (left side) some beam diagnostics including a Faraday cup are located [23].

overview will be given here as well. Once the ion beam enters RB0, it first passes through a Quadrupole Doublet which allows to steer and to focus the beam. The size of the final beamspace and the quality of the laser and ion beam overlap later on in the setup is for a significant part determined by this Quadrupole.

1.8.1 Ion/laser beam overlap

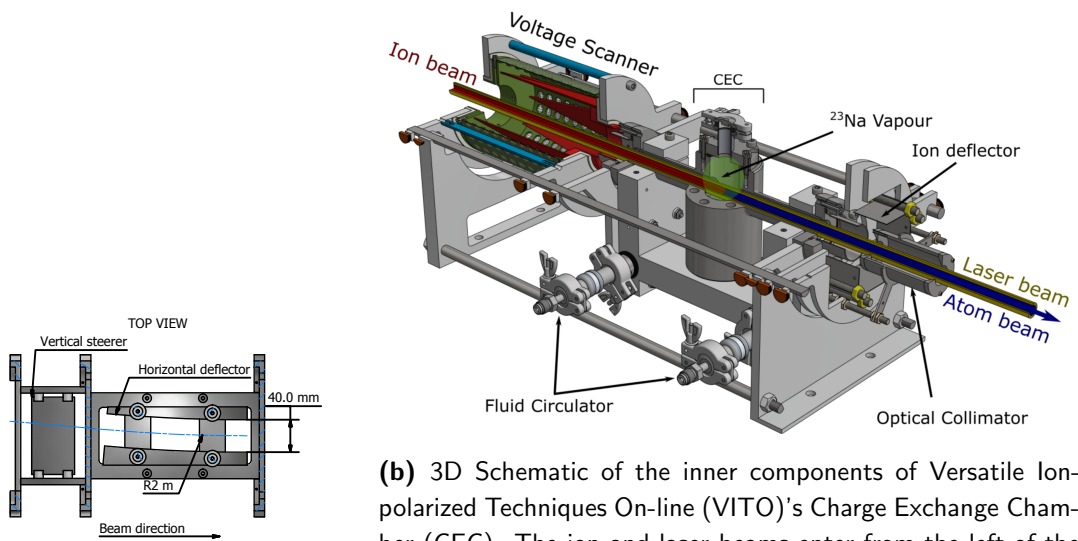
After the quadrupole, the beam passes through the 5° -deflector (see figure 1.15a). The deflector bends the ion beam by 5° with a radius of 2 m, which allows the ion beam to be overlapped with a laser beam. A top view of the VITO beamline from the 5° -deflector onward is given in figure 1.14. The 5° -deflector section ends with a gate valve. Right behind this gate valve, beam diagnostic elements are mounted on a vacuum cross. An insertable plate and an iris are used to read out the current produced by the impact of the ion beam. This gives a coarse measure of the total intensity and width of the beam.

1.8.2 Doppler tuning and neutralization

The section following the 5°-Deflector, is the Charge Exchange Chamber (CEC). The elements inside the CEC are shown in figure 1.15b. The beam first enters a voltage scanner made of a crown-shaped electrode. By applying an electrical potential of up to ± 1 kV, the beam can be de-/accelerated such that the overlapped laser light Doppler-shifts in resonance in the rest-frame of the beam. Next, the beam passes through the Charge Exchange Cell. This cell is a stainless steel cup that is kept at 230 °C by six RS Components RS-8607016 220 W heating cartridges [53]. When the cup is filled with solid Na and heated, a dense Na vapor is created within the cup. As the ion beam passes through the vapor it exchanges electrons with it and neutralizes. The neutralization efficiency of Na⁺ on Na can be up to a 100%. The arms connected to the cup are slightly slanted upwards and are cooled by a liquid-cooled heat sink to 100 °C. This is slightly above the melting point (97.8 °C) of sodium, allowing the condensed sodium to flow back into the cup. The last part of the CEC is an ion-deflector that kicks any remaining non-neutralized ions out of the beam path.

1.8.3 Optical Pumping and Spin Rotation

After the CEC, the beam enters the Optical Detection and Optical Pumping sections of the beamline. The optical detection section starts with a collimator with a pair of knife edges. The purpose of this collimator is to decrease the photon background by reducing the amount of scattered laser light that enters the optical detection region. A pair of optical lenses and Photo Multiplier Tubes (PMTs) are used for the collection of the fluorescently emitted light. The design is based on the light collection region used in the COLLAPS experiment [56]. The CEC and optical detection section, in principle, make it possible to perform collinear laser spectroscopy to determine the atomic hyperfine structure. At VITO this can be used to detect the resonant laser frequency of a reference isotope from the same chemical element by means of the fluorescence signal in order to predict the resonance position of the isotope of interest. However, for the work on sodium, this option was not needed. The optical pumping section is a 1.6 m section of vacuum pipe surrounded by a Helmholtz coils array (four coils with a diameter of 80 cm each). The Helmholtz coils provide a magnetic



(a) 2D CAD drawing of the 5° ion-deflector. The ion beam coming from ISOLDE (left) is bent 5° with a radius of 2 m to overlap the ion beam with the laser beam. [53]

(b) 3D Schematic of the inner components of Versatile Ion-polarized Techniques On-line (VITO)'s Charge Exchange Chamber (CEC). The ion and laser beams enter from the left of the diagram. The voltage scanner allows for the modulation of the ion beam energy. The Charge Exchange Cell (indicated with CEC in this figure) is filled with sodium and heated to create a sodium vapor. The arms of the cell are cooled using a liquid-cooled block, to condense the sodium traveling along the arms and allowing it to flow back into the cell. The Ion Deflector kicks any remaining non-neutralized ions out of the beam path.[23]

Figure 1.15 Internal components of the 5° Deflector and Charge Exchange Chamber of VITO beamline.

field of 2 mT, along the beam axis, which defines the spin orientation axis of the atoms. The magnitude of the field is sufficiently large to avoid the spin orientation to be impacted by stray fields from the environment. While the beam traverses this section, the atom- and laser-beam overlap is maintained and the atoms experience repeated excitation/de-excitation cycles. Through this optical pumping in the 'D2 line' of atomic sodium ($^2S_{1/2} \rightarrow ^2P_{3/2}$ transition), the ensemble of atoms is spin-polarized. The length of the optical pumping section was a compromise between achievable polarization and available space in the ISOLDE hall [53]. The typical laser power recorded at the end of the beamline is 80 mW cm^{-2} , This induces a theoretical maximum atomic spin polarisation of $\approx 60\%$ for ^{26}Na over 1.6 m [53]. The optical pumping section ends with a segmented collimator with a 1 cm diameter bore. Its four segments can be read out similarly to the plate and iris in between the 5° and CEC. These beam diagnostic elements allow the optimization of the atom- and laser-beam overlap.

Because the magnetic field supplied by the 1.2 T Bruker BE25 electromagnet is perpendicular to the beam axis, the atomic spins will need to be rotated into this reference frame. For this purpose, two solenoids and two smaller Helmholtz coils are used together with the stray field of the main magnet to generate a gradually changing field. The field produced by this combination of coils was simulated in COMSOL. The simulation results as well as the measured field can be seen in figure 1.16 [23]. As the atom beam travels through this field the spin adiabatically rotates into the direction of the magnets' field. A detailed description of this adiabatic spin rotation can be found in reference [53]. For ^{26}Na about 10% of the polarization is lost during the spin rotation. Once the magnetic field experienced by the ^{26}Na atom beam, exceeds $\approx 0.1 \text{ T}$ the electron and nuclear spin are decoupled and a purely nuclear polarisation can be observed [57]. Behind the magnet, a Faraday cup and wire scanner are located. These help with the initial tuning of the beam such that it travels through the magnet and through the sample zone.

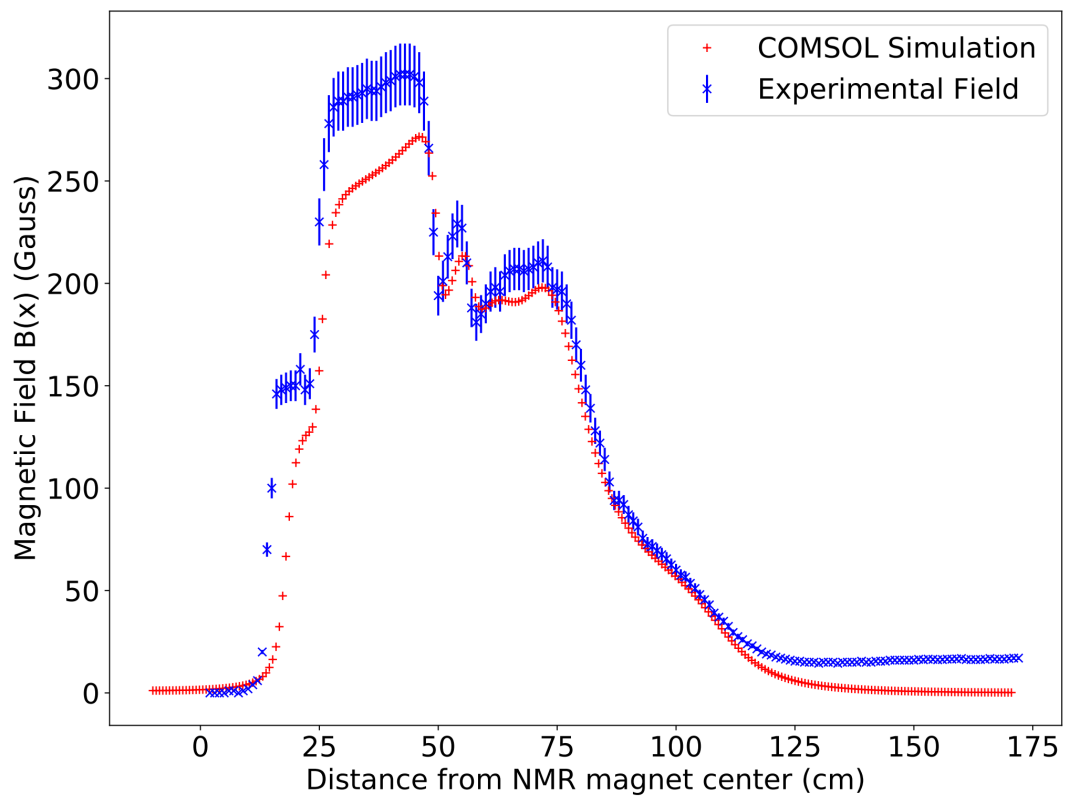
















Figure 1.16 The magnitude of the transitional field along the beam axis as a function of the distance from the crystal at the center of the magnet. The results of a COMSOL simulation are shown as red '+'s and the experimental results are shown as blue 'x's. The atom beam travels from the right to the left [23].

Chapter 2

Paper 01: High-accuracy liquid-sample β -NMR setup at ISOLDE

The following paper was published in *Nuclear Instruments and Methods in Physics Research Section A: Accelerators, Spectrometers, Detectors and Associated Equipment*. It describes in detail the remaining parts of the setup specifically focusing on the elements surrounding the experimental vacuum chamber. These components are essential for performing β -NMR measurements. They include, among others, the β -detectors, the RF-coil, and the sample holder. Instrumental to the measurements presented in chapter 3 was the shimming and locking of the magnetic field. The implementation of both systems is also presented in this chapter.

High-accuracy liquid-sample β -NMR setup at ISOLDE

J. Croese^{1,2}, *M. Baranowski*³, *M. L. Bissell*⁴,
K. M. Dziubinska-Kühn^{1,5}, *W. Gins*⁷, *R. D. Harding*^{1,8},
*R. B. Jolivet*⁹, *A. Kanellakopoulos*⁷, *B. Karg*², *K. Kulesz*^{1,2},
*M. Madurga Flores*¹¹, *G. Neyens*^{1,7}, *S. Pallada*¹, *R. Pietrzyk*³,
*M. Pomorski*¹², *P. Wagenknecht*^{1,10}, *D. Zakoucky*¹³, *M. Kowalska*¹

¹CERN, Geneva, Switzerland

²University of Geneva, Geneva, Switzerland

³Adam Mickiewicz University, Poznan, Poland

⁴University of Manchester, Manchester, United Kingdom

⁶Leipzig University, Leipzig, Germany

⁷KU Leuven, Leuven, Belgium

⁸University of York, York, United Kingdom

⁹Maastricht University, Maastricht, The Netherlands

¹⁰Oldenburg University, Oldenburg, Germany

¹¹University of Tennessee, Knoxville, USA

¹²University of Warsaw, Warsaw, Poland

¹³Nuclear Physics Institute of the Czech Academy of Sciences , Rez, Czech Re-
public

Published in Nucl. Ints. & Meth. A (1020), 2021, 165862

doi: [10.1016/j.nima.2021.165862](https://doi.org/10.1016/j.nima.2021.165862)

Abstract

Recently there has been an increased interest to apply the sensitive β -decay asymmetry detected nuclear magnetic resonance (β -NMR) technique to biological studies. A liquid-sample β -NMR setup was build at ISOLDE to allow such investigations and to use the resolution gain of liquid-state NMR in nuclear physics. As part of this setup a magnetic field locking system, a set of printed circuit board shimming coils, a sample exchange system, a set of compact β -detectors and a custom experimental vacuum chamber were developed. The main magnetic field was stabilized down to the ppm level by the locking system while allowing the direct determination of the absolute magnetic field. The homogeneity of the magnetic field was improved to ≤ 5 ppm over the sample volume by the shimming coils. Time spent on changing samples was reduced by a factor of five by the liquid sample exchange system. During experiments it was possible to continuously observe the liquid sample thanks to the custom chamber and compact β -detectors. The absolute field determination allows for a novel way to reference β -NMR measurements, removing the need for time consuming reference measurements. The improved accuracy and resolution resulting from these innovations allows the study of the distribution of nuclear magnetization and (bio)chemicals using high-accuracy liquid-sample β -NMR.

2.1 Introduction

The emission of β -radiation from an ensemble of oriented nuclei can exhibit a high degree of asymmetry. This was first observed by Wu *et al.*, with a low temperature spin-oriented sample of ^{60}Co nuclei proving that the weak force does not conserve parity[22]. Due to the magnitude of the observed asymmetry compared to other types of anisotropically emitted radiation, this effect is a promising probe for several nuclear effects[21]. In particular, it can be used as a very sensitive means of detecting nuclear magnetic resonance (NMR) signals, which can be up to ten orders of magnitude more sensitive when compared to conventional NMR on stable isotopes[3] as it allows one to measure signals from as few as 10^7 nuclei.

The β -asymmetry that is observed in β -decay asymmetry detected NMR

(β -NMR) experiments, scales linearly with the nuclear polarisation[21], i.e. the amount of first order nuclear orientation within an ensemble. Therefore, the larger the polarisation is, the better the signal to noise ratio (SNR) is. The high level of polarisation of the ensemble of nuclei is one of the reasons for the high sensitivity of the technique, the other being the detection by β -radiation.

The Larmor precession frequency of the nucleus and the spin-lattice relaxation time are directly affected by the electromagnetic (em) environment it experiences. Therefore, the implanted nuclei can be used as probes of these local environments in the host material by measuring the resonance (Larmor) frequencies and relaxation times in β -NMR experiments. To do so, nuclei that have a non-negligible beta-decay asymmetry parameter, that can be spin-polarised and have a short lifetime are required. Examples of such nuclei are $^8,^{11}\text{Li}$ [58], ^{31}Mg [59], $^{26,27,28}\text{Na}$ [11], [54]. Other experimental requirements are: a stable and homogeneous magnetic field (either externally applied or internal to the sample), a radio-frequency (rf) source, a set of beta-detectors and the sample to be studied.

Radioactive ion beam (RIB) facilities, of either the in-flight or ISOL-type[60], provide many nuclei that are suitable for β -NMR. Our experiment is located at ISOLDE, which falls into the ISOL-type category[39], [40]. This facility uses a 1.4 GeV proton beam as a light projectile impinging on heavy target materials, containing e.g. uranium or lead[61]. The diverse mixture of simultaneously produced isotopes is selectively ionised and consecutively accelerated, mass-separated, and electrostatically guided to different experimental setups[50].

The resulting low-energy ion beam does not exhibit any nuclear polarisation. Laser optical pumping, the method used at our polarisation beamline at ISOLDE [53], [54], is a very efficient method to produce a sample of highly oriented short lived isotopes[54]. This is however dependent on an available closed excitation-deexcitation loop which is generally available for alkali and alkaline-earth metals. Moreover, when multiple-frequency pumping is used other elements (e.g Argon)[53] can be efficiently polarized using this technique as well.

Using an accelerating/decelerating electrode the ion beam is tuned into resonance with the laser light to allow for the optical pumping process to happen, next (in the case of alkali metals) the beam passes through a charge exchange cell which neutralises the beam. A space of 2 m is left for the atoms to interact

with the laser light, after which the beam goes through a transition magnetic field which allows the spins to adiabatically rotate into the direction of the main magnetic field (B_0)[53], [54]. Next the beam is implanted into the sample material from where the β -radiation is emitted and observed by a set of detectors located with and against the direction of B_0 . After each ion bunch, the β -count asymmetry between the two detectors is recorded. To record a resonance spectrum the frequency of the applied rf-field is modified at each bunch. To extract from the measured Larmor frequency either the nuclear g-factor or the magnetic field felt by the nuclei, one usually performs a reference measurement. A reference measurement can be performed by implanting another isotope of the same element in the same sample, yielding then a ratio of g-factors. Alternatively, the isotope of interest can be implanted in another sample, yielding then a ratio of the magnetic fields felt by the isotope (and thus sensitivity to e.g. a chemical shift or a Knight shift).

β -NMR measurements have been applied in nuclear structure studies and in material science studies on solid-state samples compatible with the high vacuum environment present at RIB facilities[62]. In nuclear structure studies, they can be used to determine magnetic dipole and electric quadrupole moments of short-lived nuclei [59], [63]–[65]. In material science, they serve as a sensitive local probe of the internal and interface em-fields[66].

Recently, there has been increased interest in extending the scope of applications of the technique to (bio-)chemical studies, which typically make use of liquid samples in which small chemical shifts of the NMR signal are measured[1], [3]. This goal poses several design and engineering challenges: first, the need to combine the liquid environment with high vacuum and second, the requirement of a part-per-million (ppm) homogeneous and stable magnetic field. Additionally, several practical aspects that improve the operation and throughput of the setup are also important to consider. Such as minimising the footprint of the β -detectors and the time spent on changing liquid samples.

Here, we report on the developments that have led to the high-accuracy liquid-sample β -NMR experiments using our experimental setup at ISOLDE[53], [54]. The upgrades described below have enabled us to determine with unprecedented accuracy the nuclear magnetic dipole moment of the short-lived ^{26}Na isotope[11].

2.2 Methods

2.2.1 Field locking

B_0 (1.2 T) was supplied by a Bruker (Billerica MA) BE25 electromagnet corresponding to a ^1H resonance frequency around 52 MHz. This is generally considered low-field for modern day NMR spectrometers[67], [68]. Due to the crowded environment of the ISOLDE experimental hall, which contains lots of devices that generate (fluctuating) stray fields, fluctuations of B_0 are to be expected. However, a stable B_0 is essential for β -NMR experiments, especially those performed in liquid samples, where chemical shifts of a few ppm are often measured[69]. These shifts can easily become unidentifiable by peak broadening due to poor magnetic field homogeneity and/or stability. Therefore a magnetic field stability and homogeneity on the level of a few ppm or less is required. Systematic B_0 measurements showed that besides rapid fluctuations of low amplitude a significant drift could be observed.

In order to reduce these field changes and to stabilize the magnetic field, a feedback system was implemented. As part of this system the magnetic field was measured using the pulsed NMR method on ^1H inside H_2O enclosed in a 3 mm (outer) diameter vacuum-tight vial. The applied pulse length was tuned to cause a $\pi/4$ rotation of the magnetization vector. The free induction decay (FID) of ^1H nuclei in water was measured using a transmitter/receiver coil tightly wound around the outside of the vial. This signal was acquired by a PS2204a PicoScope (Pico Technology, Cambridgeshire, UK). A LabVIEW (National Instruments, Austin TX) [70] program was used to compute a zero-filled Fast Fourier Transform (FFT) of the acquired signal to obtain the ^1H Larmor frequency, which is proportional to the magnitude of the magnetic field. This frequency was in turn compared to the set point using the LabVIEW built-in PID control function. The output of the PID function was used to determine the number of steps required by a stepper-motor driving a 10 k Ω variable resistor, connected in parallel to the magnet. The variable resistor was in series with two 1 k Ω resistors, to avoid short-circuiting the power supply. When coupled to the magnet's power supply (providing 38 A) the stepper-motor afforded an adjustment range of B_0 of 350 ppm.

The ^1H frequency measurement was repeated every 200 ms. A faster repetition rate was not feasible due to the long spin lattice relaxation times (T_1) of ^1H in water, and the subdued signal strength of the FID in a low magnetic field.

2.2.2 Absolute-field measurement

The measured ^1H frequency also allowed the determination of the absolute value of the external magnetic field B_0 at the position of the ^1H magnetometer, according to the following equation:

$$B_0 = \frac{\nu_L h I}{\mu(1 - \sigma)} \quad (2.1)$$

Here, ν_L is the measured Larmor frequency, h Planck's constant, I the proton spin, $\sigma=25.71(3)$ ppm is the absolute shielding of ^1H in water at 300 K [71], [72], μ is the magnetic moment of the proton $2.79284734462(82) \mu_N$ [73]. To include the effect of the magnetic susceptibility of the probe, see Eq. (2) in ref. [11].

To determine the magnetic field in the center of the magnet, where the sample is located, the field difference between the magnetometer and the sample positions has to be taken into account. We have done so by measuring the field with the ^1H magnetometer at both locations, and the relative difference amounted to 20(3) ppm. The biggest source of uncertainty in the determination of the absolute magnetic field at the location of the sample was due to the uncertainty in the probe's position.

2.2.3 Magnetic field shimming

To address the 2^{nd} order spatial fluctuations, or inhomogeneities, of the magnetic field in the center of the magnet, two shimming coils were designed. They were installed concentric and in contact with the magnet poles. For the design of the coils, the patent of Günthard *et al.* was used [74], which states that a pair of shimming coils placed directly against the poles of a magnet with a mean radius (A) of 0.43 times the distance between the poles (G) can effectively correct for 2^{nd} order inhomogeneities, without introducing any inhomogeneities of the 4^{th} order. Günthard *et al.* [74] also describe that the required current (I) can be calculated with:

$$I = \frac{2B_2A^3}{N\mu_0 1.36} \quad (2.2)$$

where μ_0 is the magnetic permeability of air, N the number of coil windings and B_2 the second order inhomogeneous contribution to the field. For ease of use and precision, the coils were manufactured as a double-layered printed circuit board (PCB). Figure 2.1 shows a picture of one of the shimming coils.

2.2.4 β -detectors

As can be seen in the exploded view of the experimental chamber in Figure 2.2, a pair of double-layer plastic scintillator detectors were placed close to both magnet poles, i.e. along and opposite to the direction of spin polarisation. Within the detectors, both 2-mm scintillator layers (Eljen Technology EJ-212) were insulated against light travelling between them with a 23.62 μm layer of aluminum. Silicon Photon Multipliers (SiPMs) (onsemi MICROFJ-60035) were coupled to the scintillators, and the signal was amplified by on-board operational amplifiers. This kept the detector system small, power efficient, and very resistant to external electronic noise sources. Because of the use of SiPMs, the detectors were not affected by the 1.2T magnetic field, thus eliminating the need for light guides.

2.2.5 Sample exchange system

To reduce the time spent on changing liquid samples, a sample ladder shown in Figure 2.3 was developed. The entire ladder fits within the 30 mm internal diameter of the rf excitation coil. Individual sample holders, made of 8 mm diameter mica sheets (i) or reference crystals (ii), are mounted on 3D printed Polylactic acid (PLA) structures, (iii) connected to two ceramic rods (iv), which are fixed to a vacuum flange (v). This flange, in combination with a linear translation stage (vi) and tilt adjust (vii), allows for coarse and fine adjustments of the sample position in all 3 dimensions.

To align the sample a theodolite is used to look through the end of the beamline at the back of the sample ladder. The centre of the mica is indicated by a contrasting dot made at the back of the PLA structures. This dot is used



Figure 2.1 Detailed picture of a double layered printed circuit board shim coil.

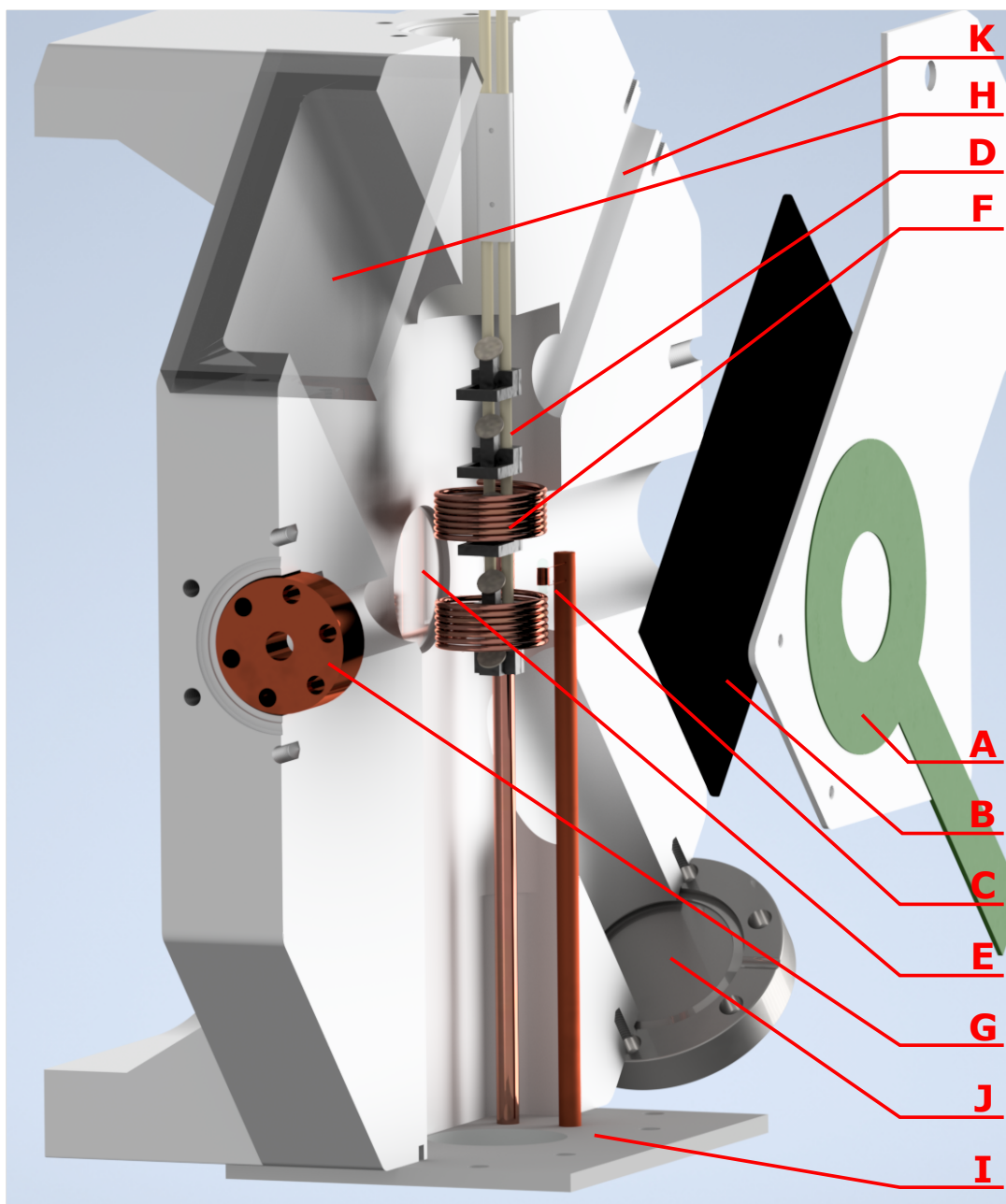


Figure 2.2 Exploded view of the experimental measurement chamber. The following parts are shown: (a) PCB shimming coil, (b) β -detectors, (c) ^1H magnetometer, (d) sample ladder, (e) β -windows, (f) rf-excitation coil, (g) collimator, (h) front viewport, (i) bottom plate with viewport, and feedthroughs, and two empty flanges for expansion purposes (j,k). See text for further details.

to position the sample in the centre of the pole axis and the vertical axis by changing the position of the linear stage and tilt adjust. To centre the sample in the beam axis a similar dot on the lowest sample holder is observed through a viewport on the bottom-plate of the experimental chamber (Figure 2.2 (i)) as the tilt adjust is changed. After the tilt adjust has been correctly set only the position of the linear stage had to be moved to change between the different sample positions.

The sample exchange system allows to measure up to five samples in rapid succession, reducing the time spent changing samples (more than an hour per sample) during the measurement time by a factor of five.

2.2.6 Experimental vacuum chamber

The experimental vacuum chamber, shown in Figure 2.2, was designed and CNC-machined to tightly fit in-between the magnet poles, and to maximize the available space inside it. On each side of the vacuum chamber, a plate housing a Printed Circuit Board (PCB) shimming coil on one side (a), and a β -detector on the other (b), is mounted on the outside of the chamber. Concentric with the magnet, 200 μm thick aluminum sheets act as " β -windows" (e). They form the boundary between the vacuum inside the chamber and the atmospheric pressure outside, while still allowing the β -particles to pass through to the detectors with as little absorption as possible. Inside, the vacuum chamber (100x40x200 mm) accommodates a 30 mm inner-diameter rf-excitation coil (f), the ^1H magnetometer (c), and movable sample ladder (d), with a NaF reference crystal and mica sample holders. At the front of the chamber, there is an in-vacuum pocket that can be used to mount a collimator (g) or a differential pumping cone. The upper part of the front side houses a large viewport for sample observation (h). The bottom of the chamber is closed off with a bottom plate equipped with a viewport for sample alignment purposes (i) and two vacuum feedthroughs with SMA connectors for rf connections. In the back, two additional flanges (j,k) are available for future setup expansions, e.g. sample manipulation and temperature control.

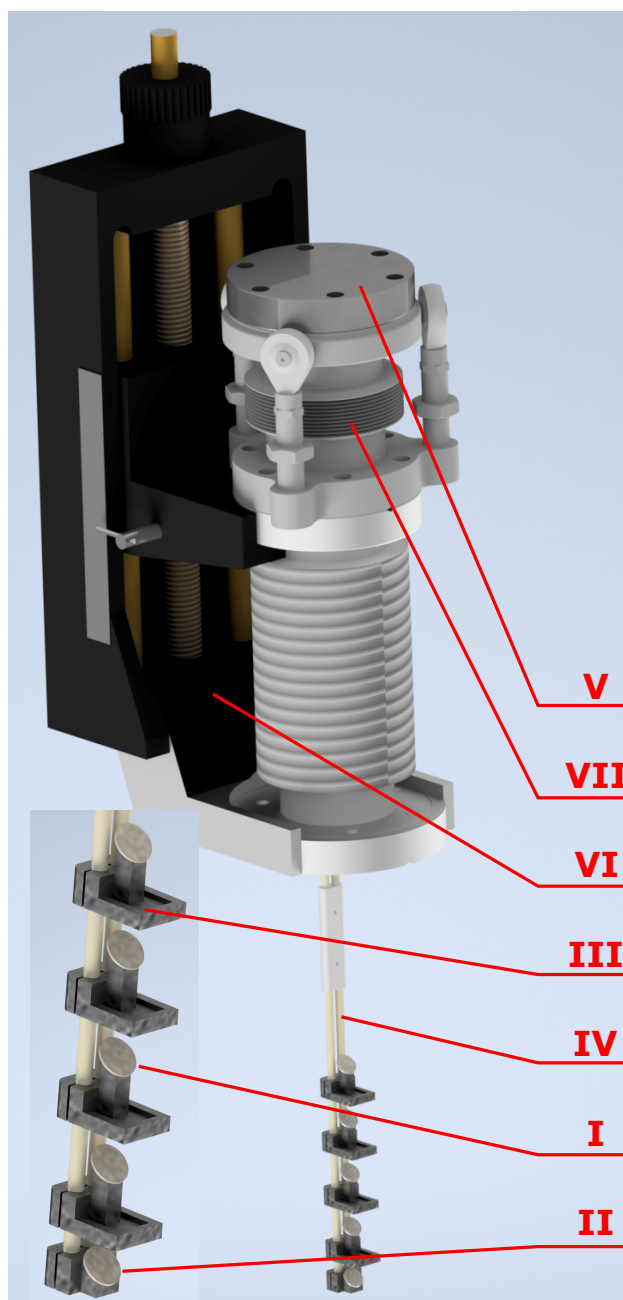


Figure 2.3 Sample exchange ladder that allows for the rapid exchange of samples. Shown are (i) the mica sheet sample holder, (ii) reference crystals, (iii) PLA mounting structures, (iv) ceramic rods, (v) vacuum flange, (vi) the linear translation stage and (vii) tilt adjust.

2.3 Results

In this part, we present the results achieved thanks to the upgrades described in the previous section.

The implemented locking system has allowed us to effectively stabilize the magnetic field down to the ppm level. As shown in Figure 2.4, the fluctuations of the magnetic field were substantial when the locking system was turned off.

When powered without the locking system, the magnet exhibited significant field instability while the power supply and magnet coils reached a temperature equilibrium. This can take up to 10 hours. The field change observed during this period has been as high as 300 ppm. Following this initial instability the field shows an oscillation with a period of roughly 5 hrs and an amplitude of 17 ppm, which correlates with periodic changes in the ISOLDE cooling water temperature. By comparison, with the locking system enabled (see the insert of Figure 2.4), the field deviates around a set point by approximately ± 0.6 ppm. The disturbances in the otherwise smooth lines are caused by manual interventions in the direct vicinity of the magnet during which the regulation system was turned off. Upon restarting the system it cycles through most of its range before finding back the locked frequency. This is the cause of the large spikes at the end of the intervention.

The shimming coils improve the homogeneity of B_0 within the sample volume to the single digit ppm level in every direction as shown in Figure 2.6. With the shimming coils turned off, B_0 follows a parabola deviating by over 20 ppm from the center to 9 mm outwards on either side along the pole-axis. With the shimming coils turned on, the deviation is reduced to only 4 ppm over the same distance.

Because the sample is oriented with a 45 degrees angle to the horizontal plane (Figure 2.3) the sample volume extends 3 mm from the magnet center in the vertical and beam axis directions, and 4mm in the magnet-pole axis. Figure 2.6 shows the final shimmed magnetic field (B_0) along all three axes around the centre of the magnet. This is the highest achieved homogeneity across the three combined dimensions, as trying to optimize the homogeneity in one axis further, decreases it in the others dimensions. Between the magnet poles and the vertical axis B_0 follows a flat parabola with the center approximately in

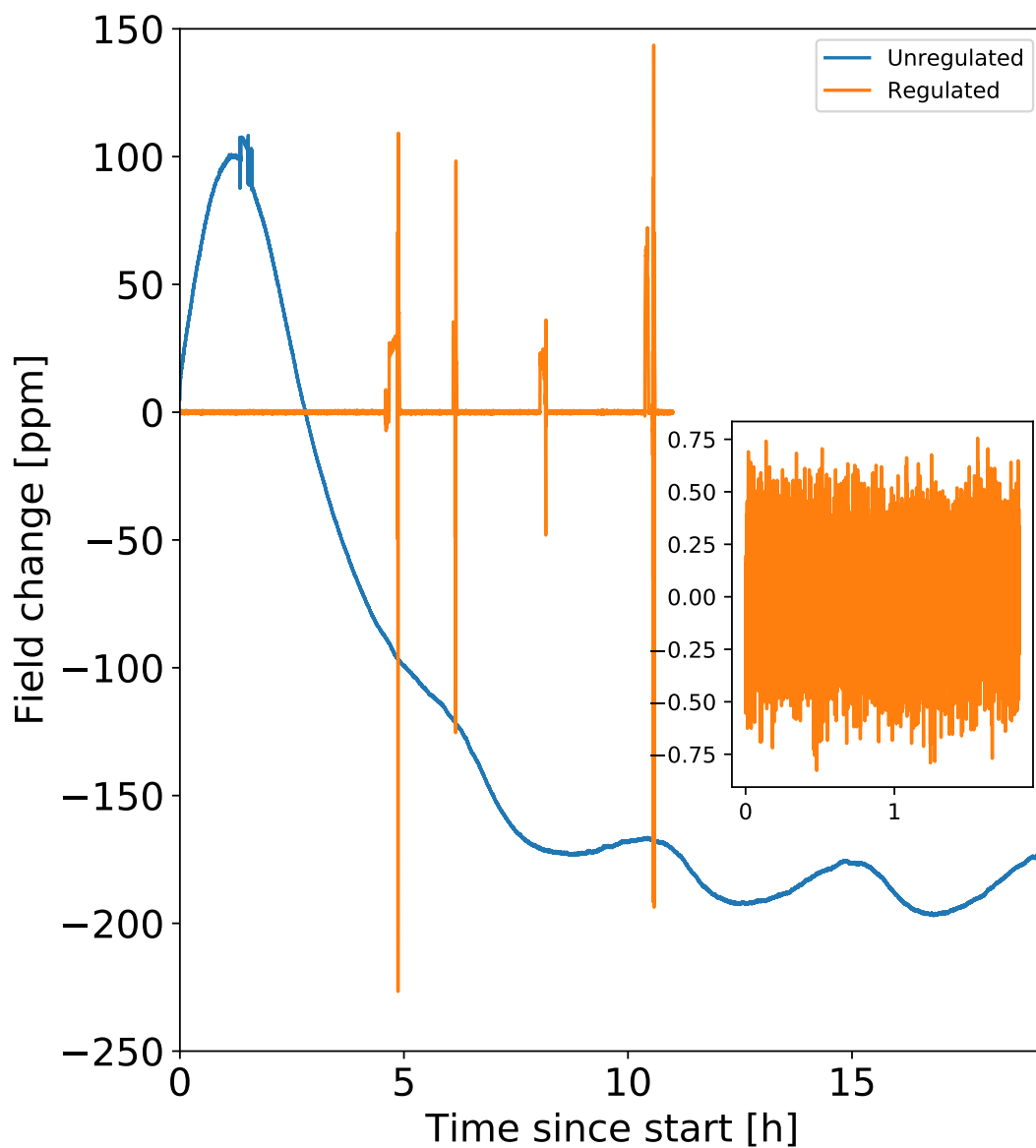


Figure 2.4 The change of the magnetic field compared to a reference value over time with the locking system off (blue) and on (orange). The insert shows a zoom of the regulated data. The spikes in the data are due to interventions on the experimental chamber requiring the regulation to be temporarily turned off. Once turned back on, the system cycles through most of its range before regaining the locked frequency. The initial drift of the unregulated data is due to slow equilibration of the magnet and power supply. The subsequent oscillations are caused by fluctuations in the cooling water and ambient temperature.

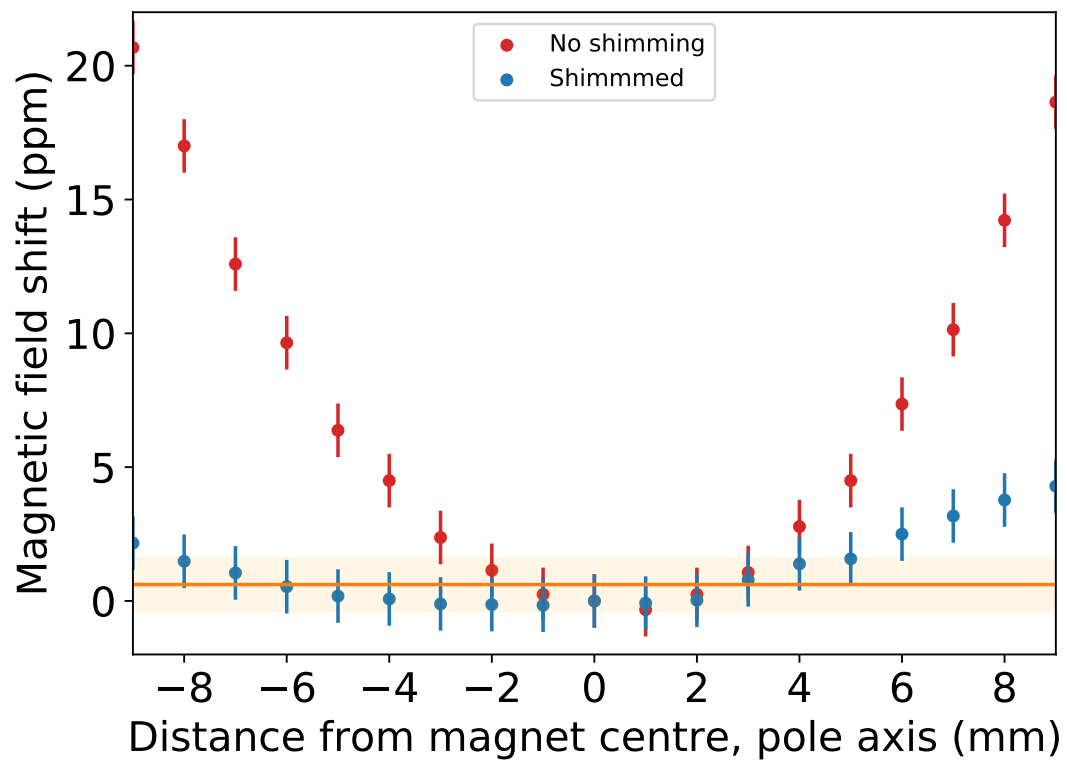


Figure 2.5 Spatial deviation of the magnetic field when going away from the magnet's center towards its poles. Red symbols: shimming coils turned off; Blue symbols: shimming coils on; Orange line shows the median field across the sample site and the shade area indicates a 1 ppm difference from this line.

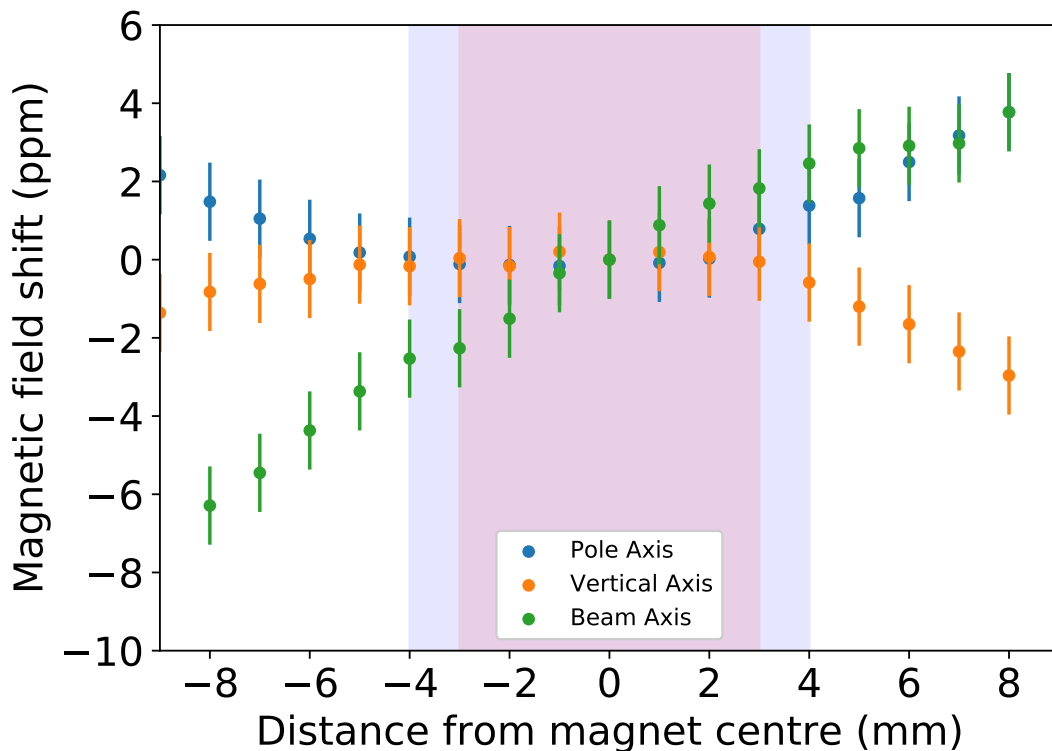


Figure 2.6 Final shimming results for the magnetic field along all three axes, relative to the magnetic field in the centre of the magnet (taken as 0 ppm). Blue symbols: field deviation along the central pole-to-pole axis, orange symbols: deviation along the vertical axis, green symbols: deviation in the horizontal (beam) direction. The shaded blue area indicates the sample space in the pole-to-pole direction, and the shaded red area the sample space in the other two directions.

the magnet’s middle, resulting in a maximum deviation from the median field along these axes at the sample site of 0.8 and 0.2 ppm respectively. However, along the beam axis B_0 follows almost a straight line, resulting in a maximum deviation from the median field of 2.1 ppm.

This field stability has allowed us to determine the magnetic moment of an unstable nucleus with two orders of magnitude higher accuracy than possible before. Until recently[11], [75], studies of the magnetic moment of exotic nuclei through β -NMR have relied on solid-state hosts as implantation sites [76]–[79]. In the case of sodium, magnetic moment studies were performed using a NaF crystal, with cubic lattice structure, which retained the nuclear spin-polarisation

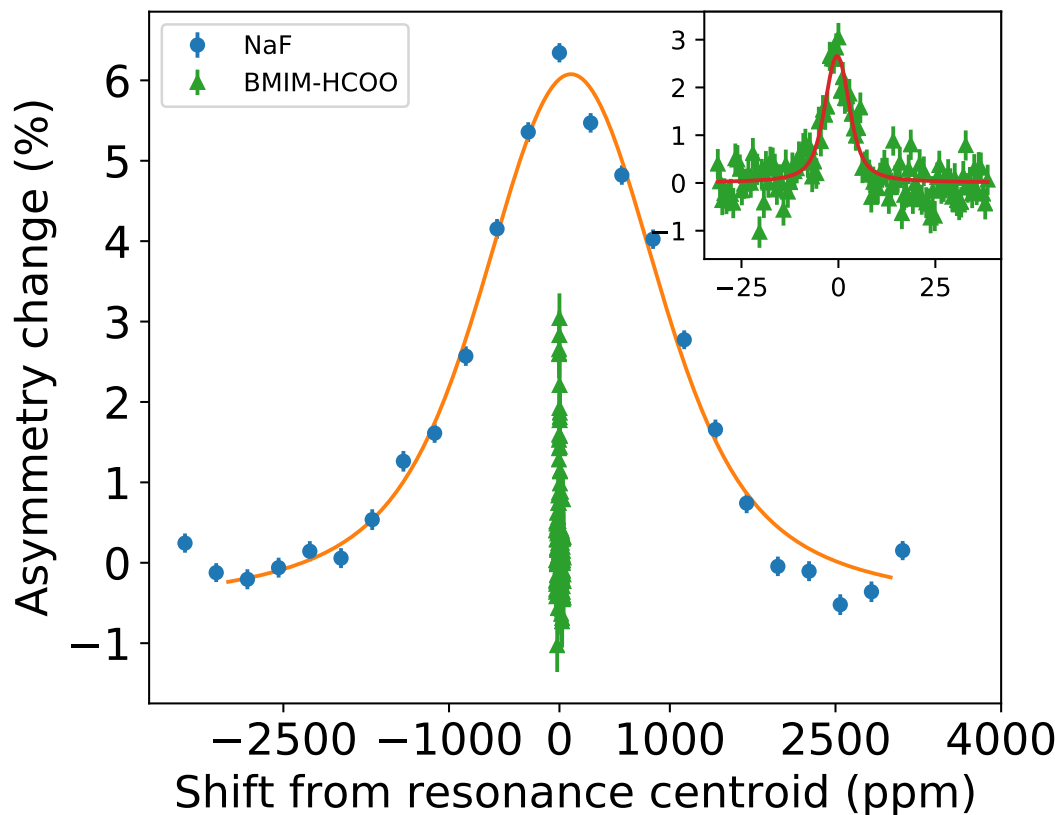


Figure 2.7 A comparison between the resonance width of ^{26}Na in a solid state host (NaF; blue), and a liquid state host (BMIM-HCOO; green). The deviation from the centre of each peak is given on the x-axis. The insert shows the resonance in the liquid host.

for up to 40 s [54], [65]. Resonances were achieved with a full width at half maximum (FWHM) in the order of 10^{-4} of the resonance frequency [65]. However, with liquid-state hosts, it is possible to obtain resonances with a FWHM down to two orders of magnitude smaller, whilst retaining the nuclear polarisation long enough to observe it through β -NMR. The narrowing of the resonance lines is due to fast molecular tumbling within the liquid sample, effectively averaging out the anisotropic contributions found in solid-state NMR spectra. Figure 2.7 shows a comparison the resonance width of ^{26}Na in a solid state host (NaF; blue), versus a liquid state host (BMIM-HCOO; green). The insert in Figure 2.7, is a zoomed in part of the spectra in order to show the resonance from the liquid host.

2.4 Discussion

In this article, we have presented in detail the technical solutions that allow to perform β -NMR studies in liquid samples with high absolute accuracy.

One of the key innovations we introduced is the magnetic field locking and measurement system that maintains the stability of the magnetic field down to the ppm level over hours and which allows us to determine the absolute value of the field with ppm accuracy. Another improvement is the PCB-shimming coils, which improve the magnetic-field homogeneity to 1-5 ppm within the volume of the sample. Furthermore, the use of state-of-the-art SiPMs has allowed us to obtain a very compact β -detection system opening up the space to observe the behavior of liquid samples in real time. Finally, a special sample handling system shortened the time spent on changing samples by a factor of 5. With the combination of these features, frequencies of β -NMR resonances in different hosts have been measured with unprecedented accuracy, paving the way for new applications of the technique. At the same time, further improvements are possible, and these and some general characteristics are covered in the following sections.

2.4.1 Locking system

The present field locking system reads out the magnetic field every 200 ms, and adjusts the current at least once per second. This measurement rate is 5 times faster than the previously used commercial Metrolab PT2025 magnetometer (Geneva, CH). In addition, the probe is smaller and is fully vacuum compatible. However, the rate at which the current in the electromagnet can be adjusted is the limiting step in the feedback loop. Specifically, the control and adjustment of the stepper-motor-driven variable resistor takes longer than the measurement time of the ^1H NMR magnetometer. Decreasing the time it takes to adjust the current can improve the field control further by making use of every measured ^1H frequency, thus reducing the time interval between consecutive field adjustments.

The ^1H magnetometer's other strength comes from the fact that it is based on the ^1H NMR frequency in water. The absolute NMR shielding for ^1H in water has been calculated much more accurately than in other liquid or solid hosts, thus leading to a more accurate magnetic field readout at the NMR probe's

position. The determination of the absolute magnetic field can be done concurrently with β -NMR measurements. Relative measurements via the resonance frequency of a reference β -NMR nucleus in a known host, which is both time-consuming and less accurate, are therefore unnecessary.

Furthermore, our ^1H magnetometer uses pulsed NMR, which eliminates the need to modulate the static magnetic field (as is done in the PT2025 probe). Thanks to this, the magnetometer does not disturb the magnetic field experienced by the probe nuclei at the sample location. Additionally the diameter of the magnetometer's rf coil is much smaller than the continuous-wave β -NMR excitation coil and the applied frequencies are far apart, excluding cross-talk between the two rf coils.

At the same time, because the β -NMR coil is relatively large, the ^1H probe is positioned 25 mm away from the sample location, where the field is different and less homogeneous than at the sample's location in the magnet's center. Though this does not affect the locking capabilities of the system, it leads to a field offset that needs to be measured and corrected for, in order to accurately determine the magnetic field at the sample position. As the field's gradient increases, so does the uncertainty of this correction. Even a small change of the probe's position can then result in a slightly different measured field. At present, this uncertainty is the largest contribution to the total uncertainty in the value of the magnetic field at the sample's position. Higher accuracy in the determination of the magnetic field at the sample position can be reached, e.g. by measuring the magnetic field very close to, or even at, the exact position of the sample. For example, in conventional NMR spectrometers, this is done by measuring the resonance frequency of ^2H present in heavy water (D_2O) mixed into the solvent. In β -NMR, protons in the solvent molecules can be used for the same purpose if an excitation and pickup coil is used to acquire a conventional ^1H NMR signal from the sample itself.

2.4.2 Shimming coils

The main achievement of the shimming coils was to reach 1 ppm homogeneity over a distance of several millimeters. Because the coils are made as PCB boards, they are very robust compared to wire wound coils. They are also cheap and

easy to manufacture reproducibly. The optimal current setting can easily be calculated using Eq. 2.2, requiring only minor fine tuning afterward.

A consequence of this design, which is dependent on the distance between the poles of the electromagnet, is that the corrections of the field in the axial and radial directions are coupled. This means a compromise must be found between the field homogeneity in different directions. Thus, a small gradient arising from the tail of the transitional field used to adiabatically rotate the atomic spin and consecutively decouple the nuclear and electron spin of the incoming beam of probe isotopes [54], can not be corrected by this system.

The magnetic field homogeneity could be further improved by analysing the field map, and by designing additional coils to correct for remaining field inhomogeneities. This would however quickly become very complicated, as one would need to take into account not only the field at the sample site, but also along the beam path, to make sure that field adjustments made by any additional shimming coils do not negatively affect the aforementioned transitional field. The extra space required for additional shimming coils will also be a limiting factor.

2.4.3 Sample handling system

Because the sample handling system reduces the time spent on exchanging samples 5 fold, it significantly increases the number of samples that can be tested during an experimental campaign. It also allows for the fine adjustment of each sample's position, resulting in reproducible sample alignment. When used in combination with the upstream collimator at the front of the experimental chamber, the sample handling system allows to have the polarised beam implanted solely in the well-aligned sample. This prevents background β -counts that could arise from parts of the beam being implanted in materials other than the sample.

During previous experiments, a NaF crystal was mounted at the bottom of the ladder, for reference and inspection purposes. The mica substrate used to hold the liquid samples is compatible with biological samples, easy to clean, and allows to create a thin, sub-millimeter layer of the liquid hosts (corresponding to 5-20 μ L of liquid), which also makes it possible to use solvents only available in

very small quantities. As with all other parts situated between, or close to the magnet poles, the sample handling system is made of non-magnetic material, and thus does not disturb the static magnetic or the rf fields.

The sample handling system is actuated manually. A clear improvement from the operational standpoint would be the automation of sample positioning. In addition, it does not yet include sample temperature measurements and control. These will be implemented in future developments of the system. Due to the lack of an efficient vacuum-liquid barrier and the sample orientation at 45° to the vertical, the sample handling system is only suitable for relatively viscous vacuum-resistant solvents. Low viscous solvents would simply flow off of the sample holder and non-vacuum-resistant solvent will evaporate and/or freeze due to the low pressure.

Ideally, for biochemical studies, one would want to perform measurements in water, as this is what is routinely done in conventional NMR studies. To achieve this goal, new technical approaches will be necessary to combine the no/low-vacuum environment required by water (because of its high vapour pressure), with the high-vacuum environment of RIB facilities. Solutions that warrant investigation for that specific purpose are differential pumping setups, allowing poor vacuum around the sample, combined with better vacuum along the path of the beam of unstable nuclei, or the encapsulation of samples to protect the high vapor pressure solvents from evaporation in the vacuum. Both of these approaches present their own hurdles. In the case of a high final pressure in a differential pumping setup, the gas present right before the sample will significantly scatter the incoming beam due to beam-gas interactions, which will significantly decrease the β -NMR SNR. In the case of encapsulation, the window material must be able to withstand the pressure gradient, but also transmit most of the beam without affecting its spin polarisation. Interactions between the beam and the window heavily depend on the material used for the window, its thickness, and the energy of the beam. For low energy beams such as in our setup (up to 50 keV), the window should be less than 100 nm thick, even possibly only 50 nm thick, which makes it very brittle. For high energy beams used at in-flight facilities, the window can be thicker. This allowed Mihara *et al.* [75], to perform a β -NMR measurement of ^{17}N in water.

2.4.4 Beta detectors

The current beta-detection system is a significant improvement compared to previous systems, which also relied on two pairs of thin plastic scintillators, however these were coupled to conventional PMs. Since conventional PMs are very sensitive to magnetic fields, they needed to be covered in Mu-metal and kept almost 1 m away from the center of the magnet, necessitating the use of light guides. The whole system took up lot of space, making any manipulation impractical, and mostly preventing visual inspection of the implantation site. It was also very heavy, and thus cumbersome to assemble and to get ready for operation. The present system is lighter and more compact, with β -detectors (scintillator and SiPMs) located inside the magnet, but still outside of the NMR chamber. In the future it should be possible to craft a set of detectors to be placed closer to the sample in vacuum. These could be made significantly smaller if the covered solid angle is kept constant. Besides this, one can consider designs with more complex geometries, so as to take full advantage of the beta decay angular distribution and the effect of the magnetic field on beta-particle trajectories.

2.4.5 Experimental chamber

Our experimental chamber design was to a large degree determined by the vacuum regime (no need for vacuum better than 10^{-6} mbar), the magnet to be used, and by respecting previously made design decisions. It allows to accommodate all necessary elements: β -NMR excitation coil, ^1H magnetometer, samples, detectors and shimming coils. Additionally, it has 2 viewports, combined with the viewport at the end of the beamline, allowing to check the alignment, circular polarisation, and power of the laser beam, to define the position of each sample holder after sample change and finally to observe the behaviour of the liquid sample on the substrate. The chamber is made of heat treated (T6) 6082 aluminium alloy and has standard-sized flanges compatible with the UHV standard CF (using elastomer instead of copper gaskets), which makes the installation and alignment easier.

The rf-excitation coil was designed to not obstructed the incoming beam, allow for the maximum solid angle of β -radiation through the " β -windows, and

the best homogeneity of the applied rf-field perpendicular to B_0 over the sample volume given these two boundary conditions.

Different magnet configurations, however, come with significantly different constraints. For example, for a solenoidal magnet, the chamber design will not easily give access to a viewport for sample observation. The design of a sample ladder would also not be a trivial task.

2.5 Conclusion

The upgrades described in the present manuscript open new avenues for β -NMR studies. They have already allowed for the determination of the magnetic moment of the short lived nucleus ^{26}Na with ppm precision [11]. This achievement, together with accurate hyperfine structure measurements [80], should allow for the study of the distribution of nuclear magnetism through the hyperfine anomaly (the effect of the non-point like size of the nucleus on the hyperfine structure[81]). The distribution of nuclear magnetisation can in turn shed light on open questions in nuclear structure physics, in particular about the distribution of neutrons inside the nucleus [8], [9].

Another application that these upgrades will be essential for, is the study of interactions between metal ions and biomolecules with β -NMR [82], [83]. One example of such interactions is the interaction between DNA G-Quadruplexes and sodium or potassium ions [84]–[87]. Presently, we are exploring the most suitable potassium probes for G-quadruplexes studies [2], as well as isotopes of several other elements relevant to protein folding [1]. Together with our previous ^{26}Na measurement [11] this will be of direct use in our current investigations into this topic.

2.6 Acknowledgements

This work was supported by the European Research Council (Starting Grant 640465), the UK Science and Technology Facilities Council (ST/P004423/1), EU project ENSAR2 (654002), the Ministry of Education of the Czech Republic (LM2018104), the Wolfgang Gentner Programme of the German Federal Min-

istry of Education and Research (05E15CHA), and by the Swiss Government
Excellence Scholarships for Foreign Scholars program.

Chapter 3

Paper 02: Magnetic Moments of Short-Lived Nuclei with Part-per-Million Accuracy

As described in the introduction one of the main observables in NMR, the Larmor frequency, is directly linked to the nuclear magnetic moment. With the beamline built and improved, the first study of magnetic moments of short-lived isotopes implanted into a liquid host could be performed.

Magnetic moments of short-lived nuclei with part-per-million accuracy

Towards novel applications of β -detected NMR in physics, chemistry and biology

R. D. Harding^{1,2}, *S. Pallada*¹, *J. Croese*^{1,3}, *A. Antušek*⁴,
*M. Baranowski*⁵, *M. L. Bissell*⁶, *L. Cerato*³,
K. M. Dziubinska-Kühn^{1,7}, *W. Gins*⁸, *F. P. Gustafsson*⁸, *A. Javaji*⁹
*R. B. Jolivet*³, *A. Kanellakopoulos*⁸, *B. Karg*³, *M. Kempka*⁵,
*V. Kocman*¹⁰, *M. Kozak*^{5,11}, *K. Kulesz*^{1,3}, *M. Madurga Flores*¹²,
G. Neyens^{1,8}, *R. Pietrzyk*⁵, *J. Plavec*¹³, *M. Pomorski*¹⁴,
*A. Skrzypczak*⁵, *P. Wagenknecht*^{1,9}, *F. Wienholtz*¹, *J. Wolak*⁵, *Z.*
*Xu*¹², *D. Zakoucky*¹⁵, *M. Kowalska*^{1,3}

¹CERN, Geneva, Switzerland

²University of York, York, United Kingdom

³University of Geneva, Geneva, Switzerland

⁴Slovak University of Technology, Bratislava, Slovakia

⁵Adam Mickiewicz University, Poznan, Poland

⁶University of Manchester, Manchester, United Kingdom

⁷Leipzig University, Leipzig, Germany

⁸KU Leuven, Leuven, Belgium

⁹Oldenburg University, Oldenburg, Germany

¹⁰National Institute of Chemistry, Ljubljana, Slovenia

¹¹Jagiellonian University, Krakow, Poland

¹²University of Tennessee, Knoxville, USA

¹³National Institute of Chemistry, Ljubljana, Slovenia

¹⁴University of Warsaw, Warsaw, Poland

¹⁵Nuclear Physics Institute of the Czech Academy of Sciences, Rez, Czech Republic

Published in *Phys. Rev. X* (10), 2020, 041061

doi: [10.1103/PhysRevX.10.041061](https://doi.org/10.1103/PhysRevX.10.041061)

Abstract

We determine for the first time the magnetic dipole moment of a short-lived nucleus with part-per-million (ppm) accuracy. To achieve this two orders of magnitude improvement over previous studies, we implement a number of innovations into our β -detected Nuclear Magnetic Resonance (β -NMR) setup at ISOLDE/CERN. Using liquid samples as hosts we obtain narrow, sub-kHz linewidth, resonances, while a simultaneous *in-situ* ^1H NMR measurement allows us to calibrate and stabilize the magnetic field to ppm precision, thus eliminating the need for additional β -NMR reference measurements. Furthermore, we use *ab initio* calculations of NMR shielding constants to improve the accuracy of the reference magnetic moment, thus removing a large systematic error. We demonstrate the potential of this combined approach with the 1.1 s half-life radioactive nucleus ^{26}Na , which is relevant for biochemical studies. Our technique can be readily extended to other isotopic chains, providing accurate magnetic moments for many short-lived nuclei. Furthermore, we discuss how our approach can open the path towards a wide range of applications of the ultra-sensitive β -NMR in physics, chemistry, and biology.

3.1 Introduction

The magnetic dipole moment μ is a fundamental property of atomic nuclei, and it is one of the primary observables used to investigate the nuclear wave-function [59], [88]–[96]. At the same time, it serves as a versatile probe to measure the local magnetic field at the nucleus. This ability lies at the core of various spectroscopic techniques, among which a prominent role is played by nuclear magnetic resonance (NMR), which is an indispensable tool for determining structural details and dynamics in chemistry, biology and materials science [97], [98].

In NMR experiments, one measures the Larmor frequency ν_L of nuclei of spin I precessing in a magnetic field. This frequency is the product of the gyromagnetic ratio γ of the nucleus and the local magnetic field B at the site of the nucleus, i.e. the applied magnetic field corrected for the effect of the electrons in the sample,

$$\nu_L = \frac{\gamma B}{2\pi} = \frac{\mu B}{hI}. \quad (3.1)$$

If one wants to employ NMR to extract a nuclear magnetic moment μ , two inputs are thus essential. First, the Larmor frequency ν_L must be measured. For stable nuclei ν_L has been determined with sub-ppm precision since the early years of NMR [99]–[102], thus is not the dominant source of uncertainty in the derived magnetic moment. The second essential input to derive μ is the NMR shielding, describing the local effect of electrons in the sample on the applied magnetic field. Until recently, this effect has been poorly quantified and sometimes even neglected [5]. However, the introduction of reliable NMR shielding constants, provided by modern *ab initio* methods [103], [104] enabled correction of this source of the systematic error in nuclear magnetic moment data [105], [106], which in extreme cases reached per-mill or per-cent levels [107]–[110]. This correction turned out to be crucial for the tests of QED in the strong electromagnetic fields of highly-charged ions [111], [112]. Here, a more accurate value of the magnetic moment of ^{209}Bi [108], [109] resolved a significant discrepancy between the measured and predicted hyperfine splitting (an effect of the interaction between μ and the magnetic field produced by the atomic electrons) of highly-charged ^{209}Bi [113], showing that QED is still valid in such a strong magnetic field. Based on the corrected magnetic moments a new referencing scheme in NMR spectroscopy was also proposed [114], which allows a direct measurement of the NMR shielding instead of a chemical shift (i.e. a difference in NMR shieldings in different hosts).

More accurate nuclear magnetic moments can clearly bring new applications in different fields of research, as shown above for stable nuclei. However, magnetic moments of short-lived nuclei have not yet been measured with equally small uncertainty. In the present work, we demonstrate for the first time the determination of a magnetic moment of a short-lived nucleus with ppm accuracy. This has been achieved for the 1.1 s half life ^{26}Na using an improved version of the β -NMR technique, combined with *ab initio* calculations of NMR shielding for the stable reference ^{23}Na . The isotope ^{26}Na was used for the proof-of-principle experiment, because of sodium importance for biochemistry applications [2].

The β -NMR technique is based on the directional asymmetry of β -particle emission from spin-polarized β -decaying nuclei [115], [116]. The most attractive feature of the method is its sensitivity, which is up to 10^{10} times higher than in conventional NMR [3], with down to 10^6 resonating nuclei leading to an NMR

spectrum. The technique has been applied to measure the magnetic moments of short-lived nuclei down to per-mill precision [59], [63]–[65], [117]–[123] and for electronic, magnetic, and structural investigations in materials science [66], [124]–[130]. However, in chemistry and biology, β -NMR is far from being a routinely applicable spectroscopic method [3], [131], [132], due to numerous experimental challenges. One of them is the requirement of time-consuming reference measurements with the same short-lived nucleus in a different chemical environment [131], [133]. Furthermore, those reference measurements are performed in a solid-state sample [131], [132], resulting in relatively wide resonance signals, thus increasing the final error on the extracted experimental value. Another challenge is due to the reduced precision and accuracy in the measured frequency and deduced magnetic moments, which prevent a direct comparison of the data with results from conventional NMR and from *ab initio* chemical calculations of local fields. The work presented here addresses all of the above limitations of the β -NMR technique, with the key ingredient being an accurate magnetic moment measurement.

The developments presented here will be crucial for future applications of high-precision β -NMR spectroscopy using a variety of radioactive probes, not only in the fields of chemistry and biology, but also for nuclear structure research. For example, determining the neutron distribution in light neutron-rich nuclei [134], [135] is experimentally very challenging as neutrons do not carry electric charge. However, one can access this information by measuring the distribution of magnetization inside exotic nuclei. This requires very high-precision magnetic moment measurements, combined with high-precision hyperfine-structure measurements on the same isotope, to be sensitive to the ‘hyperfine anomaly’ [136]–[138].

3.2 Techniques

3.2.1 β -NMR on short-lived ^{26}Na

β -NMR studies were performed on laser-polarized short-lived ^{26}Na . The nuclei were produced at the ISOLDE facility at CERN [139], in reactions induced by a 1.4-GeV proton beam of up to 2 μA , impinging every 3.6 s on a UC_x (uranium

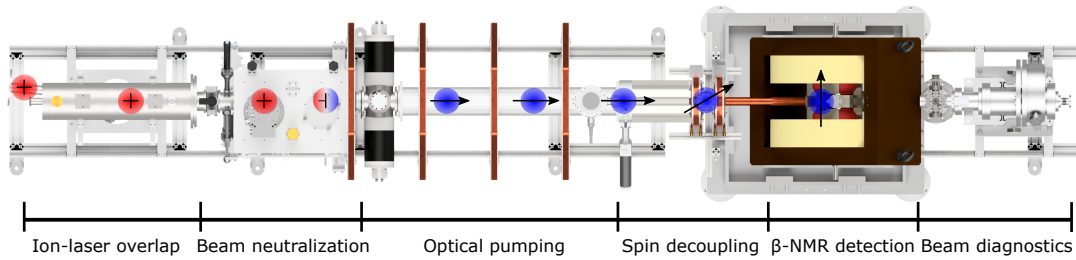


Figure 3.1 Top view of the laser-polarization and β -NMR beamline [53], [54]. The ion and laser beams enter from the left. The ions are represented by red circles with a plus sign. The neutral atoms are represented by blue circles. The polarization of the atom is represented by arrows. See text for further details.

carbide) target. After fast diffusion out of the heated target, sodium atoms were surface-ionized, accelerated to 50 keV and mass separated using the High Resolution Separator (HRS). The pure isotopic beam of ^{26}Na , with an intensity of $2 - 5 \times 10^7$ ions/second, was transported to the laser polarization beamline [53], [54] shown in Fig. 3.1.

There, the $^{26}\text{Na}^+$ beam is overlapped with circularly-polarized laser light. Next, it passes through a neutralization cell, where it picks up an electron as it travels through a vapour of stable ^{23}Na . Over the next 1.5 m the neutral atomic ^{26}Na beam is polarized via optical pumping in the D2 line at 589 nm [54]. This takes place in a weak guiding magnetic field of 2 mT (applied along the beam path), which defines the quantization axis and prevents the coupling of the electron spins to possible stray fields in the surrounding environment. Next, the atoms pass through a transitional field region of $\approx 10 - 20$ mT, where the atomic spins undergo an adiabatic rotation towards the perpendicular magnetic field of the NMR magnet. The spin-polarized atoms pass through a collimator and reach a liquid sample located in a vacuum chamber that is placed between the poles of a Bruker BE25 electromagnet set to a field of 1.2 T (Fig. 3.2). At this point, the nuclear and electronic spins are decoupled and the nuclear spin couples to the large static field.

The liquid sample is deposited on a sample holder made of mica. The collimated atom beam and the holder have a diameter of 8 mm. Four such sample holders are attached to a sample ladder that can be moved in and out of the beam path. The emitted β particles are registered in two pairs of thin organic

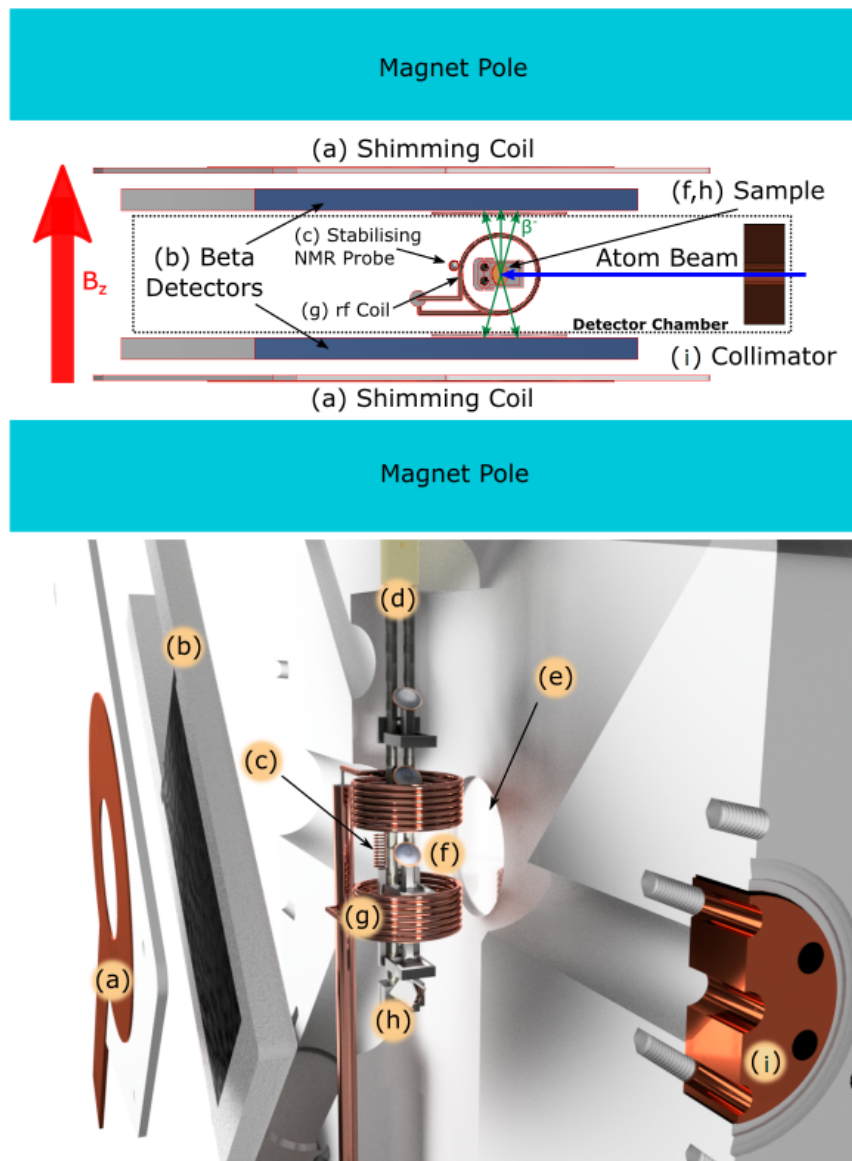


Figure 3.2 β -NMR detection chamber. Top: Schematic cross-section as viewed from the top. Bottom: 3D CAD exploded view. a) shim coil to improve field homogeneity, b) β -particle detector (plastic scintillator) and Si photomultiplier, c) ^1H -NMR probe to monitor and actively stabilize the magnetic field, d) sample ladder, e) β -particle window (100 μm aluminium), f) mica sample holder, g) main rf coil for NMR excitations, h) NaF crystal to optimise the degree of laser spin-polarization, i) 8 mm beam collimator. See text for further details.

scintillators, coupled to compact silicon photo-detectors. The sample at the center of the electromagnet is surrounded by a 30 mm diameter coil to which an rf signal can be applied. See Fig. 3.2 for details.

To record an NMR spectrum, such as the ones shown in Fig. 3.3, 200 equally spaced rf frequencies are sequentially set. For each frequency, the ^{26}Na beam is implanted over 200 ms following the proton-bunch impact. After the start of implantation the β particles are counted for up to 1 s in the detectors at 0° and 180° to the direction of the magnetic field (left and right to the beam axis). From these counts the experimental β -decay asymmetry is determined, as a normalized difference in the counts, $(N_{0^\circ} - N_{180^\circ})/(N_{0^\circ} + N_{180^\circ})$. At the same time, the sample is irradiated with a continuous wave rf field of 0.03 mT and a frequency corresponding to the point in the scan. This procedure is repeated for consecutive proton bunches (arriving every 3.6 or 4.8 s), to allow most of the nuclei from the previous bunch to decay. If required by the signal-to-noise ratio, several spectra of the same sample can be recorded and summed.

To increase the precision of the NMR measurements to the ppm level, the magnetic field across the sample had to be homogeneous with a temporal stability at the ppm level during a measurement. To ensure the former, a weak magnetic field on the order of 0.02 mT was produced by two shimming coils placed in contact with the magnet poles [74]. In this way the field homogeneity across the sample volume was improved by more than an order of magnitude in all three axes: 1 ppm along the symmetry axis of the magnet, 3 ppm in the vertical axis, and 5 ppm in the horizontal axis (ion-beam propagation). Since the magnetic field is symmetric with respect to the center of the sample, the remaining inhomogeneity contributes to a broadening of the resonance peak, without a significant shift in the resonance frequency, compared to a point-like sample. The temporal drift in the magnetic field was addressed using an active stabilization system based on the ^1H resonance frequency measured in a tailor-made vacuum-compatible H_2O NMR probe. The 3-mm diameter probe was located just outside the main excitation rf coil, as shown in Fig. 3.2, with its middle only 25 mm away from the center of the sample. The resulting temporal stability was better than 1 ppm between sub-second and 24-h timescales, compared to drifts as big as 1 ppm/minute without it.

Previous β -NMR studies of the magnetic moments of short-lived nuclei have

relied on solid-state hosts. For sodium, the studies were performed using a cubic NaF crystal which retained polarization for several dozen seconds, leading to NMR resonances with the width in the order of 10^{-3} of the resonance frequency [65]. In comparison, with liquid-state hosts it is possible to obtain resonances with over two orders of magnitude smaller width (due to molecular tumbling within a liquid [140]), whilst retaining the nuclear polarization long enough to employ β -NMR. Unfortunately, most liquid-state hosts used for NMR studies have a high vapour pressure, so when placed inside vacuum they either freeze or evaporate. However, room-temperature ionic liquids, which are salts in a liquid state at room temperature, have an extremely low vapour pressure [141], which makes them suitable hosts for high-precision NMR studies in vacuum environments, as encountered in most β -NMR setups. For measuring the Larmor frequency of ^{26}Na two different ionic liquids were selected: 1-ethyl-3-methylimidazolium dicyanamide (EMIM-DCA) and 1-butyl-3-methylimidazolium formate (BMIM-HCOO). The EMIM-DCA sample contained $\approx 1 \mu\text{M}$ of $^{23}\text{Na}^+$ while the BMIM-HCOO sample contained 0.5 M. Both samples were degassed slowly at 10^{-5} mbar pressure for several hours in a separate vacuum chamber. 20 μL of each solution was deposited as a 0.4 mm layer on one of the sample holders attached to the sample ladder. The ladder was then placed in the β -NMR chamber, as shown in Fig. 3.2, and the pressure inside was lowered slowly from atmospheric pressure to 10^{-5} mbar. The sample was oriented at 45 degrees to the atom beam. Due to the high viscosity of both liquids, the layer remained on each substrate at high vacuum for up to 24 h.

3.2.2 Conventional NMR on stable ^{23}Na

At the time of investigation, it was not possible to obtain a conventional NMR signal from ^{23}Na at the β -NMR beamline. Therefore, ^{23}Na and ^1H NMR spectra were recorded on a conventional NMR spectrometer. Our earlier systematic NMR studies showed that changing ^{23}Na concentration from micro-molar to molar ranges and degassing for an extended period shifts the ^{23}Na resonance by less than 0.5 ppm. This was taken as our experimental uncertainty for ^{23}Na and degassing was not carried out during the measurements presented here. The field of 7.05 T was provided by a Bruker Avance DMX 300 MHz spectrometer

and a basic pulsed-NMR scheme was applied (single $\frac{\pi}{2}$ rf pulse) on samples kept at room temperature. The sample preparation and Na^+ concentration were as close as possible to those in the β -NMR experiment: $\approx 1 \mu\text{M}$ in the EMIM-DCA sample and 0.5 M in the BMIM-HCOO sample.

For the measurements, 200 μL of each solution were sealed inside a 3-mm diameter NMR tube. The tube was placed inside a 5-mm diameter tube filled with D_2O , whose ^2H NMR signal was used to stabilise the magnetic field automatically during the measurements (field locking). ^1H NMR resonances were also recorded within several minutes from ^{23}Na spectra, using the same setup with two concentric tubes. Here, the 3-mm tube was filled with H_2O . Due to the way the field locking was performed, the magnetic field was the same for all measurements.

3.3 Results

In order to derive the nuclear magnetic moment from the Larmor frequency in eqn. 3.1, the effective magnetic field B needs to be known. Since the external field B_0 is modified by the bulk magnetic susceptibility of the host and by the NMR shielding of the nucleus in the host σ , B can be thus expressed as [142]

$$B = B_0[1 + (1/3 - \alpha)\kappa](1 - \sigma), \quad (3.2)$$

where κ is the volume magnetic susceptibility and α is the shape factor (see Appendix B for details). It is advantageous to use an approach where $\alpha\kappa$ or/and σ cancel out, so we started by determining the ratio R of the magnetic moment of ^{26}Na to that of ^{23}Na in the same ionic liquid host

$$R = \frac{\mu(^{26}\text{Na})}{\mu(^{23}\text{Na})} = \frac{\nu_L(^{26}\text{Na})I(^{26}\text{Na}) B(^{23}\text{Na})}{\nu_L(^{23}\text{Na})I(^{23}\text{Na}) B(^{26}\text{Na})}. \quad (3.3)$$

This value is independent of the NMR shielding (which is the same for ^{26}Na and ^{23}Na), and includes only a correction due to the difference in bulk magnetic susceptibilities of our samples (Appendix B).

The ^{26}Na β -NMR spectra in EMIM-DCA and BMIM-HCOO recorded at 1.2 T are shown in Fig. 3.3, while Tab. 3.1 shows the corresponding Larmor

frequencies, together with reference frequencies for ^{23}Na at 7.05 T. For each measurement, several spectra were analysed, which differed in the observation time and in the coincident gate to determine the experimental β -decay asymmetry. The spectra were fitted with a flat baseline and Lorentzian profiles, which were expected due to a moderate rf power broadening. The data were also fitted using Gaussian profiles and a sloped baseline, with a negligible effect on the resonance frequency and its uncertainty. To extract the ^{26}Na resonance frequencies shown in Tab. 3.1, spectra with a 250 ms observation time were used, as they provided the highest signal-to-noise ratio and the smallest non-statistical scattering between data points. Because this scattering led to the normalized (reduced) sum of residuals χ_{red}^2 being higher than 1, the fitted frequency uncertainty was scaled by $\sqrt{\chi_{red}^2}$, following the procedure by the Particle Data Group [143].

During the ^{26}Na measurements, the ^1H stabilising NMR probe had a resonance frequency of 52008500(30) Hz. This was 1050(150) Hz lower than when the probe was placed at the sample position in the middle of the magnet, which lead to a corrected frequency of 52009550(150) Hz. During the ^{23}Na measurements, the ^1H NMR Larmor frequency was 300131415(100) Hz.

Using the above Larmor frequencies and the magnetic susceptibility correction from Appendix B, the derived value of R for each measurement is shown in Tab. 3.1. The error in round brackets results from the statistical uncertainty on the ^{26}Na resonance position. The systematic error present in all measurements is shown in square brackets, and includes systematic uncertainties in the resonance frequencies of ^1H and ^{23}Na , and the uncertainty of the magnetic susceptibility correction. Here, the biggest contribution by far is the error in the frequency of ^1H during the β -NMR measurements, caused by the uncertainty in the position of the probe, which can be improved in the future. The final value of the ratio of $\mu(^{26}\text{Na})$ to $\mu(^{23}\text{Na})$ is $R = 1.284956(1)[8]$ or $R = 1.284956(8)$ with the uncertainties combined. Fig. 3.4 shows the individual results in comparison to the literature value based on the hyperfine-structure measurement [144], which is two orders of magnitude less precise than our result. Our weighted average is indicated by the purple line. The purple shaded region represents the statistical uncertainty while the orange region represents the systematic uncertainties.

In order to determine $\mu(^{26}\text{Na})$, a reliable reference $\mu(^{23}\text{Na})$ value is needed. In Nuclear Data Tables [5], the values of $\mu(^{26}\text{Na})$ based on Atomic Beam Mag-

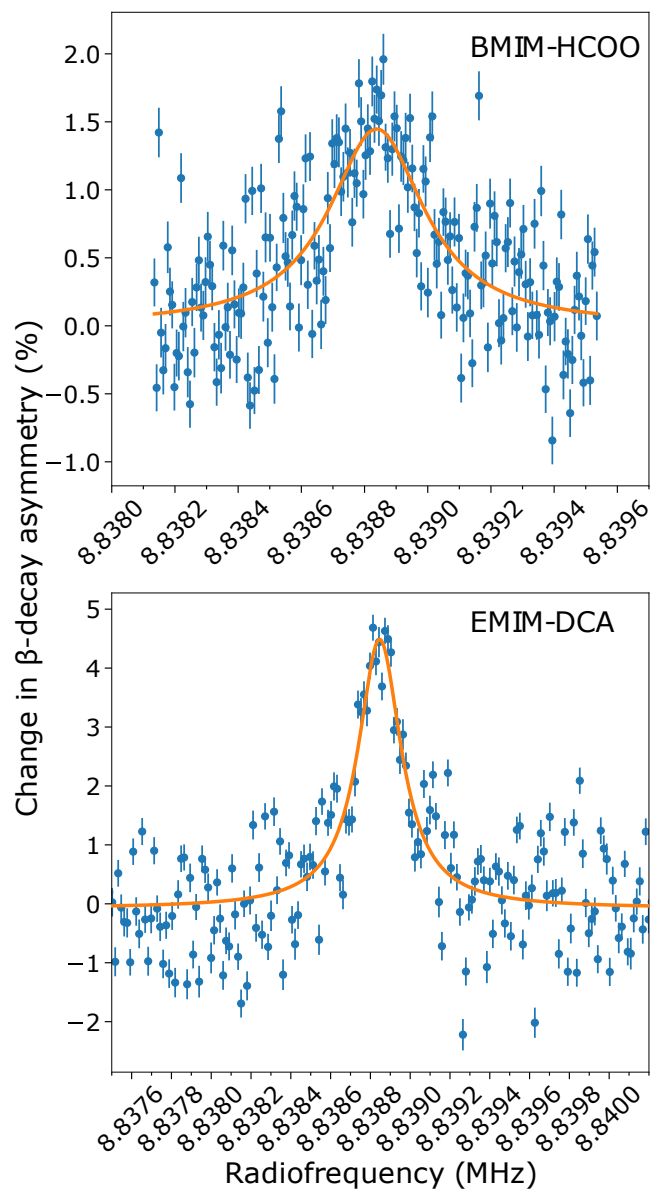


Figure 3.3 Examples of ^{26}Na β -NMR spectra in BMIM-HCOO (top) and EMIM-DCA (bottom). See text for the description of the fitting procedure. Note the different ranges of x and y axes. The fitted baseline (i.e. experimental asymmetry outside resonance) was subtracted for all data points for an easier comparison of the amplitudes of both signals. The magnetic field was locked to the same ^1H frequency for both samples.

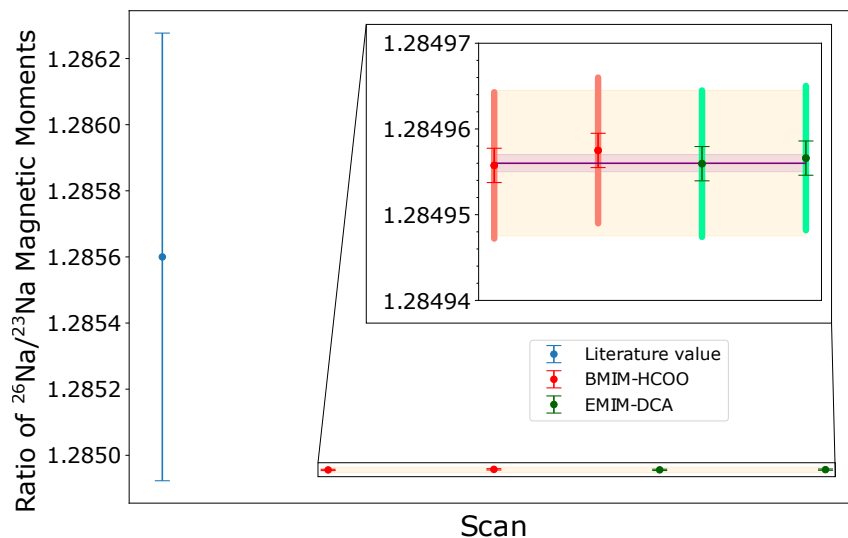


Figure 3.4 Ratio of the magnetic moments of ^{26}Na and ^{23}Na . Left: literature value [144], right: present study. Thin error-bar lines correspond to statistical uncertainty in the ^{26}Na Larmor frequency and thick lines are the systematic uncertainties. The weighted average is represented by the purple line. The statistical uncertainty from all four measurements is indicated by the pink band, while the systematic uncertainty is shown by the broader orange band. For details, see text.

Table 3.1 Larmor frequencies of ^{26}Na at 1.2 T and ^{23}Na at 7.05 T in BMIM-HCOO and EMIM-DCA, and the resulting ratio of the magnetic moments, R , based on eqn. 3.3. Errors in round brackets are due to the statistical uncertainties in the resonance frequencies. For R , this includes only the uncertainty of the ^{26}Na resonance frequency, while the square brackets are due to other contributions, including the uncertainty of the ^{23}Na resonance frequency.

Liquid host	$\nu_L(^{26}\text{Na})$ (Hz)	$\nu_L(^{23}\text{Na})$ (Hz)	R
BMIM-HCOO	8838826(14)	79390170(100)	1.284956(2)[8]
BMIM-HCOO	8838834(12)		1.284957(2)[8]
EMIM-DCA	8838838(10)	79390300(100)	1.284955(2)[8]
EMIM-DCA	8838847(13)		1.284957(2)[8]

netic Resonance (ABMR) and NMR experiments differ by $1.34 \times 10^{-4} \mu_N$, which is much larger than the individual error bars. This introduces an uncertainty that is larger than that of the frequency-ratio measurement in our β -NMR experiment. The above discrepancy stems from applying an obsolete diamagnetic correction [145] for the derivation of $\mu(^{23}\text{Na})$ from the experiments. This inconsistency can be corrected using *ab initio* NMR shielding constants calculated for the species used in both experiments: a sodium atom in ABMR and an aqueous sodium ion in the NMR experiment. The technical details of NMR shielding calculations can be found in the Appendix A.

The NMR shielding in the sodium atom calculated using the Dirac-Hartree-Fock (DHF) method is 637.1 ppm. The electron correlation contribution estimated using the Dirac-Kohn-Sham (DKS) method with various DFT functionals ranges from 0.06 ppm (PBE0) to 0.23 ppm (B3LYP). Coupled cluster codes for the NMR shielding of open-shell systems are not available. However, the accuracy of DKS correlation contributions can be estimated by the NMR shielding in the closed-shell Na^+ ion and the difference between the electron correlation contributions in the sodium atom and sodium ion from the literature [146]. The non-relativistic CCSD(T) correlation contribution calculated for the sodium ion, -0.08 ppm, should not differ from the NMR shielding in the sodium atom by more than 0.09 ppm [146]. All presented correlation contributions suggest that the electron correlation effects for the NMR shielding in the sodium atom are small. Therefore the NMR shielding in the sodium atom can be approximated with a very good accuracy by the DHF value. The electron correlation contributions can be used as an error estimate. Our final NMR shielding in the sodium atom, 637.1(2) ppm, is consistent with the shielding in ref. [147]. The NMR shielding for the solvated sodium ion was approximated by the NMR shielding in a six-coordinated $\text{Na}^+(\text{H}_2\text{O})_6$ complex (the prevalent coordination number according the experiment [148]). The five coordinated $\text{Na}^+(\text{H}_2\text{O})_5$ complex was used to estimate the error of the NMR shielding due to the structural uncertainty. The NMR shielding constants calculated using non-relativistic and relativistic approximations for the $\text{Na}^+(\text{H}_2\text{O})_6$ complex are shown in Tab. 3.2. The Hartree-Fock and DHF NMR shielding, electron correlation contributions ($\Delta_{corr}^{\text{CCSD}}$, $\Delta_{corr}^{\text{CCSD}(\text{T})}$) and relativistic contributions ($\Delta_{rel}^{\text{DHF}}$, $\Delta_{rel}^{\text{DKS}}$) reach good convergence with the basis size. The final NMR shielding for the $\text{Na}^+(\text{H}_2\text{O})_6$ com-

plex, 582.0 ppm, is a composite value of (i) the non-relativistic shielding calculated using the CCSD(T) method, (ii) relativistic correction (Δ_{rel}^{DKS}), and (iii) the PCM solvent contribution (Δ_{solv}^{PCM}). All contributions entering the final NMR shielding were calculated using the quadruple- ζ (QZ) basis set.

The systematic error of the NMR shielding in the $\text{Na}^+(\text{H}_2\text{O})_6$ complex was evaluated as the square root of the sum of squares of the following errors. The structural uncertainty (2 ppm) was evaluated as the difference between the CCSD NMR shielding for aqueous sodium complexes with the coordination number of five and six. The basis set incompleteness error (1 ppm) was estimated from the variations of the NMR shielding constants calculated using non-relativistic HF method with Dunning and Jensen basis set series. The coupled cluster expansion truncation error was approximated by $\Delta_{corr}^{CCSD(T)} \approx 1$ ppm. Considering the convergence of the PCM solvent contribution (Δ_{solv}^{PCM}), the error was estimated to be 1 ppm. The systematic error introduced by assuming an additivity of the electron correlation and the relativistic effects is negligible as indicated by the small difference between the Δ_{rel}^{DHF} and Δ_{rel}^{DKS} relativistic corrections.

The final approximation of the NMR shielding of the aqueous sodium ion is (582.0 ± 2.6) ppm. This result is consistent with the NMR shielding in ref. [149], but in the present study, the error bar was reduced by a factor of four. This was achieved by calculations with much larger basis sets, which led to a better convergence of all contributions.

Table 3.3 presents the new values of the ^{23}Na reference magnetic moment re-derived using our new NMR shielding constants. The ABMR-based magnetic moment was obtained using our *ab initio* NMR shielding of the sodium atom and the original ABMR experiment [150]. The NMR-based magnetic moment was re-derived using (i) our *ab initio* NMR shielding of the aqueous sodium ion, (ii) the experimental frequency ratio 0.26451900 [151] of ^{23}Na in 0.1 M NaCl water solution to the proton in tetramethylsilane (TMS), (iii) the reference proton magnetic moment $\mu(^1\text{H}) = 2.792847348(7) \mu_N$ [152], and (iv) the reference NMR shielding of the proton in TMS $\sigma(^1\text{H}) = 33.480 \pm 0.5$ ppm [71].

The newly extracted ABMR- and NMR-based values of ^{23}Na nuclear magnetic dipole moment are now consistent within the error bars and the discrepancy between them was decreased by a factor of ≈ 30 .

For the derivation of the ^{26}Na nuclear magnetic dipole moment, the NMR-based ^{23}Na nuclear magnetic dipole moment was used, because the corresponding NMR shielding calculations for aqueous sodium complexes are based on a better approximation and the error bar was estimated more rigorously. The resulting ^{26}Na nuclear magnetic dipole moment is $2.849390(20) \mu_N$ (Tab. 3.4).

The new ^{26}Na nuclear magnetic dipole moment is consistent with the previous experimental value based on the hyperfine-structure measurement [144] within the error bar, but the present experiment and *ab initio* calculations improved its accuracy by two orders of magnitude, to 7 ppm. The largest contribution to this error bar comes from the uncertainty in the position of the ^1H NMR probe during the β -NMR experiment, which is 2 times larger than the uncertainty from NMR shielding and 3 times larger than the other experimental uncertainties. Experimental upgrades to provide a rigorous determination of the probe position could reduce the uncertainty of the ^{26}Na magnetic moment to the level of accuracy reached for the stable ^{23}Na .

Magnetic moments which have been linked to ^{26}Na can also benefit from the improved accuracy of $\mu(^{26}\text{Na})$. This is the case for $^{27-31}\text{Na}$, which were investigated using β -NMR in solid-state hosts at the collinear laser spectroscopy beamline at ISOLDE [65], and whose g -factors $g_I = \mu/(I\mu_N) = \gamma\hbar/\mu_N$ were referenced to that of ^{26}Na . Table 3.4 presents our new values of the ^{23}Na and ^{26}Na magnetic moments, as well as the $^{27-31}\text{Na}$ magnetic moments obtained using our improved $\mu(^{26}\text{Na})$ and the aforementioned g -factors. Literature magnetic moments [65], [144] are also shown for comparison.

The new values of the $^{27-29,31}\text{Na}$ magnetic moments have a relative uncertainty of 70 ppm. This is a ten-fold improvement compared to the values deduced in [65] and up to 50 times more accurate than the values tabulated in the latest compilation of nuclear magnetic dipole and electric quadrupole moments [5] (for ^{30}Na , it is respectively two [65] and 10 [5] times smaller). Previously, the uncertainty for $^{27-31}\text{Na}$ was dominated by the precision in the magnetic moment of the reference ^{26}Na . At present, it is determined by the uncertainty in the $^{27-31}\text{Na}$ β -NMR resonance frequency in solid-state hosts. If new measurements in liquid hosts are performed, this contribution could be decreased further to the ppm level.

Table 3.2 Sodium NMR shielding in the $\text{Na}^+(\text{H}_2\text{O})_6$ complex.

	DZ ^a	TZ ^a	QZ ^a
HF	578.588	578.814	579.150
CCSD	571.625	573.837	574.140
CCSD(T)	571.011	572.909	573.127
$\Delta_{corr}^{\text{CCSD}}$	-6.963	-4.977	-5.010
$\Delta_{corr}^{\text{CCSD(T)}}$	-0.614	-0.928	-1.013
PBE0+PCM	563.355	565.609	568.197
PBE0	564.406	565.472	567.533
$\Delta_{solv}^{\text{PCM}}$	-1.051	0.137	0.664
DHF	586.860	587.263	587.346
DHF ^b	578.980	579.089	579.151
$\Delta_{rel}^{\text{DHF}}$	7.880	8.174	8.195
DKS/PBE0	574.842	574.822	574.848
DKS/PBE0 ^b	567.007	566.694	566.688
$\Delta_{rel}^{\text{DKS}}$	7.835	8.128	8.160

^a for non-relativistic calculations cc-pCVXZ.cc-pVXZ basis set series (X = D, T, Q) are used; for relativistic DHF and DKS calculations uncontracted ucc-pCVXZ.ucc-pVXZ basis set series are used

^b non-relativistic limit obtained with the speed of light re-scaled by factor of 20

Table 3.3 $\mu(^{23}\text{Na})/\mu_N$ reference nuclear magnetic dipole moment from ABMR and NMR experiments

	old reference [5]	This work
ABMR	+2.217522(2)	2.217495(2) ^a
NMR	+2.2176556(6)	2.217500(7) ^b

^a using the original ABMR experiment [150] and NMR shielding of the sodium atom (637.1 ± 0.2) ppm

^b using the standard NMR frequency ratio of ^{23}Na in NaCl water solution to proton in TMS [151] and NMR shielding of $\text{Na}^+(\text{H}_2\text{O})_6$ (582.0 ± 2.6) ppm.

See the text for details on NMR shielding calculations.

Table 3.4 Magnetic moments of $^{23,26-31}\text{Na}$ determined in this work, compared to literature values [65], [144], and other nuclear properties relevant for NMR.

Isotope	I	$t_{1/2}(\text{ms})$	$Q(\text{mb})$	old μ (μ_N)	new μ (μ_N)
^{23}Na	3/2	stable	+106(1)		2.217500(7) ^a
^{26}Na	3	1071	-5.3(2)	2.851(2)	2.849390(20) ^b
^{27}Na	5/2	301	-7.2(3)	3.894(3)	3.89212(24)
^{28}Na	1	31	+39(1)	2.420(2)	2.41844(19)
^{29}Na	3/2	44	+86(3)	2.457(2)	2.45535(17)
^{30}Na	2	48		2.069(2)	2.0681(11)
^{31}Na	3/2	17		2.298(2)	2.29670(17)

^a corrected $\mu(^{23}\text{Na})$ based on NMR experiment, Table 3.3

^b based on our improved ratio of $\mu(^{26}\text{Na})/\mu(^{23}\text{Na})$

3.4 Discussion and future perspectives

To determine precise and accurate, shielding-corrected magnetic moments, two independent steps are needed. First, the Larmor frequency of the radioactive probe is measured relative to that of a stable NMR probe, e.g. ^1H or ^2H in water. This procedure removes the need for reference measurements relative to another radioactive probe nucleus, which is the current (time consuming) reference method used in β -NMR. Furthermore, by using an ionic liquid as the host for the radioactive probe, a very precise Larmor frequency can be obtained, from which a precise (but still uncorrected) magnetic moment of a short-lived nucleus can be deduced relative to that of the stable (^1H or ^2H) probe. Second, the NMR shielding in the host is corrected, using one of two procedures. It can be calculated using modern calculation methods (if possible), or alternatively an independent NMR measurement has to be performed for the stable isotope of the element in the same host, again relative to the H-reference. The latter approach was used here. The final accuracy on the magnetic moment will then depend on the accuracy of the moment of the stable isotope, which can be deduced

from former high-precision measurements in atoms, molecules and liquids, in combination with state-of-the-art shielding calculations (as performed here).

The accurate magnetic moments of $^{26-31}\text{Na}$ presented above, together with that of ^{23}Na , provide a set of NMR probes connected through the same NMR shielding. In this way conventional NMR and the ultra-sensitive β -NMR can be used to provide complementary information on chemical and biological processes, by probing different timescales and different nucleus-environment interactions (see Tab. 3.4). For example, with the very short-lived ^{28}Na one can probe processes with ms timescales, with longer-lived ^{26}Na – timescales of seconds, while stable ^{23}Na has a much longer observation window. Furthermore, quadrupole moments of ^{26}Na and ^{27}Na are respectively 20 and 15 times smaller compared to the stable ^{23}Na . This results in a weaker interaction with the gradient of the electric field [153], leading to longer relaxation times and narrower resonances. This should permit the observation of NMR signals in hosts which display broad ^{23}Na resonances due to a strong quadrupolar interaction.

The approach presented here can be directly applied to other isotopic chains, thus expanding the palette of nuclei available for NMR spectroscopy. It can be combined with several techniques to polarize spins of short-lived nuclei. Some elements are easily polarized using element-specific laser optical pumping, as proven for several alkali and alkali-earth elements [90]. At the same time, universal polarization methods, such as pickup of polarized thermal neutrons, projectile-fragmentation or low-energy nuclear reactions can be also used to produce polarized samples of radioactive isotopes, see [88], [154], [155] and references therein.

Accurate magnetic moments of β -NMR probe nuclei are setting foundations for a novel referencing scheme in β -NMR spectroscopy. The method is based on measuring two Larmor frequencies simultaneously: for the radioactive probe in the chosen host material and a stable NMR probe like ^1H or ^2H in water placed in the experimental setup near the probe of interest. In this scheme, the absolute NMR shielding σ_X instead of a chemical shift could be measured directly, following eqns. 3.1 and 3.2:

$$\sigma_X = 1 - \frac{\nu_X |\mu_Y| I_X}{\nu_Y |\mu_X| I_Y} \frac{1 + (1/3 - \alpha_Y)\kappa_Y}{1 + (1/3 - \alpha_X)\kappa_X} (1 - \sigma_Y). \quad (3.4)$$

where X is the β -NMR probe nucleus and Y is the reference conventional nucleus

(e.g. ^1H in water). A description of the correction due to the difference in the bulk magnetic susceptibilities $\alpha\kappa$ is presented in Appendix B. Here, the β -NMR probe nucleus is related to the conventional NMR reference nucleus, which establishes a bridge between β -NMR spectroscopy and conventional NMR spectroscopy. This scheme offers the possibility to reference radioactive nuclei shielding to the stable nuclei not only within the isotopic chain, but also between different elements. This removes the dependence of β -NMR spectroscopy on the ambiguous and often *ad hoc* standards defined for every element separately [114].

In this novel referencing scheme, the uncertainty of the NMR shielding σ_X of β -NMR nuclei in different hosts, derived from eqn. 3.4, will be defined primarily by the uncertainty in their magnetic moment. For ^{26}Na , using the old value of ^{26}Na magnetic moment leads to ^{26}Na NMR shielding values with a ± 700 ppm error bar, which is about 10 times larger than the full range of chemical shifts for sodium [156]. In comparison, our new magnetic moment of ^{26}Na will lead to a 100 times more accurate shielding values (± 7 ppm), which will be sufficient to distinguish between different sodium binding sites, see e.g. [157], and will enable comparisons to theoretical Na NMR shielding values [87], [158], [159].

All of the above innovations open the path for novel applications for β -NMR in chemistry and biology. One such application is the interaction of metal ions with biomolecules [82], [83], which is important for the functions of living organisms (especially metal-ion mediated folding of proteins [160] and nucleic acids [161]). For example, half of the proteins in our body contain metal ions, but their interactions and factors influencing them are still not fully understood. This is because many metal ions are silent for most spectroscopic techniques [83] and are very challenging for conventional NMR [147], [162]. Yet, in NMR, metal nuclei are often very sensitive to small changes in geometry and coordination number, which gives rise to dozen-ppm shifts in resonance frequencies for many metals [156], [162]. The application of β -NMR will allow this field to profit from up to a billion times increased sensitivity and access to readily available β -NMR probe nuclei with smaller or even no quadrupolar moment (see e.g. [59], [65]), giving rise to longer relaxation times and narrower resonances.

Using the advances presented here, pilot applications in biology are already planned. Among the biologically relevant metal ions, sodium and potassium play an important role in the formation and dynamics of special DNA structures, G-

quadruplexes, which are promising targets for anti-cancer therapies [84]. Our present work has prepared ^{26}Na to be an immediately applicable β -NMR probe to address this topic [2], [85]–[87]. Presently, we are also exploring the most suitable potassium probes for G-quadruplex studies [2] and isotopes of several other elements relevant to protein folding [1].

In a very different field, namely in nuclear structure, our research paves the way for addressing the open question about the distribution of neutrons inside atomic nuclei [8], [163]. The neutron distribution impacts the properties of neutron stars [164], determines the limits of the nuclear landscape [165], and is responsible for novel phenomena and exotic structures in unstable nuclei [166]. It is especially important for light neutron-rich ‘halo’ nuclei, consisting of a compact nuclear core and one or several loosely bound ‘halo’ neutrons which are spatially extended [167], [168]. As neutrons do not carry an electric charge, compared to protons their distribution is much more difficult to be determined experimentally. However, because the neutron distribution is closely related to the distribution of nuclear magnetism, it can be addressed via the hyperfine anomaly, by combining the accurate magnetic moment with an accurate hyperfine structure measurement [169]. For example, in ^{11}Be the magnetism is mostly due to the ‘halo’ neutron [134], [135], so the hyperfine anomaly provides a direct probe of the halo structure [134], [170]. Because the hyperfine structure of ^{11}Be is already known with high accuracy [135], the only missing experimental input to derive the neutron distribution from the hyperfine anomaly is an accurate value of the magnetic moment of ^{11}Be , which can be achieved by applying the procedure presented in this work.

3.5 Conclusions

In summary, using ^{26}Na as an example, we have presented the first determination of a magnetic moment of a short-lived nucleus with ppm accuracy. This represents an improvement by two orders of magnitude in comparison with a previous experiment and other β -NMR based measurements of magnetic moments. The procedure described in this article represents a general protocol for measurements of magnetic dipole moments of polarized β -decaying nuclei with high accuracy, reaching the accuracy for stable nuclei.

The innovations presented here brings the following advances for the ultra-sensitive β -NMR technique: (i) Elimination of the dependence of β -NMR spectroscopy on ambiguous and often *ad hoc* references. As a result, the uncertainty related to the β -NMR reference measurement can be removed from the analysis. In addition, the direct comparison of β -NMR and conventional NMR data bridges these two techniques. (ii) Saving scarce resources of radioactive beam for acquisition of more β -NMR data on the samples of interest, since a reference measurement on a β -NMR probe is not required. This will accelerate the application of β -NMR spectroscopy as an analytical tool. (iii) Link to *ab initio* predictions through the direct measurement of NMR shielding for β -NMR probes. This will facilitate the interpretation of β -NMR experiments.

These novel features have the potential to transform β -NMR spectroscopy into a more widely applicable technique, based on a palette of ultra-sensitive β -NMR probes with accurate magnetic moments, allowing to address problems that range from neutron distribution in exotic nuclei to interactions of metal ions with biomolecules.

3.6 Acknowledgements

This work was supported by the European Research Council (Starting Grant 640465), the UK Science and Technology Facilities Council (ST/P004423/1), FWO-Vlaanderen in Belgium (G0B3415N), KU Leuven (GOA 15/010), EU project ENSAR2 (654002), Slovak Research and Development Agency grant (APVV-15-0105), European Regional Development Fund, Research and Innovation Operational Programme (ITMS2014+: 313011W085), Polish National Science Centre OPUS research grant (2017/27/B/ST4/00485), the Ministry of Education of Czech Republic (LM2015058), the Wolfgang Gentner Programme of the German Federal Ministry of Education and Research (05E15CHA), and the Swiss Excellence Scholarship programme. Computational resources of the Slovak Academy of Sciences and the Slovak University of Technology were used (projects ITMS 26230120002 and ITMS 26210120002). We thank the assistance of the ISOLDE technical team and that of L. Hemmingsen from Copenhagen University, M. Walczak from Poznan University of Technology, K. Szutkowski from A. Mickiewicz University in Poznan, M. Jankowski, R. Engel, and W.

Neu from Oldenburg University, H. Heylen, A. Beaumont, M. Van Stenis from CERN, V. Araujo from KU Leuven, A. Zhuravlova from Kiev University, K. Jackowski, M. Piersa and E. Adamska from Warsaw University, J. Klimo, R. Urban, S. Komorovsky, G. Kantay, J. Krajnak from the Slovak Academy of Sciences, E. Sistare from Geneva University, and M. Jaszuński from the Polish Academy of Sciences.

3.7 Appendix A - *Ab initio* NMR shielding calculations

NMR shielding in the sodium atom with the doublet electronic ground state was calculated using the Dirac-Hartree-Fock (DHF) method applying the paramagnetic NMR theory for open-shell systems [146], [171], [172]. Dyall-VXZ [173] basis set series were used ($X = D, T, Q$ represents double- ζ , triple- ζ and quadruple- ζ basis sets).

According to a recent experiment [148], the coordination number of the aqueous Na^+ ion depends on the NaCl solution concentration and varies between 5 and 6. Therefore, NMR shielding of the Na^+ ion in the aqueous solution was calculated for model $\text{Na}^+(\text{H}_2\text{O})_5$ and $\text{Na}^+(\text{H}_2\text{O})_6$ complexes. Their structures were optimized using Density Functional Theory (DFT) with the B3LYP density functional [174]–[176] and Def2-TZVP basis set [177]. The D3 dispersion correction [178] was applied. A distorted octahedral structure (D_{2h} symmetry) was obtained for the $\text{Na}^+(\text{H}_2\text{O})_6$ complex, with an average Na-O distance of 2.386 Å. For $\text{Na}^+(\text{H}_2\text{O})_5$ the corresponding structure was found to be a trigonal bipyramid (C_{2v} symmetry) with an average Na-O distance of 2.368 Å. The average Na-O distances for both structures are in good agreement with the experimental Na-O distances obtained with two different experimental methods giving 2.384 ± 0.003 Å and 2.37 ± 0.024 Å [148].

NMR shielding constants for aqueous sodium complexes were calculated using the non-relativistic coupled cluster (CC) method with single and double excitations (CCSD) and with non-iterative triple excitations CCSD(T) [179], [180]. All electrons were correlated. Dunning core-valence basis set series cc-pCVXZ [181] were used for sodium and valence series cc-pVXZ [182] for hydro-

gen and oxygen, combining basis sets with the same cardinal number X ($X = D, T, Q$). In order to estimate the error due to incompleteness of the basis set, the pcS-n basis set series by Jensen [183] was also used. In all NMR shielding calculations Gauge-Including Atomic Orbitals (GIAO) [184] were used.

The effect of the water solvent (outside the first solvation shell) on the NMR shielding in the sodium complex was incorporated by the polarized continuum model (PCM) COSMO [185]. This effect was evaluated using DFT with the PBE0 functional [186], [187]. The water dielectric constant of 78 was used in this implicit solvent model.

Relativistic corrections were calculated as the difference between the relativistic NMR shielding and the corresponding non-relativistic limit using two different methods: the DKS method with the PBE0 functional and the DHF method. The non-relativistic limit was obtained by re-scaling the speed of light in the Hamiltonian by a factor of 20. In the relativistic calculations, the Dunning basis sets were fully uncontracted and a restricted magnetic balance scheme was employed to generate the small component basis set [188], [189]. The nucleus was modeled by a Gaussian charge distribution [190].

For the structure optimization and for non-relativistic DFT calculations of NMR shielding constants the NWChem package was used [191]. Non-relativistic coupled cluster NMR shielding calculations were carried out in the CFOUR [192] package. For relativistic NMR shielding calculations, the ReSpect [193], [194] program was used.

3.8 Appendix B - Effect of bulk magnetic susceptibility

When using NMR to determine accurate nuclear magnetic moments or absolute NMR shielding, one should consider the differences in bulk magnetic susceptibility between the samples [142] (see. eqn. 3.2 and 3.4). This effect depends on the volume magnetic susceptibility of the host material κ and on the geometry of the sample, reflected in the shape factor α . For the shapes used in our studies, $\alpha \approx 0$ for the ^{23}Na and ^1H samples in conventional NMR, and for ^{26}Na in β -NMR at CERN (cylinders parallel to the magnetic field [142] and a disc

3.8. APPENDIX B - EFFECT OF BULK MAGNETIC SUSCEPTIBILITY

perpendicular to the magnetic field [195], respectively), whereas $\alpha \approx 1/2$ for the ^1H probe used at CERN (cylinder perpendicular to the field [142]).

In eqn. 3.3 for the ratio R of the magnetic moments, the magnetic susceptibility corrections for ^{23}Na and ^{26}Na cancel out in the term $\nu_L(^{26}\text{Na})/\nu_L(^{23}\text{Na})$, due to the same α and κ . At the same time, $B(^{23}\text{Na})/B(^{26}\text{Na}) = \nu_L(^1\text{H})/\nu'_L(^1\text{H}) \times (1 + \Delta)$, with $\Delta = (1 - \frac{1}{6}\kappa_{H_2O})/(1 + \frac{1}{3}\kappa_{H_2O}) - 1$, and prime denoting the measurement at CERN. Using $\kappa_{H_2O} = -9.04 \times 10^{-6}$, $\Delta \approx +4.5 \pm 0.5$ ppm, where we assumed a 10 % uncertainty in the shape factors due to the finite size of the samples.

When using eqn. 3.4 to measure NMR shieldings with β -NMR, one must consider the shape factor α and the volume susceptibility κ for the host of the reference nucleus (water in our case) and that of the β -NMR nucleus.

Chapter 4

Discussion & Outlook

In this thesis, a method to determine the magnetic moments of β -emitting radioisotopes with ppm accuracy using β -NMR has been established. This achievement is valuable for (bio)-chemical studies with β -NMR, especially those that are challenging with conventional NMR. It is also an essential part that could shed light on the distribution of magnetization within the nucleus.

The technical prerequisites for a precise measurement of the nuclear Larmor frequency were achieved thanks to several developments implemented at the β -NMR setup at ISOLDE. Especially important was the ppm stability and homogeneity of the magnetic field, achieved by the ^1H feedback system and the shimming coils. The other main contribution to the precision of the measurement was the ability to implant the atom bunches into room temperature ionic liquids (RTILs).

To use the improved measurement of the Larmor frequency of ^{26}Na to obtain a more accurate magnetic moment, the measurements linking it to stable ^{23}Na and new *ab initio* NMR-shielding calculations were needed. The ^{26}Na Larmor frequency was connected to that of stable ^{23}Na in the same solvent through an intermediate measurement of the ^1H frequency at different magnetic field strengths. The *ab initio* NMR-shielding calculations solved the discrepancy between the historic ^{23}Na magnetic moment measurements. All these steps combined, in turn, allowed for a more precise and accurate determination of the magnetic dipole moment of ^{26}Na with an uncertainty of 7 ppm.

Just as in conventional NMR, the resolution of β -NMR increases at higher

magnetic field strength. The absolute frequency width of any NMR peak remains constant with increasing field. However, the resonance position linearly increases with increasing magnetic field strength. Consequently, the relative peak width decreases, and the peaks get better resolved. With the current hardware, the ISOLDE β -NMR setup is limited to a magnetic field strength of 1.2 T. Going to higher field strengths will require a superconducting magnet, which can improve the field stability and homogeneity to the sub-ppm level.

The nuclear chart gives an overview of a vast number of potential isotopes with more favorable NMR properties compared to their stable counterparts e.g. with a (larger) magnetic dipole moment, with an electric quadrupole moment which is smaller or even equal to zero, and with a different spin quantum number. However, the potential amount of suitable isotopes usable in β -NMR experiments reduces significantly if the following two requirements are taken into account: First, the chosen isotopes need to be efficiently produced at the available production site. Second, the experimental β -decay asymmetry needs to be significant. The latter is determined by the amount of nuclear spin polarisation of the implanted ensemble, the β -decay asymmetry factor, the profile of the implanted beam, and the effective solid angle covered by the detectors. For a given signal to noise ratio (SNR) one can make a trade-off between beam intensity, experimental β -decay asymmetry, and measurement time. Because of this trade-off and the experimental β -decay asymmetry being setup-dependent, it is not feasible to publish a comprehensive list of suitable isotopes. Furthermore, continued development of polarisation schemes and improved production rates will further expand the number of isotopes suitable for β -NMR studies.

When comparing the work done within this thesis to previously performed measurements in solid-state samples, the most striking difference can be seen comparing the resonance of ^{26}Na in the RTIL BMIM-HCOO with the resonance in a NaF crystal (see figure 7 of chapter 2). It highlights the two orders of magnitude gain in resolution by performing β -NMR measurements in liquid hosts rather than solid-state hosts.

Although performed with different setups, field strengths, implantation energies, methods, and isotopes, it is also worth looking at β -NMR results in liquid samples from other facilities: The Heavy Ion Medical Accelerator in Chiba (HIMAC), and the ISAC-facility at TRIUMF in Vancouver. The setup

used at HIMAC for the study of the $^{12,17}\text{N}$ isotopes, as reported by Mihara et al. [75], [131], [196], operates at a similar field strength as the setup at ISOLDE. However, since it is located at an in-flight facility, the beam energies are in the order of tens of MeV/nucleon instead of 50 keV. Because of this higher energy, the sample does not have to be kept inside a vacuum chamber, and implantation directly into liquid water through a thick window is possible. This is a clear advantage for future biological applications. A drawback is that this solution leads to a reported reduction of the nuclear polarisation by 50%. Initially, the HIMAC-team was faced with large line-widths of around 1000 ppm for ^{12}N in water [131], which was even wider than the solid state (Pt) reference. However, by going to an isotope without an electric quadrupole moment (^{17}N) [75], and by optimizing the magnetic field homogeneity and stability [196] a line-width of only 5 ppm was achieved. A further reduction, down to the single ppm level, is envisaged by further optimizing the applied RF field.

Three main points stand out from the HIMAC results compared to the work presented in this thesis. First, this is a prime example of one of the strengths of β -NMR: an isotope with more beneficial nuclear properties was used (no electric quadrupole moment). In conventional NMR, this would be difficult and in most cases even impossible. For completeness, it must be mentioned that for the specific case of nitrogen, two stable isotopes exist: ^{14}N which has a nuclear spin $I = 1$ and a natural abundance of 99.64% and ^{15}N which has $I = 1/2$ and a natural abundance of 0.36%. Thus, for this element in conventional NMR, more beneficial nuclear properties could also be obtained by isotopically enriching a sample with ^{15}N . The lack of an electric quadrupole moment can lead to a reduction of the measured resonance peak width. Thus our own resonance line width could be even further reduced for non-quadrupolar nuclei. Second, the work done at HIMAC provides another example that optimizing the homogeneity and stability of the main magnetic field has a large impact on the recorded resonance. Last, an excellent SNR has been achieved using the π -pulse method, even though 50% of the nuclear polarisation is lost during implantation into the water container and ^{17}N has a moderate β -decay asymmetry factor of 0.25. Pulsed-NMR would be a valuable addition to the available techniques at the ISOLDE β -NMR setup.

The setup at ISAC [132], [197], [198], on the other hand, uses a high field

magnet that can be set at various field strengths (2.5 to 6.55T in the referenced works). The production of the radioactive beam is of the same type (ISOL) as the one used in ISOLDE. However, unlike ISOLDE, the radioactive beam is continuous, as it is produced by a continuous 500 MeV proton beam from a cyclotron. This is in contrast to the pulsed structure (every 1.2s) of the 1.4 GeV proton beam which arrives at ISOLDE. The different energy of the proton driver also means that some of the production channels for radioactive ions available at ISOLDE are not possible at ISAC. The resulting low-energy ion beam is transported, neutralized, and polarized in a very similar way as is done at ISOLDE. However, the laser light is coupled anti-co-linearly rather than co-linearly. Next, the polarized atom beam is re-ionized in a He gas cell and transported via two 45° benders to the detection chamber. The ultra-high vacuum detection chamber is located on a high-voltage platform which allows deceleration of the beam to control the implantation energy and thus the implantation depth. As the detection chamber is housed in a solenoidal superconducting magnet, the β -decay asymmetry is of the front/back orientation rather than left/right, thus an annular front detector is placed in the beam path upstream from the sample. The homogeneity of the applied field is, however, sub-optimal, with 10 ppm over the central 1 cm³ [198], while conventional NMR spectrometer magnets usually achieve a sub-ppm homogeneity. The setup was originally designed for solid-state material science studies. A sample holder for liquids has been added recently and in the referenced works ⁸Li and ³²Mg have been used to investigate both RTILs and ATP dissolved in a RTIL. Notable in these works is the high SNR. The use of an external solid-state reference, however, puts a limit on the achievable accuracy. On the other hand, the internally referenced peaks give significant chemical information not yet achieved at ISOLDE.

As already discussed in chapter 3 and during the comparison with the work done at HIMAC, the methods put forth in this thesis allow for the determination of nuclear magnetic dipole moments with high accuracy and precision for a wide array of unstable isotopes. By making use of different production techniques (ISOL/inflight/neutron capture) and polarization techniques (laser optical pumping, polarized thermal neutron capture, nuclear reactions, tilted foils) many different isotopes can potentially be studied using β -NMR. Even isotopes that would have a particularly low β -decay asymmetry factor might be

used by combining β -NMR with β - γ correlations, resulting in a γ -gated β -NMR measurement. By correlating the β -particles with the energy of the following γ -radiation the decay branch can be identified. This will allow the untangling of the contribution of the various decay branches to the measured experimental β -decay asymmetry, allowing to improve the SNR.

The significance of the above developments at CERN, HIMAC, and TRIUMF can not be understated. There is no other technique than liquid-state β -NMR that can determine the magnetic moments of short-lived nuclei with such precision. When combined with improved measurements of the hyperfine structure, it can also be used to determine the distribution of magnetization inside unstable nuclei. This distribution is affected by the valence proton and/or neutron. It thus gives an insight into the internal structure of the nucleus, complementary to the electric charge-based interactions which are purely caused by the distribution of the protons. In addition, liquid-state β -NMR opens up the way for measurements with chemical elements heretofore difficult, if not impossible, to probe using classical NMR. This could yield chemical information on e.g. interactions between ions and proteins, RNA or DNA, helping to better understand biocatalysts, solvents for new generation liquid batteries, etc.

To further expand the above studies and the possibilities of the setup at ISOLDE, the following investigations and improvements are also recommended, complementing the previously mentioned. First of all, the logical next step is performing the DNA alkali-ion interaction studies that have been one of the driving forces for this work. A prime example of this is the interaction between Na or K and GQs. Furthermore, an extension and diversification of the used isotopes would greatly improve the possible studies, and this will be beneficial for possible (bio)-chemical investigations [2], [199]. A wider selection of elements, half-lives, and nuclear properties would be essential for this application. Examples of isotopes to start with would be: $^{37,47,49}\text{K}$ and $^{39,51,53}\text{Ca}$, which would add two common biologically relevant elements to those already in the β -NMR probes palette. The reason to start with these would be the following: The asymmetry factor of ^{37}K has recently been studied with very high precision [200]. This gives an upper bound on the expected experimental β -decay asymmetry that can be observed. The half-life of 1.2s [201], the spin of 3/2 with a quadrupole moment of 0.109 barn [202] and a historical (SC) ISOLDE

yield of 7.10×10^6 ions/ μC [4] would make this isotope an example case for the β -NMR setup at ISOLDE. The only two changes to the setup needed to polarise potassium would be to add a fiber between the laser lab and the beamline that can transmit the IR, 766 nm, light needed for the polarization of K in the D2 line, and to fill the charge exchange cell with stable potassium instead of sodium to allow for resonant charge exchange. Next, adding a spin 1/2 nucleus would allow for a new type of K studies, as there is no stable isotope of K that has a spin of 1/2. ^{47}K and ^{49}K are prime candidates, especially as they have previously been studied with laser spectroscopy at the COLLAPS setup at ISOLDE [203]–[205], although they also present certain drawbacks. ^{47}K has a very simple decay scheme, which allows for a straightforward computation of the β -decay asymmetry factor (0.2), assuming 50% Gamow-Teller Decay, for the primary decay branch (79.8%) which has a $\Delta I = 0$. However, ^{47}K has a relatively long half-life of 17.5 s, which might cause problems for β -NMR. This is because if the relaxation is much shorter than the half-life, the part of the measured β -radiation coming from already relaxed nuclei will add to the unpolarised background and thus worsen the SNR. In addition, the inter-pulse delay will still have to be chosen in such a way that the majority of the activity of the previous (relaxed) bunch has decayed before the next bunch arrives, causing the data to be coming less often. With a sufficiently high yield and polarization, the problem of a long half-life might be overcome by only taking into account the β -decays that arrived within one period of relaxation. ^{49}K , on the other hand, has a half-life of 1.26 s which makes it very suitable for β -NMR applications at ISOLDE. However, due to its β -decay feeding into many excited states of ^{49}Ca with unassigned spins, no useful bounds can be set on the β -decay asymmetry factor. This is a clear risk factor compared to the other two potassium isotopes.

One optimization possible for these potassium isotopes is the installation of the PMTs in the optical detection section directly after the charge exchange cell. This allows the observation of a fluorescence signal when the resonance condition between the atom beam and the laser light is met, thus excluding a possible reason for not being able to see an asymmetry signal. The absence of an asymmetry is then inherent to the nuclei and not due to the setup. To be able to measure the fluorescence signal, care must be taken to avoid reflections of the excitation light reaching the PMTs. As this will require a narrow laser

beam it will enforce more stringent requirements to the ion beam profile as well, because the laser beam-ion beam overlap has to be maintained.

In addition to potassium, also the calcium isotopes could be a suitable physics application for the newly established method of measuring precise and accurate magnetic moments. Previously studied at ISOLDE with the ISOLTRAP [206] and COLLAPS [207]–[209] experiments, the neutron-rich calcium isotopes have been of high interest for understanding the nuclear forces and testing nuclear theory. This is due to their closed proton shell ($Z = 20$) and spanning several neutron (sub)shell closures ($N = 20, 28$, and newly established 32 and 34 [210]) in ^{40}Ca , ^{48}Ca , ^{52}Ca and ^{54}Ca . It was reported that the change in the mean-square charge radius shows an unexpectedly large increase from $N = 28$ onward [207]. This could be caused by the existence of neutron halo orbits in these neutron-rich nuclei [211]. To test this hypothesis, experimental information about neutron distribution in the nucleus is essential. The hyperfine anomaly that was mentioned earlier gives an insight into the distribution of magnetization within the nucleus and can be interpreted in terms of the radius of the nuclear magnetization. Only unpaired nucleons contribute to the nuclear magnetization, thus the proposed (valence) halo neutron would thus determine the nuclear magnetization radius. To determine the hyperfine anomaly, a precise determination of the nuclear magnetic dipole moment is needed. However, such a measurement for calcium nuclei poses several challenges. The first is the low production yields at ISOLDE, with ^{53}Ca having a reported yield of only 100 ions/s [209]. Second, it is not possible to calculate the expected β -decay asymmetry. In the case of ^{51}Ca , the majority of the spins of the excited states populated by the decay to ^{51}Sc have not been assigned. For ^{53}Ca , 44% of the decays have not even been mapped to a specific excited state in ^{53}Sc . However, 56% of the feeding which has been mapped feeds to an excited state in ^{51}Sc state which has a nuclear spin assignment of $I = \frac{3}{2}$. This results in a spin change of $\Delta I = 1$ which has a β -decay asymmetry factor of 0.33. Depending on the unmapped 44% a moderate average β -decay asymmetry factor can be possible. Last, to achieve a high degree of nuclear spin polarisation one should implement multi-step optical pumping as has been done in the selective charge exchange (ROC) experiments at the COLLAPS setup [209]. Alternatively, a multi-frequency pumping scheme has to be developed as has been done for the

³⁵Ar experiments at VITO [53].

When non-alkali metal elements will be used for β -NMR experiments, an accessible transition for optical pumping might not exist in an atom but rather in a singly-charged ion. To allow the optical pumping of ions, the beamline has to be upgraded by the addition of a long electrode in the optical pumping region which can be set at the same potential as applied to the voltage scanner.

A development that could further increase the polarization of the implanted beam is an atomic spin filter based on the Stern-Gerlach effect. This would however lower the number of nuclei in the implanted beam. Though initially considered feasible only for atomic beams, recent simulations have shown possible implementations for cooled low-energy ion beams [212]. Even though a significant engineering effort it might be worth the investment.

Another improvement would be the engineering of a low-viscosity liquid sample holder. The viscosity of the solvent impacts the ion mobility in the solution, which in turn can influence the chemical reaction/interaction speed and the rate of molecular tumbling. For these reasons the viscous liquids that were used until now, due to easier handling, might hinder the creation of the chemical species under examination within the observation window. Furthermore, the anisotropic environment might not be fully averaged out, which would lead to a broadening of the observed resonance peaks. Therefore, the use of lower-viscosity solvents might be advantageous to the setup.

Finally, beamtime at ISOLDE and similar facilities is costly and in high demand. However, with the current modus operandi at ISOLDE's β -NMR setup, only one-third or even fewer potentially available proton pulses are used during beam times, because the previously deposited activity needs to decay before the next polarized beam is added. To make better use of the beam one could envision a setup similar to the one at TRIUMF, where a He Gas Cell re-ionizes the neutralized beam. The beam then goes through a switchyard, which can send it to different and complementary measurement stations on a "pulse" by "pulse" basis.

Acronyms

NMR	nuclear magnetic resonance	16
β-NMR	beta decay asymmetry detected nuclear magnetic resonance . .	16
RIB	radioactive ion beam	16
RTIL	room temperature ionic liquid	98
HIMAC	Heavy Ion Medical Accelerator in Chiba	99
PSB	proton synchrotron booster	37
SNR	signal to noise ratio	99
GQ	Guanine Quadruplex	34
PMT	Photo Multiplier Tube	45
SC	Synchro-Cyclotron	38
HRS	High Resolution Separator	41
GPS	General Purpose Separator	41
VITO	Versatile Ion-polarized Techniques On-line	43
CEC	Charge Exchange Chamber	45
RFQ	Radio Frequency Quadrupole	38
LINAC	linear accelerator	37
EPR	Electron Paramagnetic Resonance	17
μSR	Muon Spin Resonance	17
CW	Continuous Wave	26

List of Figures

1.1	A magnetic dipole acts like a compass	19
1.2	A particle with spin start processing when placed in a magnetic field	20
1.3	Angular momentum eigen values	21
1.4	Rotating reference frame	23
1.5	longitudinal and transversal relaxation	24
1.6	Resonant field as seen from the rotating frame	25
1.7	Hyperfine structure of the ^{26}Na D2 line for optical pumping . .	32
1.8	the Paschen-Back effect	33
1.9	The G-Quadruplex structure	35
1.10	CERN's accelerator complex	37
1.11	ISOLDE Low-Energy Experimental Hall	39
1.12	ISOLDE Target Cut-through	41
1.13	ISOLDE Front End	42
1.14	VITO beamline	44
1.15	CEC and 5° internals	46
1.16	Transitional Field	48
2.1	Detailed picture of a double layered printed circuit board shim coil.	57
2.2	Exploded view of the experimental measurement chamber	58
2.3	Sample exchange ladder	60
2.4	Magnetic field stability over time	62
2.5	Magnetic field homogeneity	63
2.6	Magnetic field over the sample space	64

LIST OF FIGURES

2.7	Comparison between the resonance width of ^{26}Na in a solid state host and a liquid state host	65
3.1	Laser-polarization beam line topv view	78
3.2	β -NMR detection chamber	79
3.3	^{26}Na β -NMR spectra in BMIM-HCOO and EMIM-DCA.	84
3.4	Ratio of the magnetic moments of ^{26}Na and ^{23}Na	85

List of Tables

1.1	Asymmetry factor values	28
3.1	Larmor frequencies of ^{26}Na and ^{23}Na	85
3.2	Sodium NMR shielding in the $\text{Na}^+(\text{H}_2\text{O})_6$ complex.	89
3.3	$\mu(^{23}\text{Na})/\mu_N$ reference nuclear magnetic dipole moment	89
3.4	Magnetic moments and other nuclear properties of $^{23,26-31}\text{Na}$	90

Bibliography

- [1] A. Jancso, J. G. Correia, A. Gottberg, *et al.*, “TDPAC and β -NMR applications in chemistry and biochemistry,” *Journal of Physics G: Nuclear and Particle Physics*, vol. 44, no. 6, p. 064003, Jun. 2017, ISSN: 0954-3899. DOI: [10.1088/1361-6471/aa666b](https://doi.org/10.1088/1361-6471/aa666b). [Online]. Available: <https://iopscience.iop.org/article/10.1088/1361-6471/aa666b>.
- [2] B. Karg and M. Kowalska, “Liquid β -NMR Studies of the Interaction of Na and K Cations with DNA G-quadruplex Structures,” CERN, Geneva, Tech. Rep., 2020. [Online]. Available: <https://cds.cern.ch/record/2717964>.
- [3] A. Gottberg, M. Stachura, M. Kowalska, *et al.*, “Billion-Fold Enhancement in Sensitivity of Nuclear Magnetic Resonance Spectroscopy for Magnesium Ions in Solution,” *ChemPhysChem*, vol. 15, no. 18, pp. 3929–3932, Dec. 2014, ISSN: 14394235. DOI: [10.1002/cphc.201402619](https://doi.org/10.1002/cphc.201402619). [Online]. Available: <https://onlinelibrary.wiley.com/doi/10.1002/cphc.201402619>.
- [4] J. Ballof, A. Molander, M. Turrion, *et al.*, *ISOLDE Yield Database*, <https://isoyields2.web.cern.ch/>, Accessed: 2022-10-03.
- [5] N. Stone, “Table of nuclear magnetic dipole and electric quadrupole moments,” *Atomic Data and Nuclear Data Tables*, vol. 90, no. 1, pp. 75–176, May 2005, ISSN: 0092640X. DOI: [10.1016/j.adt.2005.04.001](https://doi.org/10.1016/j.adt.2005.04.001). [Online]. Available: <https://linkinghub.elsevier.com/retrieve/pii/S0092640X05000239>.
- [6] M. H. Levitt, *Spin Dynamics: Basics of Nuclear Magnetic Resonance*, 2nd ed. John Wiley and Sons Ltd, 2008, p. 740, ISBN: 0470511176.

-
- [7] A. Abragam, *The Principles of Nuclear Magnetism*, 1st ed. Oxford University Press, 1961, ISBN: 9780198520146. [Online]. Available: https://books.google.nl/books?id=9M8U%5C_JK7K54C.
- [8] G. Hagen, A. Ekström, C. Forssén, *et al.*, “Neutron and Weak-Charge Distributions of the ^{48}Ca Nucleus,” *Nature Physics*, vol. 12, no. 2, pp. 186–190, 2016, ISSN: 17452481. DOI: [10.1038/nphys3529](https://doi.org/10.1038/nphys3529).
- [9] M. Thiel, C. Sfienti, J. Piekarewicz, C. J. Horowitz, and M. Vanderhaeghen, “Neutron skins of atomic nuclei: per aspera ad astra,” *Journal of Physics G: Nuclear and Particle Physics*, vol. 46, no. 9, p. 093003, Sep. 2019, ISSN: 0954-3899. DOI: [10.1088/1361-6471/ab2c6d](https://doi.org/10.1088/1361-6471/ab2c6d). [Online]. Available: <https://iopscience.iop.org/article/10.1088/1361-6471/ab2c6d>.
- [10] J. Croese, M. Baranowski, M. L. Bissell, *et al.*, “High-accuracy liquid-sample β -NMR setup at ISOLDE,” *Nuclear Instruments and Methods in Physics Research Section A: Accelerators, Spectrometers, Detectors and Associated Equipment*, vol. 1020, p. 165862, 2021, ISSN: 0168-9002. DOI: <https://doi.org/10.1016/j.nima.2021.165862>. [Online]. Available: <https://www.sciencedirect.com/science/article/pii/S0168900221008470>.
- [11] R. D. Harding, S. Pallada, J. Croese, *et al.*, “Magnetic Moments of Short-Lived Nuclei with Part-per-Million Accuracy: Toward Novel Applications of β -Detected NMR in Physics, Chemistry, and Biology,” *Physical Review X*, vol. 10, no. 4, p. 41061, 2020, ISSN: 21603308. DOI: [10.1103/PhysRevX.10.041061](https://doi.org/10.1103/PhysRevX.10.041061). [Online]. Available: <https://doi.org/10.1103/PhysRevX.10.041061>.
- [12] I. I. Rabi, J. R. Zacharias, S. Millman, and P. Kusch, “A New Method of Measuring Nuclear Magnetic Moment,” *Physical Review*, vol. 53, no. 4, p. 318, Feb. 1938, ISSN: 0031-899X. DOI: [10.1103/PhysRev.53.318](https://doi.org/10.1103/PhysRev.53.318). [Online]. Available: <https://link.aps.org/doi/10.1103/PhysRev.53.318>.

BIBLIOGRAPHY

- [13] F. Bloch, W. W. Hansen, and M. Packard, “Nuclear Induction,” *Physical Review*, vol. 69, no. 3-4, pp. 127–127, Feb. 1946, ISSN: 0031-899X. DOI: [10.1103/PhysRev.69.127](https://doi.org/10.1103/PhysRev.69.127).
- [14] E. M. Purcell, H. C. Torrey, and R. V. Pound, “Resonance Absorption by Nuclear Magnetic Moments in a Solid,” *Physical Review*, vol. 69, no. 1-2, pp. 37–38, Jan. 1946, ISSN: 0031-899X. DOI: [10.1103/PhysRev.69.37](https://doi.org/10.1103/PhysRev.69.37).
- [15] M. H. Levitt, *Singlet and Other States with Extended Lifetimes*, Mar. 2010. DOI: [doi:10.1002/9780470034590.emrstm1036](https://doi.org/10.1002/9780470034590.emrstm1036). [Online]. Available: <https://doi.org/10.1002/9780470034590.emrstm1036>.
- [16] C. P. Slichter, *Principles of magnetic resonance* (Springer Series in Solid-State Sciences), en, 3rd ed. Berlin, Germany: Springer, Dec. 1989.
- [17] J. Keeler, *Understanding NMR Spectroscopy*, en, 2nd ed. John Wiley and Sons Inc, Apr. 2010.
- [18] D. J. Griffiths, *Introduction to electrodynamics*, en, 3rd ed. Upper Saddle River, NJ: Pearson, Dec. 1998.
- [19] K. Krane, *Introductory nuclear physics*, 1st ed. New York: John Wiley and Sons, 1988, p. 862, ISBN: 047180553X.
- [20] J. A. M. Cox, “Theory of the radiation from oriented nuclei,” Ph.D. dissertation, Leiden University, Leiden, The Netherlands, 1954.
- [21] N. J. Stone and H. Postma, *Low Temperature Nuclear Orientation*, 1st ed. Amsterdam: Elsevier Science Pub. Co, 1986.
- [22] C. S. Wu, E. Ambler, R. W. Hayward, D. D. Hoppes, and R. P. Hudson, “Experimental Test of Parity Conservation in Beta Decay,” *Phys. Rev.*, vol. 105, no. 4, pp. 1413–1415, Feb. 1957. DOI: [10.1103/PhysRev.105.1413](https://doi.org/10.1103/PhysRev.105.1413). [Online]. Available: <https://link.aps.org/doi/10.1103/PhysRev.105.1413>.
- [23] R. D. Harding, “Laser-assisted spectroscopy of Au and Na isotopes at ISOLDE,” Ph.D. dissertation, University of York, York, United Kingdom, 2020.

- [24] W. MacFarlane, “Implanted-ion β NMR: A new probe for nanoscience,” *Solid State Nuclear Magnetic Resonance*, vol. 68-69, pp. 1–12, Jun. 2015, ISSN: 09262040. DOI: [10.1016/j.ssnmr.2015.02.004](https://doi.org/10.1016/j.ssnmr.2015.02.004). [Online]. Available: <https://linkinghub.elsevier.com/retrieve/pii/S0926204015000181>.
- [25] M.-Y. Kim, H. Vankayalapati, K. Shin-ya, K. Wierzba, and L. H. Hurley, “Telomestatin, a potent telomerase inhibitor that interacts quite specifically with the human telomeric intramolecular g-quadruplex,” *Journal of the American Chemical Society*, vol. 124, no. 10, pp. 2098–2099, Feb. 2002. DOI: [10.1021/ja017308q](https://doi.org/10.1021/ja017308q). [Online]. Available: <https://doi.org/10.1021/ja017308q>.
- [26] T.-Y. Tseng, S.-Y. Liu, C.-L. Wang, and T.-C. Chang, “Antisense oligonucleotides used to identify telomeric g-quadruplexes in metaphase chromosomes and fixed cells by fluorescence lifetime imaging microscopy of o-BMVC foci,” *Molecules*, vol. 25, no. 18, p. 4083, Sep. 2020. DOI: [10.3390/molecules25184083](https://doi.org/10.3390/molecules25184083). [Online]. Available: <https://doi.org/10.3390/molecules25184083>.
- [27] A. M. Fleming, Y. Ding, and C. J. Burrows, “Oxidative DNA damage is epigenetic by regulating gene transcription via base excision repair,” *Proceedings of the National Academy of Sciences*, vol. 114, no. 10, pp. 2604–2609, Jan. 2017. DOI: [10.1073/pnas.1619809114](https://doi.org/10.1073/pnas.1619809114). [Online]. Available: <https://doi.org/10.1073/pnas.1619809114>.
- [28] C. Wang, G. Jia, J. Zhou, *et al.*, “Enantioselective Diels–Alder Reactions with G-Quadruplex DNA- Based Catalysts,” *Angewandte Chemie (International ed. in English)*, vol. 2, no. 3, pp. 9352–9355, 2012. DOI: [10.1002/anie.201204850](https://doi.org/10.1002/anie.201204850).
- [29] J. Zhou and J. Rossi, “Aptamers as targeted therapeutics: Current potential and challenges,” *Nature Reviews Drug Discovery*, vol. 16, no. 3, pp. 181–202, Nov. 2016. DOI: [10.1038/nrd.2016.199](https://doi.org/10.1038/nrd.2016.199). [Online]. Available: <https://doi.org/10.1038/nrd.2016.199>.
- [30] A. Ambrus, D. Chen, J. Dai, R. A. Jones, and D. Yang, “Solution structure of the biologically relevant g-quadruplex element in the human c-MYC promoter. implications for g-quadruplex stabilization,” *Biochem-*

BIBLIOGRAPHY

- istry*, vol. 44, no. 6, pp. 2048–2058, Jan. 2005. DOI: [10.1021/bi048242p](https://doi.org/10.1021/bi048242p). [Online]. Available: <https://doi.org/10.1021/bi048242p>.
- [31] A. Bohr, “Nuclear magnetic moments and atomic hyperfine structure,” *Physical Review*, vol. 81, no. 3, pp. 331–335, 1951, ISSN: 0031899X. DOI: [10.1103/PhysRev.81.331](https://doi.org/10.1103/PhysRev.81.331).
- [32] A. Antusek, N. Azaryan, M. Baranowski, *et al.*, “Magnetic moment of ^{11}Be with ppm accuracy,” CERN, Geneva, Tech. Rep., 2023. [Online]. Available: <https://cds.cern.ch/record/2845944>.
- [33] E. Mobs, *The CERN Accelerator complex*, <https://cds.cern.ch/record/2684277>, Accessed: 2021-08-05, Jul. 2019.
- [34] E. Kugler, “The ISOLDE facility,” *Hyperfine Interactions*, vol. 129, no. 1/4, pp. 23–42, 2000, ISSN: 03043834. DOI: [10.1023/A:1012603025802](https://doi.org/10.1023/A:1012603025802).
- [35] *Supercycles for LHC commissioning and Operation*, CERN, Geneva: CERN, 2001, pp. 37–40. [Online]. Available: <https://cds.cern.ch/record/567170>.
- [36] C. CERN Education and O. Group, “CERN Annual report 2017,” CERN, Geneva, Tech. Rep., 2018, pp. 22–23. [Online]. Available: <https://cds.cern.ch/record/2624296>.
- [37] C. CERN Education and O. Group, “CERN Annual report 2018,” CERN, Geneva, Tech. Rep., 2019, p. 25. DOI: [10.17181/AnnualReport2018](https://doi.org/10.17181/AnnualReport2018). [Online]. Available: <https://cds.cern.ch/record/2671714>.
- [38] B. Jonson and A. Richter, “More than three decades of ISOLDE physics,” *Hyperfine Interactions*, vol. 129, no. 1/4, pp. 1–22, 2000, ISSN: 03043834. DOI: [10.1023/A:1012689128103](https://doi.org/10.1023/A:1012689128103).
- [39] M. J. G. Borge and B. Jonson, “ISOLDE past, present and future,” *Journal of Physics G: Nuclear and Particle Physics*, vol. 44, no. 4, p. 044011, Apr. 2017, ISSN: 0954-3899. DOI: [10.1088/1361-6471/aa5f03](https://doi.org/10.1088/1361-6471/aa5f03).
- [40] M. Borge, “Highlights of the ISOLDE facility and the HIE-ISOLDE project,” *Nuclear Instruments and Methods in Physics Research Section B: Beam Interactions with Materials and Atoms*, vol. 376, pp. 408–412, Jun. 2016, ISSN: 0168583X. DOI: [10.1016/j.nimb.2015.12.048](https://doi.org/10.1016/j.nimb.2015.12.048).

-
- [41] T. Giles, “Isolde V,” *Nuclear Instruments and Methods in Physics Research Section B: Beam Interactions with Materials and Atoms*, vol. 463, pp. 254–257, Jan. 2020, ISSN: 0168583X. DOI: [10.1016/j.nimb.2019.05.025](https://doi.org/10.1016/j.nimb.2019.05.025).
- [42] R. Catherall, T. Giles, and G. Neyens, “Exploiting the Potential of ISOLDE at CERN (the EPIC Project),” in *Proc. 10th International Particle Accelerator Conference (IPAC’19), Melbourne, Australia, 19-24 May 2019*, (Melbourne, Australia), ser. International Particle Accelerator Conference, Geneva, Switzerland: JACoW Publishing, Jun. 2019, pp. 3706–3708, ISBN: 978-3-95450-208-0. DOI: [doi:10.18429/JACoW-IPAC2019-THPGW053](https://doi.org/10.18429/JACoW-IPAC2019-THPGW053). [Online]. Available: <http://jacow.org/ipac2019/papers/thpgw053.pdf>.
- [43] M. Borge and Y. Kadi, “ISOLDE at CERN,” *Nuclear Physics News*, vol. 26, no. 4, pp. 6–13, Oct. 2016, ISSN: 1061-9127. DOI: [10.1080/10619127.2016.1249214](https://doi.org/10.1080/10619127.2016.1249214).
- [44] *ISOLDE Layouts and Logos*, <https://isolde.web.cern.ch/isolde-logos-layouts-and-templates>, Accessed: 2023-01-09.
- [45] E. Bouquerel, R. Catherall, M. Eller, *et al.*, “Purification of a Zn radioactive ion beam by alkali suppression in a quartz line target prototype,” *The European Physical Journal Special Topics*, vol. 150, no. 1, pp. 277–280, Nov. 2007, ISSN: 1951-6355. DOI: [10.1140/epjst/e2007-00323-4](https://doi.org/10.1140/epjst/e2007-00323-4). [Online]. Available: <http://link.springer.com/10.1140/epjst/e2007-00323-4>.
- [46] R. Catherall, J. Lettry, S. Gilardoni, and U. Köster, “Radioactive ion beams produced by neutron-induced fission at ISOLDE,” *Nuclear Instruments and Methods in Physics Research Section B: Beam Interactions with Materials and Atoms*, vol. 204, pp. 235–239, May 2003, ISSN: 0168583X. DOI: [10.1016/S0168-583X\(02\)01915-8](https://doi.org/10.1016/S0168-583X(02)01915-8). [Online]. Available: <https://linkinghub.elsevier.com/retrieve/pii/S0168583X02019158>.
- [47] J. Ramos, M. Ballan, L. Egoriti, *et al.*, “Design and tests for the new CERN-ISOLDE spallation source: an integrated tungsten converter surrounded by an annular UC target operated at 2000°C,” *Nuclear In-*

- struments and Methods in Physics Research Section B: Beam Interactions with Materials and Atoms*, vol. 463, pp. 357–363, Jan. 2020, ISSN: 0168583X. DOI: [10.1016/j.nimb.2019.04.060](https://doi.org/10.1016/j.nimb.2019.04.060). [Online]. Available: <https://linkinghub.elsevier.com/retrieve/pii/S0168583X19302484>.
- [48] J. P. Fernandes Pinto Ramos, “Titanium carbide-carbon porous nanocomposite materials for radioactive ion beam production: processing, sintering and isotope release properties,” Ph.D. dissertation, EPFL, Lausanne, Switzerland, 2017. DOI: [10.5075/epfl-thesis-7363](https://doi.org/10.5075/epfl-thesis-7363).
- [49] J. F. Baugh, C. E. Burkhardt, J. J. Leventhal, and T. Bergeman, “Precision Stark spectroscopy of sodium 2P and 2D states,” *Physical Review A*, vol. 58, no. 2, p. 1585, Aug. 1998, ISSN: 10941622. DOI: [10.1103/PhysRevA.58.1585](https://doi.org/10.1103/PhysRevA.58.1585). [Online]. Available: <https://journals.aps.org/prabstract/10.1103/PhysRevA.58.1585>.
- [50] R. Catherall, W. Andreazza, M. Breitenfeldt, *et al.*, “The ISOLDE facility,” *Journal of Physics G: Nuclear and Particle Physics*, vol. 44, no. 9, p. 094002, Sep. 2017, ISSN: 0954-3899. DOI: [10.1088/1361-6471/aa7eba](https://doi.org/10.1088/1361-6471/aa7eba). [Online]. Available: <https://iopscience.iop.org/article/10.1088/1361-6471/aa7eba>.
- [51] E. Mane, J. Billowes, K. Blaum, *et al.*, “An ion cooler-buncher for high-sensitivity collinear laser spectroscopy at ISOLDE,” *EUROPEAN PHYSICAL JOURNAL A*, vol. 42, no. 3, pp. 503–507, Dec. 2009, ISSN: 1434-6001. DOI: [10.1140/epja/i2009-10828-0](https://doi.org/10.1140/epja/i2009-10828-0).
- [52] M. Stachura, A. Gottberg, K. Johnston, *et al.*, “Versatile Ion-polarized Techniques On-line (VITO) experiment at ISOLDE-CERN,” *Nuclear Instruments and Methods in Physics Research Section B: Beam Interactions with Materials and Atoms*, vol. 376, pp. 369–373, Jun. 2016, ISSN: 0168583X. DOI: [10.1016/j.nimb.2016.02.030](https://doi.org/10.1016/j.nimb.2016.02.030).
- [53] W. Gins, R. D. Harding, M. Baranowski, *et al.*, “A new beamline for laser spin-polarization at ISOLDE,” *Nuclear Instruments and Methods in Physics Research Section A: Accelerators, Spectrometers, Detectors and Associated Equipment*, vol. 925, no. 1, pp. 24–32, 2019. DOI: [https://](https://doi.org/10.1016/j.nucphysa.2019.03.001)

- doi.org/10.1016/j.nima.2019.01.082. [Online]. Available: <http://www.sciencedirect.com/science/article/pii/S0168900219301536>.
- [54] M. Kowalska, P. Aschenbrenner, M. Baranowski, *et al.*, “New laser polarization line at the ISOLDE facility,” *Journal of Physics G: Nuclear and Particle Physics*, vol. 44, no. 8, p. 084005, Aug. 2017, ISSN: 0954-3899. DOI: [10.1088/1361-6471/aa77d7](https://doi.org/10.1088/1361-6471/aa77d7). [Online]. Available: <http://dx.doi.org/10.1088/1361-6471/aa77d7%20http://stacks.iop.org/0954-3899/44/i=8/a=084005?key=crossref.07759a8b6b4dbbf8d3c47fb20b5dae8e>.
- [55] W. Gins, “Development of a dedicated laser-polarization beamline for ISOLDE-CERN,” Ph.D. dissertation, University of Leuven, Leuven, Belgium, 2019.
- [56] K. Kreim, M. L. Bissell, J. Papuga, *et al.*, “Nuclear charge radii of potassium isotopes beyond $N = 28$,” *Physics Letters, Section B: Nuclear, Elementary Particle and High-Energy Physics*, vol. 731, pp. 97–102, 2014, ISSN: 03702693. DOI: [10.1016/j.physletb.2014.02.012](https://doi.org/10.1016/j.physletb.2014.02.012). [Online]. Available: <http://dx.doi.org/10.1016/j.physletb.2014.02.012>.
- [57] H. T. Törnqvist, “Tilted Foils Nuclear Spin Polarization at REX-ISOLDE,” Ph.D. dissertation, Chalmers University of Technology, Göteborg, Sweden, 2013. [Online]. Available: <https://cds.cern.ch/record/1640821>.
- [58] R. Neugart, D. L. Balabanski, K. Blaum, *et al.*, “Precision Measurement of Li11 Moments: Influence of Halo Neutrons on the Li9 Core,” *Physical Review Letters*, vol. 101, no. 13, 2008. DOI: [10.1103/physrevlett.101.132502](https://doi.org/10.1103/physrevlett.101.132502). [Online]. Available: <https://doi.org/10.1103/physrevlett.101.132502>.
- [59] G. Neyens, M. Kowalska, D. Yordanov, *et al.*, “Measurement of the spin and magnetic moment of ^{31}Mg : Evidence for a strongly deformed intruder ground state,” *Physical Review Letters*, vol. 94, no. 2, Jan. 2005, ISSN: 00319007. DOI: [10.1103/PhysRevLett.94.022501](https://doi.org/10.1103/PhysRevLett.94.022501).
- [60] Y. Blumenfeld, T. Nilsson, and P. V. Duppen, “Facilities and Methods for Radioactive Ion Beam Production,” *Physica Scripta*, vol. T152, p. 014023, 2013. DOI: [10.1088/0031-8949/2013/t152/014023](https://doi.org/10.1088/0031-8949/2013/t152/014023). [Online]. Available: <https://doi.org/10.1088/0031-8949/2013/t152/014023>.

- [61] A. Gottberg, “Target Materials for Exotic ISOL Beams,” *Nuclear Instruments and Methods in Physics Research Section B: Beam Interactions with Materials and Atoms*, vol. 376, pp. 8–15, Jun. 2016. DOI: [10.1016/j.nimb.2016.01.020](https://doi.org/10.1016/j.nimb.2016.01.020). [Online]. Available: <https://doi.org/10.1016/j.nimb.2016.01.020>.
- [62] M. Kowalska and *et al.*, “NMR on unstable nuclei,” *Progress in Nuclear Magnetic Resonance Spectroscopy*, under review, 2021.
- [63] E. Arnold, J. Bonn, R. Gegenwart, *et al.*, “NUCLEAR SPIN AND MAGNETIC MOMENT OF ^{11}Li ,” *Phys. Lett. B*, vol. 197, no. 3, p. 311, 1987. DOI: [10.1016/0370-2693\(87\)90390-X](https://doi.org/10.1016/0370-2693(87)90390-X).
- [64] W. Geithner, S. Kappertz, M. Keim, *et al.*, “Measurement of the magnetic moment of the one-neutron halo nucleus ^{11}Be ,” *Physical Review Letters*, vol. 83, no. 19, pp. 3792–3795, Jan. 1999, ISSN: 10797114. DOI: [10.1103/PhysRevLett.83.3792](https://doi.org/10.1103/PhysRevLett.83.3792).
- [65] M. Keim, U. Georg, A. Klein, *et al.*, “Measurement of the electric quadrupole moments of $^{26-29}\text{Na}$,” *The European Physical Journal A*, vol. 8, no. 1, pp. 31–40, 2000, ISSN: 1434-601X. DOI: [10.1007/s100500070117](https://doi.org/10.1007/s100500070117). [Online]. Available: <https://doi.org/10.1007/s100500070117>.
- [66] W. A. MacFarlane, Q. Song, N. J. Ingle, *et al.*, “ β -detected NMR spin relaxation in a thin film heterostructure of ferromagnetic EuO ,” *Physical Review B - Condensed Matter and Materials Physics*, vol. 92, no. 6, pp. 1–7, 2015, ISSN: 1550235X. DOI: [10.1103/PhysRevB.92.064409](https://doi.org/10.1103/PhysRevB.92.064409).
- [67] B. Blümich, “Low-field and Benchtop NMR,” *Journal of Magnetic Resonance*, vol. 306, pp. 27–35, 2019. DOI: [10.1016/j.jmr.2019.07.030](https://doi.org/10.1016/j.jmr.2019.07.030). [Online]. Available: <https://doi.org/10.1016/j.jmr.2019.07.030>.
- [68] M. J. Minkler, J. M. Kim, V. V. Shinde, and B. S. Beckingham, “Low-Field ^1H NMR Spectroscopy: Factors Impacting Signal-to-Noise Ratio and Experimental Time in the Context of Mixed Microstructure Polyisoprenes,” *Magnetic Resonance in Chemistry*, vol. 58, pp. 1168–1176, 12 2020. DOI: [10.1002/mrc.5022](https://doi.org/10.1002/mrc.5022). [Online]. Available: <https://doi.org/10.1002/mrc.5022>.

- [69] R. A. Scott, Ed., *Encyclopedia of Inorganic and Bioinorganic Chemistry*, 1st ed. Wiley, 2011. DOI: [10.1002/9781119951438](https://doi.org/10.1002/9781119951438). [Online]. Available: <https://doi.org/10.1002/9781119951438>.
- [70] C. Elliott, V. Vijayakumar, W. Zink, and R. Hansen, “National Instruments LabVIEW: A Programming Environment for Laboratory Automation and Measurement,” *Journal of Laboratory Automation*, vol. 12, no. 1, pp. 17–24, 2007, ISSN: 15402452. DOI: [10.1016/j.jala.2006.07.012](https://doi.org/10.1016/j.jala.2006.07.012).
- [71] P. Garbacz, K. Jackowski, W. Makulski, and R. E. Wasylshen, “Nuclear magnetic shielding for hydrogen in selected isolated molecules,” *Journal of Physical Chemistry A*, vol. 116, no. 48, pp. 11 896–11 904, 2012, ISSN: 10895639. DOI: [10.1021/jp309820v](https://doi.org/10.1021/jp309820v).
- [72] W. Makulski, “The Radiofrequency NMR Spectra of Lithium Salts in Water; Reevaluation of Nuclear Magnetic Moments for ^6Li and ^7Li Nuclei,” *Magnetochemistry*, vol. 4, no. 1, p. 9, Jan. 2018, ISSN: 2312-7481. DOI: [10.3390/magnetochemistry4010009](https://doi.org/10.3390/magnetochemistry4010009). [Online]. Available: <http://www.mdpi.com/2312-7481/4/1/9>.
- [73] G. Schneider, A. Mooser, M. Bohman, *et al.*, “Double-Trap Measurement of the Proton Magnetic Moment at 0.3 Parts Per Billion Precision,” *Science*, vol. 358, pp. 1081–1084, 6366 2017. DOI: [10.1126/science.aan0207](https://doi.org/10.1126/science.aan0207). [Online]. Available: <https://doi.org/10.1126/science.aan0207>.
- [74] H. H. Günthard and J. J. Primas, *Generating of Homogeneous Static Magnetic Fields*, 1960. [Online]. Available: <https://patentimages.storage.googleapis.com/66/ae/22/9e7cda1eed807b/US2953727.pdf>.
- [75] M. Mihara, T. Sugihara, M. Fukuda, *et al.*, “Beta-NMR of short-lived nucleus ^{17}N in liquids,” *Hyperfine Interactions*, vol. 240, no. 1, p. 113, Dec. 2019, ISSN: 0304-3843. DOI: [10.1007/s10751-019-1650-3](https://doi.org/10.1007/s10751-019-1650-3). [Online]. Available: <http://link.springer.com/10.1007/s10751-019-1650-3>.
- [76] D. T. Yordanov, M. Kowalska, K. Blaum, *et al.*, “Spin and magnetic moment of ^{33}Mg : Evidence for a negative-parity intruder ground state,” *Physical Review Letters*, vol. 99, no. 21, Nov. 2007. DOI: [10.1103/](https://doi.org/10.1103/PhysRevLett.99.211101)

- [physrevlett.99.212501](https://doi.org/10.1103/physrevlett.99.212501). [Online]. Available: <https://doi.org/10.1103/physrevlett.99.212501>.
- [77] W. Rogers, D. Clark, S. Dutta, and A. Martin, "Measurement of the Magnetic Moment of ^{33}Cl using On-Line Beta-Nuclear Magnetic Resonance," *Physics Letters B*, vol. 177, no. 3-4, pp. 293–298, 1986. DOI: [10.1016/0370-2693\(86\)90755-0](https://doi.org/10.1016/0370-2693(86)90755-0). [Online]. Available: [https://doi.org/10.1016/0370-2693\(86\)90755-0](https://doi.org/10.1016/0370-2693(86)90755-0).
- [78] D. Connor and T. Tsang, "Sign of the Li8 Magnetic Moment," *Physical Review*, vol. 126, no. 4, pp. 1506–1507, 1962. DOI: [10.1103/physrev.126.1506](https://doi.org/10.1103/physrev.126.1506). [Online]. Available: <https://doi.org/10.1103/physrev.126.1506>.
- [79] K. Matsuta, M. Fukuda, M. Tanigaki, *et al.*, "Magnetic Moment of Proton Drip-Line Nucleus ^9C ," *Nuclear Physics A*, vol. 588, pp. 153–156, 1995. DOI: [10.1016/0375-9474\(95\)00115-h](https://doi.org/10.1016/0375-9474(95)00115-h). [Online]. Available: [https://doi.org/10.1016/0375-9474\(95\)00115-h](https://doi.org/10.1016/0375-9474(95)00115-h).
- [80] H. Stroke, H. Duong, and J. Pinard, "Bohr–Weisskopf effect: influence of the distributed nuclear magnetization on hfs," *Hyperfine Interactions*, vol. 129, no. 1/4, pp. 319–335, 2000. DOI: [10.1023/a:1012630404421](https://doi.org/10.1023/a:1012630404421). [Online]. Available: <https://doi.org/10.1023/a:1012630404421>.
- [81] J. R. Persson, "Table of hyperfine anomaly in atomic systems," *Atomic Data and Nuclear Data Tables*, vol. 99, no. 1, pp. 62–68, 2013, ISSN: 0092640X. DOI: [10.1016/j.adt.2012.04.002](https://doi.org/10.1016/j.adt.2012.04.002). [Online]. Available: <http://dx.doi.org/10.1016/j.adt.2012.04.002>.
- [82] R. R. Crichton, *Biological Inorganic Chemistry: A New Introduction to Molecular Structure and Function*, 3rd ed. Elsevier, 2019, ISBN: 978-0-12-811741-5.
- [83] R. R. Crichton and R. O. Louro, *Practical Approaches to Biological Inorganic Chemistry*, 2nd ed. Elsevier, 2020.
- [84] J. Carvalho, J.-L. Mergny, G. F. Salgado, J. A. Queiroz, and C. Cruz, "G-quadruplex, Friend or Foe: The Role of the G-quartet in Anticancer Strategies," *Trends in Molecular Medicine*, vol. 26, no. 9, pp. 848–861,

2020. DOI: [10.1016/j.molmed.2020.05.002](https://doi.org/10.1016/j.molmed.2020.05.002). [Online]. Available: <https://doi.org/10.1016/j.molmed.2020.05.002>.
- [85] G. Wu, A. Wong, Z. Gan, and J. T. Davis, “Direct Detection of Potassium Cations Bound to G-Quadruplex Structures by Solid-State ^{39}K NMR at 19.6 T,” *Journal of the American Chemical Society*, vol. 125, no. 24, pp. 7182–7183, Jun. 2003, ISSN: 0002-7863. DOI: [10.1021/ja0340634](https://doi.org/10.1021/ja0340634).
- [86] A. Wong, R. Ida, and G. Wu, “Direct NMR detection of the “invisible” alkali metal cations tightly bound to G-quadruplex structures,” *Biochemical and Biophysical Research Communications*, vol. 337, no. 1, pp. 363–366, 2005, ISSN: 0006-291X. DOI: <https://doi.org/10.1016/j.bbrc.2005.08.275>. [Online]. Available: <http://www.sciencedirect.com/science/article/pii/S0006291X05019674>.
- [87] A. Wong, F. W. Kotch, I. C. Kwan, J. T. Davis, and G. Wu, “Probing the Na^+ binding site in a calix[4]arene-guanosine conjugate dimer by solid-state ^{23}Na NMR and quantum chemical calculation,” *Chemical Communications*, no. 16, pp. 2154–2156, 2009, ISSN: 13597345. DOI: [10.1039/b900442d](https://doi.org/10.1039/b900442d).
- [88] G. Neyens, “Nuclear magnetic and quadrupole moments for nuclear structure research on exotic nuclei,” *Reports on Progress in Physics*, vol. 66, no. 4, pp. 633–689, Apr. 2003. DOI: [10.1088/0034-4885/66/4/205](https://doi.org/10.1088/0034-4885/66/4/205).
- [89] S. Raeder, D. Ackermann, H. Backe, *et al.*, “Probing Sizes and Shapes of Nobelium Isotopes by Laser Spectroscopy,” *Physical Review Letters*, vol. 120, no. 23, p. 232 503, 2018, ISSN: 10797114. DOI: [10.1103/PhysRevLett.120.232503](https://doi.org/10.1103/PhysRevLett.120.232503). [Online]. Available: <https://doi.org/10.1103/PhysRevLett.120.232503>.
- [90] R. Neugart and G. Neyens, “Nuclear Moments,” in *The Euroschool Lectures on Physics with Exotic Beams*, edited by J. Al-Khalili and E. Roeckl (Springer Berlin Heidelberg, Berlin, Heidelberg): Vol.II, 2006, pp. 135–189.
- [91] K. Asahi and K. Matsuta, “Nuclear Electromagnetic Moments β -NMR and its Applications,” *Nuclear Physics A*, vol. 693, pp. 63–76, 2001.

BIBLIOGRAPHY

- [92] T. Ohtsubo, N. J. Stone, J. R. Stone, *et al.*, “Magnetic Dipole Moment of the Doubly-Closed-shell Plus One Proton Nucleus ^{49}Sc ,” *Physical Review Letters*, vol. 109, p. 032 504, 3 2012.
- [93] X. Yang, C. Wraith, L. Xie, *et al.*, “Isomer Shift and Magnetic Moment of the Long-Lived $1/2^+$ Isomer in ^{49}Zn 3079: Signature of Shape Coexistence near ^{78}Ni ,” *Physical Review Letters*, vol. 116, no. 18, 2016, ISSN: 10797114. DOI: [10.1103/PhysRevLett.116.182502](https://doi.org/10.1103/PhysRevLett.116.182502).
- [94] J. Thielking, M. V. Okhapkin, P. Głowacki, *et al.*, “Laser spectroscopic characterization of the nuclear-clock isomer $^{229\text{m}}\text{Th}$,” *Nature*, vol. 556, no. 7701, pp. 321–325, 2018, ISSN: 14764687. DOI: [10.1038/s41586-018-0011-8](https://doi.org/10.1038/s41586-018-0011-8).
- [95] N. Minkov and A. Pálffy, “Theoretical Predictions for the Magnetic Dipole Moment of $^{229\text{m}}\text{Th}$,” *Physical Review Letters*, vol. 122, no. 16, p. 162 502, 2019, ISSN: 10797114. DOI: [10.1103/PhysRevLett.122.162502](https://doi.org/10.1103/PhysRevLett.122.162502). [Online]. Available: <https://doi.org/10.1103/PhysRevLett.122.162502>.
- [96] Y. Ichikawa, H. Nishibata, Y. Tsunoda, *et al.*, “Inter-play Between Nuclear Shell Evolution and Shape Deformation Revealed by the Magnetic Moment of ^{75}Cu ,” *Nature Physics*, vol. 15, pp. 321–325, 2019.
- [97] G. A. Webb, Ed., *Modern Magnetic Resonance*, 2nd ed. Springer International Publishing, 2018, ISBN: 978-3-319-28387-6. DOI: [10.1007/978-3-319-28388-3](https://doi.org/10.1007/978-3-319-28388-3). [Online]. Available: <https://doi.org/10.1007/978-3-319-28388-3>.
- [98] The Nuclear Magnetic Resonance Society of Japan, Ed., *Experimental Approaches of NMR Spectroscopy: Methodology and Application to Life Science and Materials Science*, 1st ed. Springer Singapore, 2018, ISBN: 978-981-10-5965-0. DOI: [10.1007/978-981-10-5966-7](https://doi.org/10.1007/978-981-10-5966-7). [Online]. Available: <https://doi.org/10.1007/978-981-10-5966-7>.
- [99] E. M. Purcell, “Research in Nuclear Magnetism,” *Science*, vol. 118, pp. 431–436, 1953.

-
- [100] E. B. Baker and L. W. Build, “Spectrometer for all Nuclei Using a Frequency Synthesizer,” *Review of Scientific Instruments*, vol. 34, pp. 238–243, 1963.
- [101] B. W. Epperlein, H. Kruger, and L. A. Schwenk, “The Magnetic Moment of ^{67}Zn and the Shielding of Zinc Ions by Water,” *Physics Letters*, vol. 45, pp. 255–256, 1973.
- [102] O. Lutz and H. Oehler, “Zeitschrift Physik A ^{63}Cu and ^{65}Cu Fourier Transform Nuclear Magnetic Resonance Studies,” *Zeitschrift für Physik A Hadrons and nuclei*, vol. 21, pp. 17–21, 1978. [Online]. Available: <https://link.springer.com/article/10.1007%2F01408195>.
- [103] T. Helgaker, M. Jaszunski, and K. Ruud, “Ab Initio Methods for the Calculation of NMR Shielding and In-direct Spin-Spin Coupling Constants,” *Chemical Reviews*, vol. 99, pp. 293–352, 1999.
- [104] M. Kaupp, M. Bühl, and V. G. Malkin, Eds., *Calculation of NMR and EPR Parameters*, 1st ed. Wiley, 2004. DOI: [10.1002/3527601678](https://doi.org/10.1002/3527601678). [Online]. Available: <https://doi.org/10.1002/3527601678>.
- [105] A. Antušek, K. Jackowski, M. Jaszunski, W. Makulski, and M. Wilczek, “Nuclear Magnetic Dipole Moments from NMR Spectra,” *Chemical Physics Letters*, vol. 411, no. 1-3, pp. 111–116, 2005. DOI: [10.1016/j.cplett.2005.06.022](https://doi.org/10.1016/j.cplett.2005.06.022). [Online]. Available: <https://doi.org/10.1016/j.cplett.2005.06.022>.
- [106] M. Jaszunski, A. Antušek, P. Garbacz, K. Jackowski, W. Makulski, and M. Wilczek, “The Determination of Accurate Nuclear Magnetic Dipole Moments and Direct Measurement of NMR Shielding Constants,” *Progress in Nuclear Magnetic Resonance Spectroscopy*, vol. 67, pp. 49–63, 2012.
- [107] B. Adrjan, W. Makulski, K. Jackowski, *et al.*, “NMR Absolute Shielding Scale and Nuclear Magnetic Dipole Moment of ^{207}Pb ,” *Physical Chemistry Chemical Physics*, vol. 18, pp. 16483–16490, 2016. DOI: [10.1039/C6CP01781A](https://doi.org/10.1039/C6CP01781A). [Online]. Available: <http://dx.doi.org/10.1039/C6CP01781A>.

BIBLIOGRAPHY

- [108] L. V. Skripnikov, S. Schmidt, J. Ullmann, *et al.*, “New Nuclear Magnetic Moment of ^{209}Bi : Resolving the Bismuth Hyperfine Puzzle,” *Physical Review Letters*, vol. 120, no. 9, p. 93001, Feb. 2018. DOI: [10.1103/PhysRevLett.120.093001](https://doi.org/10.1103/PhysRevLett.120.093001). [Online]. Available: <https://link.aps.org/doi/10.1103/PhysRevLett.120.093001>.
- [109] A. Antušek, M. Repisky, M. Jaszuński, K. Jackowski, W. Makulski, and M. Misiak, “Nuclear Magnetic Dipole Moment of ^{209}Bi from NMR Experiments,” *Physical Review A*, vol. 98, p. 052509, 5 2018. DOI: [10.1103/PhysRevA.98.052509](https://doi.org/10.1103/PhysRevA.98.052509). [Online]. Available: <https://link.aps.org/doi/10.1103/PhysRevA.98.052509>.
- [110] A. Antušek and M. Repisky, “NMR Absolute Shielding Scales and Nuclear Magnetic Dipole Moments of Transition Metal Nuclei,” *Physical Chemistry Chemical Physics*, vol. 22, pp. 7065–7076, 13 2020. DOI: [10.1039/D0CP00115E](https://doi.org/10.1039/D0CP00115E). [Online]. Available: <http://dx.doi.org/10.1039/D0CP00115E>.
- [111] M. G. H. Gustavsson and A.-M. Mårtensson-Pendrill, “Need for Remeasurements of Nuclear Magnetic Dipole Moments,” *Physical Review A*, vol. 58, pp. 3611–3618, 5 1998. DOI: [10.1103/PhysRevA.58.3611](https://doi.org/10.1103/PhysRevA.58.3611). [Online]. Available: <https://link.aps.org/doi/10.1103/PhysRevA.58.3611>.
- [112] P. Indelicato, “QED tests with highly charged ions,” *Journal of Physics B: Atomic, Molecular and Optical Physics*, vol. 52, no. 23, 2019, ISSN: 13616455. DOI: [10.1088/1361-6455/ab42c9](https://doi.org/10.1088/1361-6455/ab42c9).
- [113] J. Ullmann, Z. Andelkovic, C. Brandau, *et al.*, “High Precision Hyperfine Measurements in Bismuth Challenge Bound-state Strong-field QED,” *Nature Communications*, vol. 8, no. 1, p. 15484, 2017, ISSN: 2041-1723. [Online]. Available: <http://www.nature.com/articles/ncomms15484>.
- [114] K. Jackowski, M. Jaszuński, and M. Wilczek, “Alternative Approach to the Standardization of NMR Spectra. Direct Measurement of Nuclear Magnetic Shielding in Molecules,” *The Journal of Physical Chemistry A*, vol. 114, no. 7, pp. 2471–2475, 2010. DOI: [10.1021/jp9096056](https://doi.org/10.1021/jp9096056). [Online]. Available: <https://doi.org/10.1021/jp9096056>.

- [115] N. Bloembergen and G. M. Temmer, “Nuclear Magnetic Resonance of Aligned Radioactive Nuclei,” *Physical Review*, vol. 89, pp. 883–883, 4 1953. DOI: [10.1103/PhysRev.89.883](https://doi.org/10.1103/PhysRev.89.883). [Online]. Available: <https://link.aps.org/doi/10.1103/PhysRev.89.883>.
- [116] D. A. Shirley, “Radiative Detection of Nuclear Magnetic Resonance,” *Analytical Chemistry*, vol. 41, no. 8, pp. 69–74, 1969. DOI: [10.1021/ac60277a764](https://doi.org/10.1021/ac60277a764).
- [117] D. Connor, “Measurement of the Nuclear g Factor of Li^8 ,” *Physical Review Letters*, vol. 3, pp. 429–431, 9 1959. DOI: [10.1103/PhysRevLett.3.429](https://doi.org/10.1103/PhysRevLett.3.429). [Online]. Available: <https://link.aps.org/doi/10.1103/PhysRevLett.3.429>.
- [118] H. Ogawa, K. Asahi, H. Ueno, *et al.*, “Assignment of the Ground-State Spin-Parity for ^{17}C through g -Factor Measurement,” *Progress of Theoretical Physics Supplements*, vol. 146, pp. 607–608, 2002, ISSN: 0375-9687. DOI: [10.1143/PTPS.146.607](https://doi.org/10.1143/PTPS.146.607). eprint: <https://academic.oup.com/ptps/article-pdf/doi/10.1143/PTPS.146.607/5275115/146-607.pdf>. [Online]. Available: <https://doi.org/10.1143/PTPS.146.607>.
- [119] A. Winnacker, H. Ackermann, D. Dubbers, M. Grupp, P. Heitjans, and H.-J. Stoeck-Mann, “Nuclear Moments of the β -emitters ^{108}Ag and ^{110}Ag ,” *Nuclear Physics A*, vol. 261, no. 2, pp. 261–268, 1976, ISSN: 0375-9474. DOI: [https://doi.org/10.1016/0375-9474\(76\)90569-8](https://doi.org/10.1016/0375-9474(76)90569-8). [Online]. Available: <http://www.sciencedirect.com/science/article/pii/0375947476905698>.
- [120] H. Okuno, K. Asahi, H. Ueno, *et al.*, “Measurement of the Magnetic Moments of ^{14}B and ^{15}B Using Projectile Fragmentation Spin Polarization,” *Physics Letters B*, vol. 354, no. 1, pp. 41–45, 1995, ISSN: 0370-2693. DOI: [https://doi.org/10.1016/0370-2693\(95\)00630-4](https://doi.org/10.1016/0370-2693(95)00630-4). [Online]. Available: <http://www.sciencedirect.com/science/article/pii/0370269395006304>.
- [121] T. Onishi and K. Yoshida, “Nuclear Magnetic Moment of Proton Drip-line Nucleus ^9C ,” *Nuclear Physics A*, vol. 588, pp. 153–156, 1995.

- [122] K. Matsuta, T. Minamisono, M. Tanigaki, *et al.*, “Magnetic moments of proton drip-line nuclei ^{13}O and ^9C ,” *Hyperfine Interactions*, vol. 97-98, no. 1, pp. 519–526, Dec. 1996, ISSN: 0304-3834. DOI: [10.1007/BF02150194](https://doi.org/10.1007/BF02150194). [Online]. Available: <http://link.springer.com/10.1007/BF02150194>.
- [123] H. Ueno, K. Asahi, H. Izumi, *et al.*, “Magnetic Moments of ^{17}N and ^{17}B ,” *Physical Review C*, vol. 53, pp. 2142–2151, 5 1996. DOI: [10.1103/PhysRevC.53.2142](https://doi.org/10.1103/PhysRevC.53.2142). [Online]. Available: <https://link.aps.org/doi/10.1103/PhysRevC.53.2142>.
- [124] M. Mihara, R. Matsumiya, K. Shimomura, *et al.*, “Shallow Nitrogen Acceptor in TiO_2 Studied by β -NMR Spectroscopy,” *Physica B: Condensed Matter*, vol. 401-402, pp. 430–432, 2007, ISSN: 0921-4526. DOI: <https://doi.org/10.1016/j.physb.2007.08.204>. [Online]. Available: <http://www.sciencedirect.com/science/article/pii/S0921452607007491>.
- [125] Z. Salman, O. Ofer, M. Radovic, *et al.*, “Nature of Weak Magnetism in $\text{SrTiO}_3/\text{LaAlO}_3$ Multilayers,” *Physical Review Letters*, vol. 109, no. 25, p. 257 207, 2012. DOI: [10.1103/physrevlett.109.257207](https://doi.org/10.1103/physrevlett.109.257207). [Online]. Available: <https://doi.org/10.1103/physrevlett.109.257207>.
- [126] W. A. MacFarlane, C. B. L. Tschense, T. Buck, *et al.*, “ β -Detected NMR of $^8\text{Li}^+$ in Bi, Sb, and the Topological Insulator $\text{Bi}_{0.9}\text{Sb}_{0.1}$,” *Physical Review B*, vol. 90, no. 21, p. 214 422, 2014. DOI: [10.1103/PhysRevB.90.214422](https://doi.org/10.1103/PhysRevB.90.214422). [Online]. Available: <https://doi.org/10.1103/physrevb.90.214422>.
- [127] I. McKenzie, M. Harada, R. F. Kiefl, *et al.*, “ β -NMR Measurements of Lithium Ion Transport in Thin Films of Pure and Lithium-Salt-Doped Poly(ethylene oxide),” *Journal of the American Chemical Society*, vol. 136, no. 22, pp. 7833–7836, 2014. DOI: [10.1021/ja503066a](https://doi.org/10.1021/ja503066a). [Online]. Available: <https://doi.org/10.1021/ja503066a>.
- [128] D. L. Cortie, T. Buck, M. H. Dehn, *et al.*, “Spin fluctuations in the exotic metallic state of Sr_2RuO_4 studied with β -NMR,” *Physical Review B - Condensed Matter and Materials Physics*, vol. 91, no. 24, pp. 1–6, 2015, ISSN: 1550235X. DOI: [10.1103/PhysRevB.91.241113](https://doi.org/10.1103/PhysRevB.91.241113).

- [129] D. L. Cortie, T. Buck, M. H. Dehn, *et al.*, “ β -NMR Investigation of the Depth-Dependent Magnetic Properties of an Antiferromagnetic Surface,” *Physical Review Letters*, vol. 116, no. 10, pp. 1–5, 2016, ISSN: 10797114. DOI: [10.1103/PhysRevLett.116.106103](https://doi.org/10.1103/PhysRevLett.116.106103).
- [130] J. Sugiyama, I. Umegaki, T. Uyama, *et al.*, “Lithium Diffusion in Spinel $\text{Li}_4\text{Ti}_5\text{O}_{12}$ and LiTi_2O_4 Films Detected with ^8Li β -NMR,” *Physical Review B*, vol. 96, p. 094402, 9 2017. DOI: [10.1103/PhysRevB.96.094402](https://doi.org/10.1103/PhysRevB.96.094402). [Online]. Available: <https://link.aps.org/doi/10.1103/PhysRevB.96.094402>.
- [131] T. Sugihara, M. Mihara, J. Shimaya, *et al.*, “NMR detection of short-lived β -emitter ^{12}N implanted in water,” *Hyperfine Interactions*, vol. 238, no. 1, p. 20, Nov. 2017, ISSN: 0304-3843. DOI: [10.1007/s10751-017-1401-2](https://doi.org/10.1007/s10751-017-1401-2). [Online]. Available: <http://link.springer.com/10.1007/s10751-017-1401-2>.
- [132] D. Szunyogh, R. M. L. McFadden, V. L. Karner, *et al.*, “Direct observation of Mg^{2+} complexes in ionic liquid solutions by ^{31}Mg β -NMR spectroscopy,” *Dalton Transactions*, vol. 47, no. 41, pp. 14431–14435, 2018, ISSN: 1477-9226. DOI: [10.1039/C8DT02350F](https://doi.org/10.1039/C8DT02350F). [Online]. Available: <http://xlink.rsc.org/?DOI=C8DT02350F>.
- [133] W. A. MacFarlane, T. J. Parolin, D. L. Cortie, *et al.*, “ ^8Li in the Cubic Insulator MgO ,” *Journal of Physics: Conference Series*, vol. 551, p. 012033, 2014. DOI: [10.1088/1742-6596/551/1/012033](https://doi.org/10.1088/1742-6596/551/1/012033).
- [134] M. Puchalski and K. Pachucki, “Ground-state hyperfine splitting in the Be^+ ion,” *Physical Review A - Atomic, Molecular, and Optical Physics*, vol. 89, no. 3, pp. 1–7, 2014, ISSN: 10502947. DOI: [10.1103/PhysRevA.89.032510](https://doi.org/10.1103/PhysRevA.89.032510).
- [135] A. Takamine, M. Wada, K. Okada, *et al.*, “Towards High Precision Measurements of Nuclear g-Factors for the Be Isotopes,” *Nuclear Instruments and Methods in Physics Research Section B: Beam Interactions with Materials and Atoms*, vol. 376, pp. 307–310, 2016. DOI: [10.1016/j.nimb.2015.12.027](https://doi.org/10.1016/j.nimb.2015.12.027). [Online]. Available: <https://doi.org/10.1016/j.nimb.2015.12.027>.

BIBLIOGRAPHY

- [136] A. Bohr and V. F. Weisskopf, “The influence of nuclear structure on the hyperfine structure of heavy elements,” *Physical Review*, vol. 77, no. 1, pp. 94–98, 1950, ISSN: 0031899X. DOI: [10.1103/PhysRev.77.94](https://doi.org/10.1103/PhysRev.77.94).
- [137] F. F. Karpeshin and M. B. Trzhaskovskaya, “The Theory of the Bohr–Weisskopf Effect in the Hyperfine Structure,” *Nuclear Physics A*, vol. 941, pp. 66–77, 2015, ISSN: 0375-9474. DOI: [10.1016/j.nuclphysa.2015.06.001](https://doi.org/10.1016/j.nuclphysa.2015.06.001). [Online]. Available: <http://dx.doi.org/10.1016/j.nuclphysa.2015.06.001>.
- [138] J. R. Persson, “Hyperfine anomalies in Gd and Nd,” *Atoms*, vol. 6, no. 4, pp. 2–6, 2018, ISSN: 22182004. DOI: [10.3390/atoms6040063](https://doi.org/10.3390/atoms6040063).
- [139] M. J. Borge and K. Blaum, “Focus on Exotic Beams at ISOLDE: A Laboratory Portrait,” *Journal of Physics G: Nuclear and Particle Physics*, vol. 45, no. 1, pp. 1–2, Jan. 2018. DOI: [10.1088/1361-6471/aa990f](https://doi.org/10.1088/1361-6471/aa990f).
- [140] A. Abragam, *The Principles of Nuclear Magnetism* (International series of monographs on physics), 3rd ed. Oxford: Clarendon Press, 1989. [Online]. Available: <https://cds.cern.ch/record/109195>.
- [141] M. Bier and S. Dietrich, “Vapour Pressure of Ionic Liquids,” *Molecular Physics*, vol. 108, no. 2, pp. 211–214, 2010, ISSN: 00268976. DOI: [10.1080/00268971003604609](https://doi.org/10.1080/00268971003604609).
- [142] E. D. Becker, *High Resolution NMR: Theory and Chemical Applications*, 3rd ed. Academic Press, 2000, ISBN: 9780120846627.
- [143] S. Eidelman, K. Hayes, K. Olive, *et al.*, “Review of Particle Physics,” *Physics Letters B*, vol. 592, no. 1, pp. 1–5, 2004, Review of Particle Physics, ISSN: 0370-2693. DOI: <https://doi.org/10.1016/j.physletb.2004.06.001>. [Online]. Available: <https://www.sciencedirect.com/science/article/pii/S0370269304007579>.
- [144] G. Huber, F. Touchard, S. Büttgenbach, *et al.*, “Spins, Magnetic Moments, and Isotope Shifts of $^{21-31}\text{Na}$ by High Resolution Laser Spectroscopy of the Atomic D_1 Line,” *Physical Review C*, vol. 18, pp. 2342–2354, 5 1978. DOI: [10.1103/PhysRevC.18.2342](https://doi.org/10.1103/PhysRevC.18.2342). [Online]. Available: <https://link.aps.org/doi/10.1103/PhysRevC.18.2342>.

- [145] P. Raghavan, “Table of Nuclear Moments,” *Atomic Data and Nuclear Data Tables*, vol. 42, pp. 189–291, 2 1989. DOI: [10.1016/0092-640X\(89\)90008-9](https://doi.org/10.1016/0092-640X(89)90008-9).
- [146] N. C. Pyper, “Do Theory and Experiment Agree for the Nuclear Shielding Difference Between Alkali Atoms and Ions in Magnetic Resonance?” *Journal of Physics B: Atomic and Molecular Physics*, vol. 18, no. 7, pp. 1317–1332, 1985. DOI: [10.1088/0022-3700/18/7/013](https://doi.org/10.1088/0022-3700/18/7/013).
- [147] J. Mason, Ed., *Multinuclear NMR*, 1st ed. Springer US, 1987. DOI: [10.1007/978-1-4613-1783-8](https://doi.org/10.1007/978-1-4613-1783-8). [Online]. Available: <https://doi.org/10.1007/978-1-4613-1783-8>.
- [148] M. Galib, M. D. Baer, L. B. Skinner, *et al.*, “Revisiting the Hydration Structure of Aqueous Na⁺,” *The Journal of Chemical Physics*, vol. 146, no. 8, p. 084504, 2017. DOI: [10.1063/1.4975608](https://doi.org/10.1063/1.4975608). [Online]. Available: <https://doi.org/10.1063/1.4975608>.
- [149] A. Antušek, D. Kędziera, A. Kaczmarek-Kędziera, and M. Jaszurki, “Coupled Cluster Study of NMR Shielding of Alkali Metal Ions in Water Complexes and Magnetic Moments of Alkali Metal Nuclei,” *Chemical Physics Letters*, vol. 532, pp. 1–8, 2012. DOI: [10.1016/j.cplett.2012.02.036](https://doi.org/10.1016/j.cplett.2012.02.036). [Online]. Available: <https://doi.org/10.1016/j.cplett.2012.02.036>.
- [150] A. Beckmann, K. D. Böklen, and D. Elke, “Precision measurements of the nuclear magnetic dipole moments of ⁶Li, ⁷Li, ²³Na, ³⁹K and ⁴¹K,” *Zeitschrift für Physik*, vol. 270, no. 3, pp. 173–186, 1974, ISSN: 0044-3328. DOI: [10.1007/BF01680407](https://doi.org/10.1007/BF01680407). [Online]. Available: <https://doi.org/10.1007/BF01680407>.
- [151] R. K. Harris, E. D. Becker, S. M. C. de Menezes, R. Goodfellow, and P. Granger, “NMR Nomenclature. Nuclear Spin Properties and Conventions for Chemical Shifts (IUPAC Recommendations 2001),” *Pure and Applied Chemistry*, vol. 73, no. 11, pp. 1795–1818, 2001, reprinted in *Magn. Reson. in Chem.* 40 (2002). DOI: [10.1351/pac200173111795](https://doi.org/10.1351/pac200173111795). [Online]. Available: <https://doi.org/10.1351/pac200173111795>.

- [152] A. Mooser, S. Ulmer, K. Blaum, *et al.*, “Direct High-Precision Measurement of the Magnetic Moment of the Proton,” *Nature*, vol. 509, no. 7502, pp. 596–599, 2014. DOI: [10.1038/nature13388](https://doi.org/10.1038/nature13388). [Online]. Available: <https://doi.org/10.1038/nature13388>.
- [153] C. P. Slichter, “Electric Quadrupole Effects,” in *Principles of Magnetic Resonance*, Berlin, Heidelberg: Springer Berlin Heidelberg, 1990, pp. 485–502, ISBN: 978-3-662-09441-9. DOI: [10.1007/978-3-662-09441-9_10](https://doi.org/10.1007/978-3-662-09441-9_10). [Online]. Available: https://doi.org/10.1007/978-3-662-09441-9_10.
- [154] H. Ackermann, P. Heitjans, and H. -. Stöckmann, “Radiation defects and spin-lattice relaxation studied with neutron-activated β emitters,” *Hyperfine Interactions*, vol. 25, no. 1, pp. 395–417, 1985, ISSN: 1572-9540. DOI: [10.1007/BF02354657](https://doi.org/10.1007/BF02354657). [Online]. Available: <https://doi.org/10.1007/BF02354657>.
- [155] Y. Nojiri and B. I. Deutch, “Polarized β Emitters For NMR Probes,” *Hyperfine Interactions*, vol. 21, pp. 197–207, 1-4 1985. DOI: [10.1007/BF02061985](https://doi.org/10.1007/BF02061985). [Online]. Available: <https://doi.org/10.1007/BF02061985>.
- [156] T. P. Hanusa, “Solution NMR of the Light Main Group Metals,” in *Encyclopedia of Inorganic and Bioinorganic Chemistry*, Chichester, UK: John Wiley and Sons, Ltd, Dec. 2015, pp. 1–25. DOI: [10.1002/9781119951438.eibc2292](https://doi.org/10.1002/9781119951438.eibc2292). [Online]. Available: <https://onlinelibrary.wiley.com/doi/10.1002/9781119951438.eibc2292>.
- [157] M. Schmeisser, P. Illner, R. Puchta, A. Zahl, and R. van Eldik, “Gutmann Donor and Acceptor Numbers for Ionic Liquids,” *Chemistry A European Journal*, vol. 18, no. 35, pp. 10969–10982, 2012. DOI: [10.1002/chem.201200584](https://doi.org/10.1002/chem.201200584). eprint: <https://chemistry-europe.onlinelibrary.wiley.com/doi/pdf/10.1002/chem.201200584>. [Online]. Available: <https://chemistry-europe.onlinelibrary.wiley.com/doi/abs/10.1002/chem.201200584>.
- [158] J. A. Tossell, “Na⁺ Complexes with Crown Ethers: Calculation of ²³Na NMR Shieldings and Quadrupole Coupling Constants,” *The Journal of Physical Chemistry B*, vol. 105, no. 45, pp. 11060–11066, 2001. DOI:

- 10.1021/jp0115143. eprint: <https://doi.org/10.1021/jp0115143>. [Online]. Available: <https://doi.org/10.1021/jp0115143>.
- [159] C. H. McMillen, C. K. Gren, T. P. Hanusa, and A. L. Rheingold, “A Tetrameric Allyl Complex of Sodium, and Computational Modeling of the ^{23}Na Allyl Chemical Shift,” *Inorganica Chimica Acta*, vol. 364, no. 1, pp. 61–68, 2010, Special Volume: Dedication to Professor Rheingold, ISSN: 0020-1693. DOI: <https://doi.org/10.1016/j.ica.2010.07.079>. [Online]. Available: <http://www.sciencedirect.com/science/article/pii/S0020169310005566>.
- [160] A. Sigel, Ed., *Metal Ions in Biological Systems*, 1st ed. CRC Press, 2001. DOI: [10.1201/9781482270150](https://doi.org/10.1201/9781482270150). [Online]. Available: <https://doi.org/10.1201/9781482270150>.
- [161] P. J. Sadler, “Interplay between Metal Ions and Nucleic Acids. Metal Ions in Life Sciences Series, Vol. 10. Edited by Astrid Sigel, Helmut Sigel and Roland K. O. Sigel,” *Angewandte Chemie International Edition*, vol. 51, no. 31, pp. 7632–7632, 2012. DOI: <https://doi.org/10.1002/anie.201203501>. eprint: <https://onlinelibrary.wiley.com/doi/pdf/10.1002/anie.201203501>. [Online]. Available: <https://onlinelibrary.wiley.com/doi/abs/10.1002/anie.201203501>.
- [162] F. G. Riddell, “NMR spectroscopy of alkali metal nuclei in solution,” *Encyclopedia of Spectroscopy and Spectrometry*, vol. 2, pp. 239–246, 2016. DOI: [10.1016/B978-0-12-803224-4.00096-0](https://doi.org/10.1016/B978-0-12-803224-4.00096-0).
- [163] M. Thiel, C. Sfienti, J. Piekarewicz, C. J. Horowitz, and M. Vanderhaeghen, “Neutron Skins of Atomic Nuclei: Per Aspera ad Astra,” *Journal of Physics G: Nuclear and Particle Physics*, vol. 46, no. 9, p. 093003, 2019. DOI: [10.1088/1361-6471/ab2c6d](https://doi.org/10.1088/1361-6471/ab2c6d).
- [164] T. Aumann, C. A. Bertulani, F. Schindler, and S. Typel, “Peeling Off Neutron Skins from Neutron-Rich Nuclei: Constraints on the Symmetry Energy from Neutron-Removal Cross Sections,” *Physical Review Letters*, vol. 119, p. 262501, 26 2017. DOI: [10.1103/PhysRevLett.119.262501](https://doi.org/10.1103/PhysRevLett.119.262501). [Online]. Available: <https://link.aps.org/doi/10.1103/PhysRevLett.119.262501>.

BIBLIOGRAPHY

- [165] J. Erler, N. Birge, M. Kortelainen, *et al.*, “The Limits of the Nuclear Landscape,” *Nature*, vol. 486, no. 7404, pp. 509–512, 2012, ISSN: 00280836. DOI: [10.1038/nature11188](https://doi.org/10.1038/nature11188).
- [166] I. Tanihata, H. Hamagaki, O. Hashimoto, *et al.*, “Measurements of Interaction Cross Sections and Nuclear Radii in the Light p -Shell Region,” *Physical Review Letters*, vol. 55, pp. 2676–2679, 24 1985. DOI: [10.1103/PhysRevLett.55.2676](https://doi.org/10.1103/PhysRevLett.55.2676). [Online]. Available: <https://link.aps.org/doi/10.1103/PhysRevLett.55.2676>.
- [167] I. Tanihata, “Neutron Halo Nuclei,” *Journal of Physics G: Nuclear and Particle Physics*, vol. 22, no. 2, pp. 157–198, 1996. DOI: [10.1088/0954-3899/22/2/004](https://doi.org/10.1088/0954-3899/22/2/004).
- [168] J. Al-Khalili, “An Introduction to Halo Nuclei,” in *The Euroschool Lectures on Physics with Exotic Beams, Vol. I*, Springer Berlin Heidelberg, 2004, pp. 77–112. DOI: [10.1007/978-3-540-44490-9_3](https://doi.org/10.1007/978-3-540-44490-9_3). [Online]. Available: https://doi.org/10.1007/978-3-540-44490-9_3.
- [169] H. H. Stroke, H. T. Duong, and J. Pinard, “Bohr-Weisskopf Effect: Influence of the Distributed Nuclear Magnetization on HFS,” *Hyperfine Interactions*, vol. 129, pp. 319–335, 2000.
- [170] Y. L. Parfenova and C. Leclercq-Willain, “Hyperfine Anomaly in Be Isotopes and the Neutron Spatial Distribution: A Three-Cluster Model for Be9,” *Physical Review C - Nuclear Physics*, vol. 72, no. 5, pp. 1–7, 2005, ISSN: 1089490X. DOI: [10.1103/PhysRevC.72.054304](https://doi.org/10.1103/PhysRevC.72.054304).
- [171] G. Malli and C. Froese, “Nuclear Magnetic Shielding Constants Calculated from Numerical Hartree-Fock Wave Functions,” *International Journal of Quantum Chemistry*, vol. 1, no. S1, pp. 95–98, 2009. DOI: [10.1002/qua.560010610](https://doi.org/10.1002/qua.560010610). [Online]. Available: <https://doi.org/10.1002/qua.560010610>.
- [172] S. Komorovsky, M. Repisky, K. Ruud, O. L. Malkina, and V. G. Malkin, “Four-Component Relativistic Density Functional Theory Calculations of NMR Shielding Tensors for Paramagnetic Systems,” *The Journal of Physical Chemistry A*, vol. 117, no. 51, pp. 14209–14219, 2013. DOI:

- [10.1021/jp408389h](https://doi.org/10.1021/jp408389h). [Online]. Available: <https://doi.org/10.1021/jp408389h>.
- [173] K. G. Dyall, “Relativistic Quadruple-Zeta and Revised Triple-Zeta and Double-Zeta Basis Sets for the 4p, 5p, and 6p Elements,” *Theoretical Chemistry Accounts*, vol. 115, no. 5, pp. 441–447, 2006. DOI: [10.1007/s00214-006-0126-0](https://doi.org/10.1007/s00214-006-0126-0). [Online]. Available: <https://doi.org/10.1007/s00214-006-0126-0>.
- [174] A. D. Becke, “Density-Functional Exchange-Energy Approximation with Correct Asymptotic Behavior,” *Physical Review A*, vol. 38, no. 6, pp. 3098–3100, 1988. DOI: [10.1103/physreva.38.3098](https://doi.org/10.1103/physreva.38.3098). [Online]. Available: <https://doi.org/10.1103/physreva.38.3098>.
- [175] C. Lee, W. Yang, and R. G. Parr, “Development of the Colle-Salvetti Correlation-Energy Formula into a Functional of the Electron Density,” *Physical Review B*, vol. 37, no. 2, pp. 785–789, 1988. DOI: [10.1103/physrevb.37.785](https://doi.org/10.1103/physrevb.37.785). [Online]. Available: <https://doi.org/10.1103/physrevb.37.785>.
- [176] S. H. Vosko, L. Wilk, and M. Nusair, “Accurate Spin-Dependent Electron Liquid Correlation Energies for Local Spin Density Calculations: A Critical Analysis,” *Can. J. Phys.*, vol. 58, pp. 1200–1211, 1980. DOI: [10.1103/PhysRevB.37.785](https://doi.org/10.1103/PhysRevB.37.785).
- [177] F. Weigend and R. Ahlrichs, “Balanced Basis Sets of Split Valence, Triple Zeta Valence and Quadruple Zeta Valence Quality for H to Rn: Design and Assessment of Accuracy,” *Physical Chemistry Chemical Physics*, vol. 7, pp. 3297–3305, 2005. DOI: [10.1039/b508541a](https://doi.org/10.1039/b508541a).
- [178] S. Grimme, S. Ehrlich, and L. Goerigk, “Effect of the Damping Function in Dispersion Corrected Density Functional Theory,” *Journal of Computational Chemistry*, vol. 32, no. 7, pp. 1456–1465, 2011. DOI: [10.1002/jcc.21759](https://doi.org/10.1002/jcc.21759). [Online]. Available: <https://doi.org/10.1002/jcc.21759>.
- [179] J. Gauss and J. F. Stanton, “Gauge-Invariant Calculation of Nuclear Magnetic Shielding Constants at the Coupled-Cluster Singles and Doubles Level,” *The Journal of Chemical Physics*, vol. 102, no. 1, pp. 251–

- 253, 1995. DOI: [10.1063/1.469397](https://doi.org/10.1063/1.469397). [Online]. Available: <https://doi.org/10.1063/1.469397>.
- [180] J. D. Watts, J. Gauss, and R. J. Bartlett, "Coupled-Cluster Methods with Noniterative Triple Excitations for Restricted Open-Shell Hartree–Fock and Other General Single Determinant Reference Functions. Energies and Analytical Gradients," *The Journal of Chemical Physics*, vol. 98, no. 11, pp. 8718–8733, 1993. DOI: [10.1063/1.464480](https://doi.org/10.1063/1.464480). [Online]. Available: <https://doi.org/10.1063/1.464480>.
- [181] K. L. Schuchardt, B. T. Didier, T. Elsethagen, *et al.*, "Basis Set Exchange: A Community Database for Computational Sciences," *Journal of Chemical Information and Modeling*, vol. 47, pp. 1045–1052, 2007. DOI: [10.1021/ci600510j](https://doi.org/10.1021/ci600510j).
- [182] T. H. Dunning, "Gaussian Basis Sets for Use in Correlated Molecular Calculations. I. The Atoms Boron Through Neon and Hydrogen," *The Journal of Chemical Physics*, vol. 90, no. 2, pp. 1007–1023, 1989. DOI: [10.1063/1.456153](https://doi.org/10.1063/1.456153). [Online]. Available: <https://doi.org/10.1063/1.456153>.
- [183] F. Jensen, "Basis Set Convergence of Nuclear Magnetic Shielding Constants Calculated by Density Functional Methods," *Journal of Chemical Theory and Computation*, vol. 4, pp. 719–727, 2008. DOI: [10.1021/ct800013z](https://doi.org/10.1021/ct800013z).
- [184] K. Wolinski, J. F. Hinton, and P. Pulay, "Efficient Implementation of the Gauge-Independent Atomic Orbital Method for NMR Chemical Shift Calculations," *Journal of the American Chemical Society*, vol. 112, no. 23, pp. 8251–8260, 1990. DOI: [10.1021/ja00179a005](https://doi.org/10.1021/ja00179a005). [Online]. Available: <https://doi.org/10.1021/ja00179a005>.
- [185] A. Klamt and G. Schuurmann, "COSMO: A New Approach to Dielectric Screening in Solvents with Explicit Expressions for the Screening Energy and Its Gradient," *Journal of the Chemical Society, Perkin Transactions 2*, pp. 799–805, 5 1993. DOI: [10.1039/P29930000799](https://doi.org/10.1039/P29930000799). [Online]. Available: <http://dx.doi.org/10.1039/P29930000799>.

- [186] J. P. Perdew, M. Ernzerhof, and K. Burke, “Rationale for Mixing Exact Exchange with Density Functional Approximations,” *The Journal of Chemical Physics*, vol. 105, no. 22, pp. 9982–9985, 1996. DOI: [10.1063/1.472933](https://doi.org/10.1063/1.472933). [Online]. Available: <https://doi.org/10.1063/1.472933>.
- [187] C. Adamo and V. Barone, “Toward Reliable Density Functional Methods without Adjustable Parameters: The PBE0 Model,” *The Journal of Chemical Physics*, vol. 110, no. 13, pp. 6158–6170, 1999. DOI: [10.1063/1.478522](https://doi.org/10.1063/1.478522). [Online]. Available: <https://doi.org/10.1063/1.478522>.
- [188] S. Komorovský, M. Repiský, O. L. Malkina, V. G. Malkin, I. M. Ondík, and M. Kaupp, “A Fully Relativistic Method for Calculation of Nuclear Magnetic Shielding Tensors with a Restricted Magnetically Balanced Basis in the Framework of the Matrix Dirac–Kohn–Sham Equation,” *The Journal of Chemical Physics*, vol. 128, no. 10, p. 104 101, 2008. DOI: [10.1063/1.2837472](https://doi.org/10.1063/1.2837472). [Online]. Available: <https://doi.org/10.1063/1.2837472>.
- [189] S. Komorovský, M. Repiský, O. L. Malkina, and V. G. Malkin, “Fully Relativistic Calculations of NMR Shielding Tensors using Restricted Magnetically Balanced Basis and Gauge Including Atomic Orbitals,” *The Journal of Chemical Physics*, vol. 132, no. 15, p. 154 101, 2010. DOI: [10.1063/1.3359849](https://doi.org/10.1063/1.3359849). [Online]. Available: <https://doi.org/10.1063/1.3359849>.
- [190] L. Visscher and K. G. Dyall, “Dirac-Fock Atomic Electronic Structure Calculations Using Different Nuclear Charge Distributions,” *Atomic Data and Nuclear Data Tables*, vol. 67, no. 2, pp. 207–224, 1997. DOI: [10.1006/adnd.1997.0751](https://doi.org/10.1006/adnd.1997.0751).
- [191] M. Valiev, E. J. Bylaska, N. Govind, *et al.*, “NWChem: A Comprehensive and Scalable Open-Source Solution for Large Scale Molecular Simulations,” *Computer Physics Communications*, vol. 181, p. 1477, 2010. DOI: [10.1016/j.cpc.2010.04.018](https://doi.org/10.1016/j.cpc.2010.04.018).
- [192] CFOUR, a quantum chemical program package written by J. F. Stanton, J. Gauss, M. E. Harding, P. G. Szalay with contributions from A. A. Auer, R. J. Bartlett, U. Benedikt, C. Berger, D. E. Bernholdt, J. Bomble,

- L. Cheng, O. Christiansen, M. Heckert, O. Heun, C. Huber, T.-C. Jagau, D. Jonsson, J. Jusélius, K. Klein, W. J. Lauderdale, D. A. Matthews, T. Metzroth, L. A. Mück, D. P. O'Neill, D. R. Price, E. Prochnow, C. Puzzarini, K. Ruud, F. Schiffmann, W. Schwalbach, C. Simmons, S. Stopkowicz, A. Tajti, J. Vázquez, F. Wang, J. D. Watts and the integral packages MOLECULE (J. Almlöf and P. R. Taylor), PROPS (P. R. Taylor), ABACUS (T. Helgaker, H. J. Aa. Jensen, P. Jørgensen, and J. Olsen), and ECP routines by A. V. Mitin and C. van Wüllen. For the current version, see <http://www.cfour.de>, 2020. [Online]. Available: <https://www.psc.edu/user-resources/software/cfour>.
- [193] ReSpect 5.0.1 (2018), relativistic spectroscopy DFT program of authors M. Repisky, S. Komorovsky, V. G. Malkin, O. L. Malkina, M. Kaupp, K. Ruud, with contributions from R. Bast, R. Di Remigio, U. Ekstrom, M. Kadek, S. Knecht, L. Konecny, E. Malkin, I. Malkin Ondik (see <http://www.respectprogram.org>), 2020.
- [194] M. Repisky, S. Komorovsky, M. Kadek, *et al.*, “ReSpect: Relativistic Spectroscopy DFT Program Package,” *The Journal of Chemical Physics*, vol. 152, no. 18, p. 184101, May 2020.
- [195] J. F. Schenck, “The Role of Magnetic Susceptibility in Magnetic Resonance Imaging: MRI Magnetic Compatibility of the First and Second Kinds,” *Medical Physics*, vol. 23, no. 6, pp. 815–850, 1996. DOI: [10.1118/1.597854](https://doi.org/10.1118/1.597854). eprint: <https://aapm.onlinelibrary.wiley.com/doi/pdf/10.1118/1.597854>. [Online]. Available: <https://aapm.onlinelibrary.wiley.com/doi/abs/10.1118/1.597854>.
- [196] M. Mihara, Y. Otani, Y. Kimura, *et al.*, “High-resolution β -NMR of short-lived spin-1/2 nucleus ^{17}N implanted into water,” *Hyperfine Interactions*, vol. 242, no. 1, p. 49, Dec. 2021, ISSN: 0304-3843. DOI: [10.1007/s10751-021-01773-z](https://doi.org/10.1007/s10751-021-01773-z). [Online]. Available: <https://link.springer.com/10.1007/s10751-021-01773-z>.
- [197] M. Stachura, R. M. L. McFadden, A. Chatzichristos, *et al.*, “Towards ^{31}Mg - β -NMR resonance linewidths adequate for applications in magnesium chemistry,” *Hyperfine Interactions*, vol. 238, no. 1, p. 32, Nov. 2017,

- ISSN: 0304-3843. DOI: [10.1007/s10751-017-1408-8](https://doi.org/10.1007/s10751-017-1408-8). [Online]. Available: <http://link.springer.com/10.1007/s10751-017-1408-8>.
- [198] R. M. L. McFadden, D. Szunyogh, N. Bravo-Frank, *et al.*, “Magnesium(II)-ATP Complexes in 1-Ethyl-3-Methylimidazolium Acetate Solutions Characterized by ^{31}Mg β -Radiation-Detected NMR Spectroscopy,” *Angewandte Chemie International Edition*, vol. 61, no. 35, Aug. 2022, ISSN: 1433-7851. DOI: [10.1002/anie.202207137](https://doi.org/10.1002/anie.202207137). [Online]. Available: <https://onlinelibrary.wiley.com/doi/10.1002/anie.202207137>.
- [199] B. Karg and M. Kowalska, “Liquid β -NMR Studies of the Interaction of Na and K Cations with DNA G-quadruplex Structures,” CERN, Geneva, Tech. Rep., 2022. [Online]. Available: <https://cds.cern.ch/record/2798880>.
- [200] B. Fenker, A. Gorelov, D. Melconian, *et al.*, “Precision Measurement of the β Asymmetry in Spin-Polarized K 37 Decay,” *Physical Review Letters*, vol. 120, no. 6, p. 62502, 2018, ISSN: 10797114. DOI: [10.1103/PhysRevLett.120.062502](https://doi.org/10.1103/PhysRevLett.120.062502). [Online]. Available: <https://doi.org/10.1103/PhysRevLett.120.062502>.
- [201] P. D. Shidling, D. Melconian, S. Behling, *et al.*, “Precision half-life measurement of the beta+ decay of K37,” *Physical Review C*, vol. 90, no. 3, p. 032501, Sep. 2014, ISSN: 0556-2813. DOI: [10.1103/PhysRevC.90.032501](https://doi.org/10.1103/PhysRevC.90.032501).
- [202] K. Minamisono, P. Mantica, H. Crawford, *et al.*, “Quadrupole moment of ^{37}K ,” *Physics Letters B*, vol. 662, no. 5, pp. 389–395, May 2008, ISSN: 03702693. DOI: [10.1016/j.physletb.2008.03.049](https://doi.org/10.1016/j.physletb.2008.03.049). [Online]. Available: <https://linkinghub.elsevier.com/retrieve/pii/S0370269308003900>.
- [203] J. Papuga, M. L. Bissell, K. Kreim, *et al.*, “Spins and magnetic moments of K49 and K51: Establishing the $1/2+$ and $3/2+$ level ordering beyond $N=28$,” *Physical Review Letters*, vol. 110, no. 17, pp. 1–5, 2013, ISSN: 00319007. DOI: [10.1103/PhysRevLett.110.172503](https://doi.org/10.1103/PhysRevLett.110.172503).
- [204] J. Papuga, M. L. Bissell, K. Kreim, *et al.*, “Shell structure of potassium isotopes deduced from their magnetic moments,” *Physical Review C* -

BIBLIOGRAPHY

- Nuclear Physics*, vol. 90, no. 3, pp. 1–12, 2014, ISSN: 1089490X. DOI: [10.1103/PhysRevC.90.034321](https://doi.org/10.1103/PhysRevC.90.034321).
- [205] J. Papuga, “Structure of potassium isotopes studied with collinear laser spectroscopy,” Ph.D. dissertation, KU Leuven, Leuven, Apr. 2015.
- [206] F. Wienholtz, D. Beck, K. Blaum, *et al.*, “Masses of exotic calcium isotopes pin down nuclear forces,” *Nature*, vol. 498, no. 7454, 2013, ISSN: 14764687. DOI: [10.1038/nature12226](https://doi.org/10.1038/nature12226).
- [207] R. F. Garcia Ruiz, M. L. Bissell, K. Blaum, *et al.*, “Unexpectedly large charge radii of neutron-rich calcium isotopes,” *Nature Physics*, vol. 12, no. 6, pp. 594–598, Jun. 2016, ISSN: 1745-2473. DOI: [10.1038/nphys3645](https://doi.org/10.1038/nphys3645). [Online]. Available: <http://www.nature.com/articles/nphys3645>.
- [208] R. F. G. Ruiz, M. L. Bissell, K. Blaum, *et al.*, “Ground-state electromagnetic moments of calcium isotopes,” *Physical Review C*, vol. 91, no. 4, p. 041304, Apr. 2015, ISSN: 0556-2813. DOI: [10.1103/PhysRevC.91.041304](https://doi.org/10.1103/PhysRevC.91.041304). [Online]. Available: <https://link.aps.org/doi/10.1103/PhysRevC.91.041304>.
- [209] R. F. G. Ruiz, C. Gorges, M. Bissell, *et al.*, “Development of a sensitive setup for laser spectroscopy studies of very exotic calcium isotopes,” *Journal of Physics G: Nuclear and Particle Physics*, vol. 44, no. 4, p. 044003, Apr. 2017, ISSN: 0954-3899. DOI: [10.1088/1361-6471/aa5a24](https://doi.org/10.1088/1361-6471/aa5a24). [Online]. Available: <https://iopscience.iop.org/article/10.1088/1361-6471/aa5a24>.
- [210] D. Steppenbeck, S. Takeuchi, N. Aoi, *et al.*, “Evidence for a new nuclear ‘magic number’ from the level structure of ^{54}Ca ,” *Nature*, vol. 502, no. 7470, pp. 207–210, Oct. 2013, ISSN: 0028-0836. DOI: [10.1038/nature12522](https://doi.org/10.1038/nature12522).
- [211] J. Bonnard, S. M. Lenzi, and A. P. Zuker, “Neutron Skins and Halo Orbits in the sd and pf Shells,” *Physical Review Letters*, vol. 116, no. 21, pp. 1–5, 2016, ISSN: 10797114. DOI: [10.1103/PhysRevLett.116.212501](https://doi.org/10.1103/PhysRevLett.116.212501).
- [212] C. Henkel, G. Jacob, F. Stopp, *et al.*, “Stern–Gerlach splitting of low-energy ion beams,” *New Journal of Physics*, vol. 21, no. 8, p. 083022, Aug. 2019, ISSN: 1367-2630. DOI: [10.1088/1367-2630/ab36c7](https://doi.org/10.1088/1367-2630/ab36c7).